Heliyon 9 (2023) e13853

Contents lists available at ScienceDirect

Heliyon

journal homepage: www.cell.com/heliyon

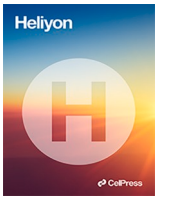

Research article

Integrative network pharmacology and in silico analyses identify the anti-omicron SARS-CoV-2 potential of eugenol

Yang Liu

Graduated Student of Harbin Medical University, Cardiology. Baojian Road#105, Nangang Distinct, Harbin, Heilongjiang, China

ARTICLE INFO

Keywords:
SARS-CoV-2
COVID-19
Omicron
Eugenol
RNA-Dependent RNA polymerase
Spike protein

ABSTRACT

Eugenol as a natural product is the source of isoniazid, and purified eugenol is extensively used in the cosmetics industry and the productive processes of edible spices. Accumulating evidence suggested that eugenol exerted potent anti-microorganism and anti-inflammation effects. Application of eugenol effectively reduced the risk of atherosclerosis, arterial embolism, and Type 2 diabetes. A previous study confirmed that treatment with eugenol attenuated lung inflammation and improved heart functions in SARS-CoV-2 spike S1-intoxicated mice. In addition to the study, based on a series of public datasets, computational analyses were conducted to characterize the acting targets of eugenol and the functional roles of these targets in COVID-19. The binding capacities of eugenol to conservative sites of SARS-CoV-2 like RNA-dependent RNA polymerase (RdRp) and mutable site as spike (S) protein, were calculated by using molecular docking following the molecular dynamics simulation with RMSD, RMSF, and MM-GBSA methods. The results of network pharmacology indicated that six targets, including PLAT, HMOX1, NUP88, CTSL, ITGB1 andTMPRSS2 were eugenol-SARS-CoV-2 interacting proteins. The omics results of in-silico study further implicated that eugenol increased the expression of SCARB1, HMOX1 and GDF15, especially HMOX1, which were confirmed the potential interacting targets between eugenol and SARS-CoV-2 antigens. Enrichment analyses indicated that eugenol exerted extensive biological effects such as regulating immune infiltration of macrophage, lipid localization, monooxyenase activity, iron ion binding and PPAR signaling. The results of the integrated analysis of eugenol targets and immunotranscription profile of COVID-19 cases shows that eugenol also plays an important role in strengthen of immunologic functions and regulating cytokine signaling. As a complement to the integrated analysis, the results of molecular docking indicated the potential binding interactions between eugenol and four proteins relating to cytokine production/release and the function of T type lymphocytes, including human TLR-4, TCR, NF-κB, JNK and AP-1. Furthermore, results of molecular docking and molecular dynamics (100ns) simulations implicated that stimulated modification of eugenol to the SARS-CoV-2 Omicron Spike-ACE2 complex, especially for human ACE2, and the molecular interaction of eugenol to SARS-CoV-2 RdRp, were no less favorable than two positive controls, molnupiravir and nilotinib. Dynamics (200ns) simulations indicated that the binding capacities and stabilities of eugenol to finger subdomain of RdRp is no less than molnupiravir. However, the simulated binding capacity of eugenol to SARS-CoV-2 wild type RBD and Omicron mutant RBD were less than nilotinib. Eugenol was predicted to have more favor LD50 value and lower cytotoxicity than two positive controls, and eugenol can pass through the blood-brain barrier (BBB). In a brief, eugenol is helpful for attenuating systemic inflammation induced by SARS-CoV-2 infection, due to the direct interaction of eugenol to SARS-CoV-2 proteins and extensive bio-manipulation of pro-

E-mail address: Yangliu19830722@126.com.

https://doi.org/10.1016/j.heliyon.2023.e13853
Received 3 April 2022; Received in revised form 6 February 2023; Accepted 13 February 2023
Available online 18 February 2023

inflammatory factors. This study carefully suggests eugenol is a candidate compound of developing drugs and supplement agents against SARS-CoV-2 and its Omicron variants.

1. Introduction

The great communicability of severe acute respiratory syndrome coronavirus 2 (SARS-CoV-2) led to more than six hundreds of millions of people infected so far and millions of people infected to death world over. In response to the pandemic, large-scale immunization with Corona Virus Disease 2019 (COVID-19) vaccinations significantly attenuated severe illness [1,2]. Vaccine regimens also lowered the rate of contracting the earlier virus by 50% [3,4]. Nevertheless, as one of the fastest-evolving viruses, high mutation rate of viral nucleotide makes the virus easier to escape the recognition of host's immune system than invariant. A new variant christened "Omicron" (B.1.1.529) and its evolutionary branch have gradually replaced delta variant as the dominant strain of SARS-CoV-2 in some countries, which spreads faster than its predecessor [5–9]. Lately, BA.4/BA.5 variants of Omicron were identified in South Africa, the two variants were presumed the dominated strains in EU countries and the US in the summer 2022. There may be a prospective COVID wave together with the seasonal influenza or new variants of Omicron SARS-CoV-2 around the end of 2022 [10]. To be different from Omicron BA.1 and BA.2 variants with similar clinical symptoms, BA.4/5 variants with more adaptable and pathogenic traits, expanded at higher levels than BA.2.12.1. Omicron sublineage BQ.1.1 has shown resistance to the existing monoclonal antibodies [11]. They primarily replicate in human alveolar epithelial cells and the BA.4/5 variants may also increase the risk of reinfection [12,13]. Besides, pathogenicity of more infectious sub-variants of Omicron such as BQ.1, BQ.1.1, XBB and BF.7 remain to be estimated.

As several studies suggested, SARS-CoV-2 Omicron infection was upper airways preferred, limiting primarily to the nasal cavity, throat and tracheae beside earlier variants. It seems to be less pathogenic to lungs [14,15]. Apart from the lethality and infectivity of the virus, a concept as "Long COVID" was previously described and used to evaluate the lasting impacts of viral infection on confirmed cases. An UK population-based study has estimated the risk of "Long COVID" by delta and omicron variants after vaccination, this study suggested the risk of "Long COVID" by Omicron variants (4.5%/56,000) is lower than delta variants (10.8%/41,000) [3]. Nevertheless, "Long COVID" in unvaccinated individuals and children were undetermined in this study. Results from a large-scale South Africa study previously indicated that the hospital admission for Omicron infected cases was significantly reduced compared with other infections during the same period. Meanwhile, the SARS-CoV-2 Omicron contracting cases had a lower risk of severe illness compared to the infection by earlier delta variant. Previously, Hastie and colleagues estimated asymptomatic infection by SARS-CoV-2, they found asymptomatic infection was not associated with adverse outcomes. COVID vaccination could improve a part of infection related symptoms [16]. Despite all this, among generally young South Africans, 21% of hospitalized patients suffering Omicron infection showed a severe clinical outcome [17,18]. In contrast, two Large-US population based studies implicated menace by Omicron variants is not lower than Delta, even in a highly vaccinated and increasingly immune population [19,20]. Hence, Omicron infection should still be given enough vigilance, because subsequent cumulative reinfection puts elderly, children, population with chronic diseases, and immunocompromised population at cumulative risk of severe disease and death [21,22]. It is also noted that a highly contagious virus could lead to considerable financial burden, additional pressure on health-care systems and the loss of productivity [18], especially in countries or regions with unbalanced resource allocation. We also cannot discount the potential impacts of the pandemic on life expectancy (LE) losses [23]. As pharmaceutical and non-pharmaceutical public health interventions have offered a positive influence on the LE of 2020 and 2021, keep exploring more efficient vaccines and therapeutic drugs against Omicron variants remains critical important.

Recently, Food and Drug Administration (FDA) approved Paxlovid (nirmatrevir plus ritonavir), a 3CL protease inhibitor of SARS-CoV-2, for the treatment of mild or moderate COVID-19. Paxlovid significantly reduce the risk of COVID-19 related hospitalization and all-cause mortality [24]. Another 3CL protease inhibitor EDP-235 (ENTA.US) showed favorable enzymological inhibitory effects against a variety of SARS-CoV-2 variants, including Omicron variants. Synchronously, SARS-CoV-2 RdRp inhibitor-Molnupiravir (Merck sharp & dohme) was approved by medicines and healthcare products regulatory agency (MHRA) and Emergency-Use-Administration (EUA) [25]. Molnupiravir is powerful ribonucleoside analogues that can inhibit the replication of multiple RNA viruses, and significantly reduce the risk of infection related hospital admission and death [26]. Molnupiravir also showed inhibitory effects on the proliferation of SARS-CoV-2 omicron [27]. Other drugs, including SARS-CoV-2 Mpro inhibitor, VV116 and SIM0417 are under development. Apart from these new inhibitors, some natural compounds such as plant phenols/polyphenols have properties of anti-inflammatory against SARS-CoV-2 infection, reinforcing intrinsic immune function and inhibiting viral transcription. Besides that, these phenolic compounds have the advantages of more pan-corona antiviral characteristics, low toxicity and fewer side effects, which can be used as a complement to existing drugs and vaccines [28].

Historically, phenolic compounds and their derivatives processes potent anti-oxidant activity due to their high reactivity of hydroxyl substitution and the ability to phagocytize free radicals [28–30]. Polyphenols can inhibit key enzymes and viral genomes related to viral transcription. Cho and colleagues found prenylated phenolic compounds isolated from the leaves of Sabia limoniacea significantly inhibit the expression of nucleocapsid and Spike protein of porcine epidemic diarrhea virus (PEDv) in a dose-dependent manner [31]. The results of Kim et al. implicated that flavonoids/polyphenols efficiently block the enzymatic activity of SARS-CoV papain-like protease (PLpro), a key player in the maturation process of SARS-CoV [32,33]. Additionally, a previous study suggested that eugenol is a candidate natural compound against COVID-19. In human cell lines, eugenol can block the binding of SARS-CoV-2 spike S1and ACE2, and suppressed the entry of pseudotyped SARS-CoV-2 into human cells, and inhibit SARS-CoV-2 spike S1-induced

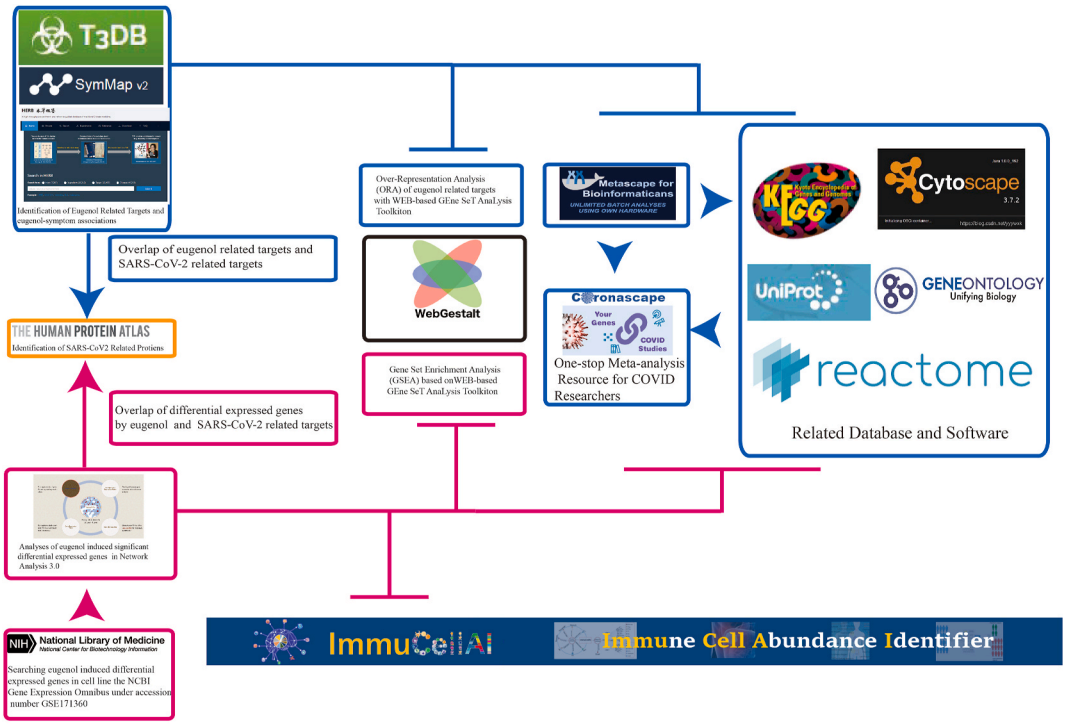

A) Identification of Biological and Functional Roles of Eugenol Targets in COVID-19

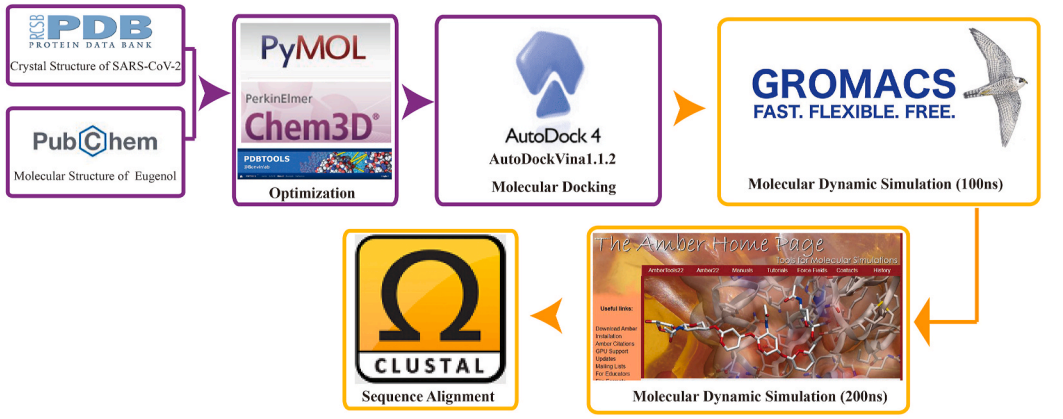

B) Identification of the Binding Capacities of Eugenol to Pathogenic Components of SARS-CoV-2 Variant

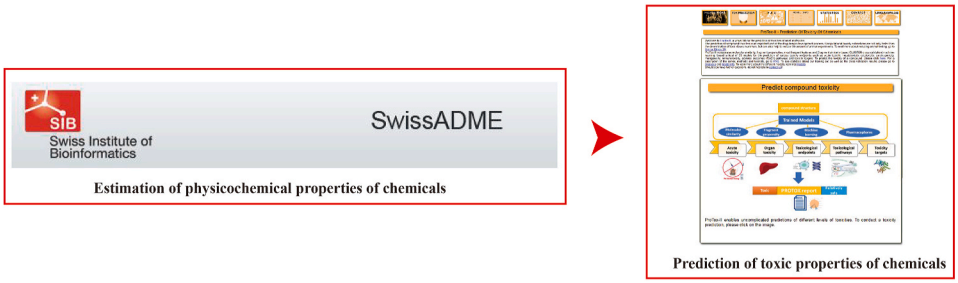

C) Estimation of the physicochemical and toxic properties of chemicals

Fig. 1. Flowchart indicates the antiviral action and mechanisms of eugenol against COVID-19 using computational analysis approach.

activation of NF-κB signaling and the expression of inflammatory cytokines in human A549 lung cells. Based on a model of SARS-CoV-2 spike S1-intoxicated mice, they found oral administration of eugenol attenuated lung inflammation, alleviated fever, protected heart function, and improved locomotor activities [34]. However, the core interacting genes and pathways related to SARS-CoV-2 infection and eugenol pharmacological actions both were not fully understood. It is still unclear the binding capacities of eugenol to SARS-CoV-2 RdRp and Omicron SARS-CoV-2 Spike antigen. At any rate, the results of Paidi et al. are important basis and reference for investigating the chemicals against SARS-CoV-2.

As drug delivery and metabolism are important parts of drug design, candidate chemicals should have the advantages that the compounds can be easily absorbed/metabolized, tissue permeability and the safety of human application. From the prospective of eugenol delivery, encapsulated eugenol is preferable, which can avoid early absorption and ameliorate the water-solubility and efficacy. Ordinarily, Chitosan can be used for encapsulation of eugenol to enhance its thermal stability. Plant essential oils (EOs) containing eugenol can be rapidly absorbed by stomach and small intestine following dermal, pulmonary, and oral intake. Ingested eugenol is metabolized quickly in liver, while 95% of the dosis is evacuated within 24 h. Zhao et al. demonstrated that eugenol ester can be used to prepare ibuprofen microemulsion, which reduced the risk of ibuprofen-induced ulcer [35]. The delivered quantity of eugenol afforded in the form of solid lipid nanoparticles increased at least six-fold in the infectious cells. Hence, diversified delivery approaches of eugenol make it have wide applications in the field of chemistry, biology and medicine [35].

Given the fact that pharmacological targets of eugenol against SARS-CoV-2 and its variants have not be fully revealed. There is also no comprehensive study on the use of eugenol as a potential inhibitor of SARS-CoV-2 proliferation. In line with the results of Paidi et al. and existing evidence, the author conducted a synthetical study covering literature review, in-silico analysis, genomics analysis and molecular dynamics simulation, to calculate the hub interacting genes, immunomodulatory characteristics of eugenol against COVID-19, and the binding capacities of eugenol to SARS-CoV-2 virulence domains related to viral invasion and proliferating. This comprehensive work aims to provide ideas for developing drugs and adjuvant therapy against SARS-CoV-2 and its variants.

2. Methods

2.1. Study protocol of the study

In order to explore the anti-SARS-CoV-2 potential of eugenol, a series of public databases and web tools were used for conducting the analysis procedure. The current study was divided into the following seven major parts. (1) Searching and identifying the eugenol targets; performing enrichment analyses of these targets to find the core BPs and pathways that regulated by eugenol; identifying the targets of SARS-CoV-2 antigens; identifying intersecting genes; investigating the roles of eugenol targets in immune response signaling of COVID-19. (2) Selecting an external genome dataset (GSE171360) to further verify the results from the single analysis above, including omics analyses, enrichment analyses, GSEA, immune infiltration analysis and integrative matching analysis in COVID-19. (3) For clarifying the immunoregulatory role of eugenol in COVID-19, binding probability of eugenol to human Toll Like Receptor (TLR-4)/AP-1 axis and T type lymphocyte receptor were calculated, as human TLR-4 is a known inflammatory signal promotor of COVID-19. (4) Initial estimation of the binding probability of eugenol to SARS-CoV-2 RdRp, spike protein-ACE2 complex of earlier strain and the omicron variant with molecular docking. (5) Calculating the interaction of eugenol to SARS-CoV-2 RdRp and SARS-CoV-2 Omicron S protein-human ACE2 complex with molecular dynamic simulation (100ns). Then the binding of eugenol to SARS-CoV-2 Spike protein (wild type) and Omicron Spike protein (mutant type), and finger subdomain of RdRp were subjected to separate calculation (200ns) by removing the ACE2 form the crystal structure of complexes. (6) Sequence alignment with wild and omicron spikes of SARS-CoV-2. (7) Estimating and predicting the physicochemical, aberration and toxic properties of chemicals. A visible graphical summary for the work flowchart is provided (Fig. 1).

2.2. Identification of eugenol targets

Pharmacotranscriptomics is a powerful approach for discovering novel drug targets. HERB (BenCaoZuJian) (URL: http://herb.ac.cn/) is a high throughput experiment and reference guided database of TCM (Traditional Chinese Medicine), and the database collected 17,886 TCM-related papers published since 2011 by PubMed text mining, and then manually extracted 1241 gene targets and 494 modern diseases for herbs/ingredients from 1966 unique references (137 references for herbs and 1860 references for ingredients, total 1997 records) among them [36]. Eugenol targets are available through searching HERB. As supplements, further query was conducted in SymMap, version 2.0 (URL: http://www.symmap.org) and T3DB (URL: http://www.t3db.org/). SymMap integrates traditional Chinese medicine (TCM) with modern medicine (MM) through both internal molecular mechanism and external symptom mapping, thus provides massive information on herbs/ingredients (698/26,035), targets (20,965), as well as the clinical symptoms (MM symptoms: 1148; TCM symptoms and syndromes: 2518) and diseases (14,086). They are used to treat for drug screening efforts [37]. T3DB as a comprehensive database, which can provided additional targets of common chemicals was also used in the initial screening [38].

2.3. Identification of SARS-CoV-2 antigen-related targets in human

The Human Protein Atlas (HPA) consortium is engaged in the corona epidemic in various ways to aid in the fight against the health consequences of this pandemic outbreak (URL: https://www.proteinatlas.org/). The program involves both efforts to increase the knowledge-base of the disease and efforts to develop diagnostic tools and therapeutic drugs to combat the pandemic. The database

provides a summary of the tissue and cell expression patterns of known SARS-CoV-2 interacting human proteins, based on transcriptomics and antibody-based proteomics [39,40]. SARS-CoV-2 antigen interacting proteins are available by searching this database.

2.4. Gene enrichment analyses of eugenol targets identified from HERB and SymMap

WebGestalt (WEB-based Gene SeT AnaLysis Toolkit) is a functional enrichment analysis web tool, the new version WebGestalt 2019 (URL: http://www.webgestalt.org/) with the R package provides an interface to integrate into other pipelines or run batch jobs locally [41]. Using WebGestalt, gene Over Representation Analysis (ORA) was performed for the enrichment of eugenol targets collected from HERB and SymMap. Geneontology enrichment, including biological process (BP), cellular component (CC), molecular function (MF), KEGG pathway enrichment, and disease enrichment can be identified.

2.5. Intersection of eugenol targets and SARS-CoV-2 interacting targets for discovering co-regulated genes

An integrative tool, jvenn (URL: http://jvenn.toulouse.inra.fr/app/example.html) for comparing lists with Venn Diagrams, was used for an overlap of eugenol targets and SARS-CoV-2 interacting genes [42]. Thereby, the co-regulated genes can be obtained.

2.6. Verification of eugenol induced gene expression through external dataset GSE171360

In addition to single analysis, an external dataset, GSE171360 (URL: https://www.ncbi.nlm.nih.gov/geo/query/acc.cgi?acc=GSE171360) was used to validate eugenol induced transcriptomics change in specific cell line. GSE171360 is the dataset of expression profiling by high throughput sequencing, which measured and classified DNA damaging agents in human HepaRG™ Cells [43]. In this study, eugenol was classified as a non-DDI (DNA damage-inducing) chemical and 5 doses (C0: baseline; C1:156.25 μM; C2: 312.5 μM; C3: 625 μM, C4: 1250 μM and C5: 2500 μM) of eugenol induced genomics transcription was tested in HepaRG™ Cells. According to the results of this study, two high doses (1250 μM and 2500 μM) were excluded, and three low or moderate doses were reserved, because eugenol at a dose of 1250 and 2500 μM will lead to a decrease in cell viability, and the genomic transcription of the two doses indicated a positive DDI classification. The raw data were downloaded from PubMed.gov (URL: https://pubmed.ncbi.nlm.nih.gov/), screening and validation of differentially expressed genes were conducted in NetworkAnalyst 3.0 (URL: https://www.networkanalyst.ca) [44]. C0 (Baseline) was set as the control, and original data was normalized with Log 2-counts per million, and analyzed with EdgeR. Adjusted P-value was set as lower than 0.05 and Log 2 fold change was set as ≥ 1. The differentially expressed genes were reserved.

2.7. Immune cell infiltration analyses of eugenol-induced gene transcription in GSE171360

ImmuCellAI (Immune Cell Abundance Identifier) is a tool to estimate the abundance of 24 immune cells from gene expression dataset including RNA-Seq and microarray data, in which the 24 immune cells are comprised of 18 T-cell subtypes and 6 other immune cells: B cell, NK cell, Monocyte cell, Macrophage cell, Neutrophil cell and DC cell (URL: http://bioinfo.life.hust.edu.cn/ImmuCellAI). ImmuCellAI can be applied to predict the difference of immune cell infiltration in diverse groups will be analyzed with the immune cell abundance in groups being checked [45]. Immune cell infiltration of transcribed genes induced by eugenol were calculated in ImmuCellAI. Raw data of different dose groups extracted from GSE171360 were normalized with Log 2 before inducing into the web tool. An adjusted P value lower than 0.05 was considered statistic significant.

2.8. Gene enrichment analyses of eugenol targets identified from GSE171360

Gene set enrichment analysis (GSEA) of differentially expressed genes by eugenol was performed in WebGestalt. The FDR value was set as 1, the enriched items involved BP, CC, MF, KEGG, drug and disease.

2.9. Single-cell RNA sequencing dataset of COVID-19 cases

Single-Cell RNA sequencing dataset used in the matching analyses is derived from peripheral blood samples of 5 healthy donors and 13 patients of COVID-19, including moderate, severe and convalescent cases according to Zhang et al. [46]. The dataset involves four types of immune cells (Monocytes, NK (Nature Killer) cells, T- and B- lymphocytes), and the transcriptional profiles of these immune cells of severe COVID-19 were selected in the current study. The dataset contains SARS-CoV-2 severe patients ($n = 4$) vs. healthy donors ($n = 5$). The significantly expressed genes of this dataset is defined by P-value <0.01 and Log2 FC$\geq$0.5. The dataset can be analyzed at Coronascape platform (URL: https://metascape.org/COVID) [47].

2.10. Integrative enrichment analyses of eugenol targets in COVID-19

Metascape network tool is a bioinformatics platform and one-stop meta-analysis resource for COVID researchers [47]. To investigate potential contributions of eugenol targets to the immune responses of COVID-19, identified eugenol targets from single analysis and omics analyses were matched to the single-cell RNA sequencing dataset of severe COVID-19 cases respectively [46]. Integrative analyses were conducted in Metascape-Coronascape (URL: https://metascape.org/COVID/). Then the results of gene ontology and

pathway enrichment analyses were visible. The data for enriched terms are presented with "Count" and "-log 10 (P-value)", the results of PPI network analyses were summarized, and the bar charts were used for visualizing the final results.

2.11. Molecular docking of eugenol and SARS-CoV-2 omicron Spike-ACE2 complex, RdRp, TLR-4 axis and clone18 TCR

To assess the binding capacities of eugenol with the pathogenic components of SARS-CoV-2, molecular docking analysis was conducted. Molecular structure of eugenol was available in Pubchem (URL: https://pubchem.ncbi.nlm.nih.gov/compound/CID: 3314/eugenol), then the downloaded molecular structure was optimized with Chem 3D [48]. Crystal structure of spike receptor-ACE2 complex from earlier SARS-CoV-2 strain and omicron variant, and replicating SARS-CoV-2 polymerase were downloaded from RCSB_PDB database (URL: https://www.pdbus.org/) with PDB ID: 6M0J; 7T9L; 6YYT [49–51]. Furthermore, Toll-like receptor-4 (TLR-4)/AP-1 axis facilitates the inflammatory cytokine production/release mediated by LPS and SARS-CoV-2. Therefore, the binding affinities of eugenol with the TLR-4 (2z63), clone18 TCR (4g8e), NF-κB (1le5), JNK/MAPK (30xi), and AP-1(4hmy) protein were further calculated. Crystal structure of these proteins were available in PDB database [52].

The methods were detailed in previous studies [53,54]. Briefly, the primordial pdb file format was transformed to the pdbqt file format, which can be recognized by the Autodock program, providing a ligand basis to molecular docking. Furthermore, the active center for docking (involving residues around the primordial ligand) was set with the grid box function of the corresponding software. The non-interacting redundant water molecules and the original ligand were removed using pymol 2.4.0 software. Then the potential probability of eugenol binding with components of SARS-CoV-2/Omicron Spike-ACE2 complexes, RdRp and other proteins were determined by assigning Autodock and AutoDock Vina 1.1.2. The binding probability was defined comprehensively, as low binding energy, the number of hydrogen bonds, appreciable binding score and the interacting amino acids.

2.12. Molecular dynamics simulation of eugenol and SARS-CoV-2 omicron spike-ACE2 complex, SARS-CoV-2 RdRp (100 ns)

Molecular docking can depict the possibility of spatial structure of the chemical matching to the interest protein, however, the results need further investigation such as molecular dynamic simulation. Therefore, the author selected molnupiravir (Pubchem: https://pubchem.ncbi.nlm.nih.gov/compound/145996610) and nilotinib (Pubchem: https://pubchem.ncbi.nlm.nih.gov/compound/644241) as the positive controls to study interacting of eugenol (Pubchem: https://pubchem.ncbi.nlm.nih.gov/compound/3314) to SARS-CoV-2 RdRp and Omicron Spike protein-ACE2 complex respectively. The two positive inhibitors were confirmed effective against SARS-CoV-2 previously, molnupiravir is orally active RdRp inhibitor, and nilotinib is identified a potential inhibitor of SARS-CoV-2 S protein [25,55–59].

GROMACS package (version 2021.03) was applied to run conventional MD simulations to investigate binding mode. ChemBio3D was used to minimize the energy of small molecules, and Autodock Vina was applied for addition of hydrogen atoms to small molecule ligands (protonation), addition of charges, confirming the ligands of root and choosing torsionable bonds for fitting low energy conformation. The force field amber14sb ff was employed to parameterize protein. The TIP3P was used for the waters. Compounds was parameterized using the AnteChamber Python Parser Interface (ACPYPE) with amber14 force field. This compound-protein complexes were solvated in an octahedral water box, and then the charge of the system was neutralized by adding 0.150 M chloride and sodium ions. First, the steepest descent minimization method was used to minimize the energy of the system by 50,000 steps. In the next step, we restricted the position of heavy atoms to run both NVT equilibration and NPT equilibration by 50,000 steps. The system temperature was maintained at 300 K, and the system pressure was maintained at 1 bar. Upon completion of the two equilibration phases, the system is now well-equilibrated at the desired temperature and pressure. A 100-ns unrestrained simulation was carried out. Every 10 ps, the energy and coordinate system of the trajectory were saved. In the simulation trajectory, use Pymol to map interaction patterns and animate kinetic trajectories [60–62].

MM-GBSA method has been widely adopted in the estimation of binding free energy in drug research. In brief, the MM-GBSA calculation was performed using the gmx_MMPBSA, a tool of GROMACS for MM-PB(GB)SA calculations. To understand the binding of proteins and compounds at the molecular level, we used gmx_MMPBSA to decompose the free energy of binding to the contribution of each residue to the free energy of binding [63,64].

2.13. Molecular docking and dynamics simulation of eugenol and SARS-CoV-2 wild type and omicron mutant spike RBD, finger subdomain of SARS-CoV-2 RdRp (200ns)

Molecular docking of eugenol and SARS-CoV-2 wt/mutant spike RBD was used to predict the binding pattern. Crystal structures of SARS-CoV-2 wild type RBD (6m0j), Omicron mutant RBD (7t9l) and RdRp (6m71) were obtained from PDB, 3D structure of small molecule molnupiravir, nilotinib and eugenol were downloaded from PUBCHEM. AutoDock Vina 1.1.2 was used to conduct the docking [65]. Energy-minimised with MMFF94 force field. At the beginning of the formal docking action, PyMol 2.5.4 [65] was used for the preparation of target proteins, as addition of hydrogen atoms, removal of no-interacting redundant water molecules and non-ligand small molecule. Subsequently, the box of docking was set to enclose the pocket of protein activity. PDB format of proteins were converted to PDBQT format using ADFRsuite 1.0 [66]. The parameter of conformation search was set as 32, while other parameters were kept defaut values, and click OK. The exported conformation affinity with the highest score was considered the correct conformation. PyMol 2.5.4 was used for visualization analysis.

The small-molecule complex system what has been built was the original structure, Amber18 soft package was applied through the whole simulation [67]. At the beginning of the simulation, Maestro 12.9 software was used for the preparation of the complexes.

Prediction of protonation of small molecule chemicals and proteins were performed under the condition of PH = 7.4, correction of valence bond, etc. After preparation of the complexes, antechamber module of AMBER18 was applied to calculate the BBC electric charge of small molecules, and to fit force fields. We descried the complexes based on GAFF2 small force field and ff14SB protein force field with LEaP module, and added the hydrogen atoms correctly [68,69]. Solvent box of truncated octahedron TIP3P was added at the distance of 10 Å of the system [70]. Na+/Cl-was used to equilibrate the electric charges, then these were exported for simulated topology and the parameter files.

The simulation involved four parts, as energy minimization, warming, equalization, end product simulation. Firstly, 200 kcal/mol/Å limiting force was added to the ternary complex to optimize solvent water molecule. Afterwards, the limiting force was removed and we optimized the energy of the whole system. The two process of optimization performed by either method of steepest descent (5000 steps) or by the method of conjugate gradient (5000 steps) method. After the energy optimization was finished, warming (50ps) process was conducted from zero to 300 K. Limiting forces (200 kcal/mol/Å) was added to the complex to conduct the simulation (500ps, NVT, isothermay, equivolume), under the condition of 300 K holding temperature of the system. Thereby, solvent molecules uniformly distributed in the solvent box. Subsequently, limiting force was removed while the temperature remained constant, simulation of the whole system was conducted with 1ns NPT (constant-temperature/constant-pressure). During the collection process of molecular trajectory, we performed the ensemble simulation of the system (200ns NPT, constant-temperature/constant-pressure) under periodic boundary condition. No bonding truncated distance was set as 10 Å, Particle mesh Ewald (PME) method was applied to analyze the long-range electrostatic interaction [71,72]. SHAKE methods was used to limited the bond length of involved hydrogen atom bond [73]. Langevin algorithm was used for temperature control, and the dynamical collision frequency γ was set as 2ps-1.

The pressure of the system was set as 1atm, the integral step-size was 2fs, and trajectory was preserved every 10ps. The exported trajectory was used for further analysis. Furthermore, the binding free energy of proteins and legends of all system were estimated with MM-GBSA method [63,74,75], the calculation of MD trajectory was 190–200 ns with the following formula:

$$\Delta Gbind = \Delta Gcomplex - (\Delta Greceptor + \Delta Gligand) = \Delta E\ internal + \Delta EVDW + \Delta Eelec + \Delta GGB + \Delta GSA \quad (1)$$

In formula (A), ΔE internal denote internal energy, ΔEVDW denote the Van der waals interaction, and ΔEelec denote the electrostatic interaction. Internal energy involved Ebond, Eangle and Etorsion. ΔGGB and ΔGGA were solvent free energy, and GGB was polar solvation energy. GSA was nonpolar solvation energy. Regarding ΔGGB, we used GB model (igb = 2) of Nguyen to perform the analysis [76], nonpolar solvation energy (ΔGSA) was calculated depending on the product of the surface tension (γ) and the solvent accessibility surface (surface area, SA). GSA = 0.0072 × SASA [77]. Entropy change was neglected due to high consumption of computing resources and low accuracy [75].

2.14. Sequence alignment with wild and omicron spike of SARS-CoV-2

Sequence alignment with wild and omicron spike of SARS-CoV-2 was conducted, sequences of SARS-CoV-2 RBD and SARS-CoV-2 Omicron was extracted based on PDB structure with pdb_tools software [78]. Clustal Omega server (https://www.ebi.ac.uk/Tools/msa/clustalo/) was used to perform the final comparison [79].

2.15. Predicting "ADME" parameters, pharmacokinetic properties, and druglike nature of chemicals

This website of Swiss ADME allows utilizers to compute physicochemical descriptors as well as to predict ADME parameters, pharmacokinetic properties, druglike nature and medicinal chemistry friendliness of one or multiple small molecules to support drug discovery [80]. In the current study, absorption (A), distribution (D), metabolism (M) and excretion (E) of aiming chemicals, as eugenol, molnupiravir and nilotinib were predicted with Swiss ADME (URL: http://www.swissadme.ch/), Structure 2D sdf files were downloaded from PubChem (eugenol_3314; molnupiravir_145996610; nilotinib_644,241). SDF files were introduced in clipboard of Swiss ADME, then the recognized molecular structure of chemicals were plotted and transformed to a list of SMILES number. Calculated ADME parameters were grouped in six sections involving physicochemical properties, lipophilicity, water solubility, pharmacokinetics, drug-likeness and medicinal chemistry. The discrepancy of these parameters were compared among chemicals.

2.16. Estimating aberration and toxic properties of chemicals

The prediction of compound toxicities is an important part of the drug design development process. ProTox-II incorporates molecular similarity, fragment propensities, most frequent features and (fragment similarity based CLUSTER cross-validation) machine-learning, based a total of 33 models for the prediction of various toxicity endpoints such as acute toxicity, hepatotoxicity, cytotoxicity, carcinogenicity, mutagenicity, immunotoxicity, adverse outcomes (Tox21) pathways and toxicity targets of small molecules [81]. In the current study, aberration and toxic properties of chemicals were estimated with ProTox-II (URL: http://tox.charite.de/protox_II).

3. Results

3.1. Eugenol-related targets

In HERB database, ingredient-based query was performed, and a total of 295 eugenol targets was identified (Supplemental Table 1). A further query was conducted in SymMap, identical eugenol targets was determined due to the interaction of the two databases to TCM. In addition to the two datasets, three unclear hormone receptors as ESR1/2 and AR, one unclear target as PPARG, one Ca^{2+} channel related target as TRPV3 were identified in T3DB (Fig. 2 A).

3.2. Enrichment analyses of eugenol targets identified in HERB

Gene over representation analysis (ORA) was performed in WebGestalt, 292 out of 295 genes was discriminated. The significant enrichment items of BPs were response to oxidative stress, blood circulation, circulatory system process, response to inorganic substance, inflammatory response, regulation of response to external stimulus, defense response, response to oxygen-containing compound, proteolysis, and homeostatic process (Fig. 2B and Supplemental Table 2). Furthermore, the significant enrichment items of KEGG pathways involved complement and coagulation cascades, calcium signaling pathway, small cell lung cancer, prostate cancer, hepatitis B, kaposi sarcoma-associated herpesvirus infection, malaria, pathways in cancer, human cytomegalovirus infection, and Influenza A (Fig. 2C and Supplemental Table 3).

3.3. Eugenol associated clinical symptoms

Sixty-one eugenol associated clinical symptoms were obtained. The clinical symptoms were manually divided into six categories, including headache (12/19.6%), other pain (15/24.6%), sensory and neurological symptoms (17/27.9%), upper respiratory tract symptoms (6/9.8%), gastrointestinal symptoms (7/11.5%) and other symptoms (4/6.6%). Among these symptoms, adjusted P value lower than 0.05 were meaningful symptoms (Supplemental Table 4). The statistic significant symptoms for headache (12 symptoms) were sharp headache, headache (periorbital), bilateral headache, ocular headache, headache throbbing, orthostatic headache, generalised headache, vertex headache, headache (retro-ocular), headache unilateral, headache, and headache (Dull) (Fig. 3 A); For other pain (1 symptom) was tenderness (Fig. 3 B); For sensory and neurological symptoms (4 symptoms) were anosmia, disorder of smell, dysomia and parosmia (Fig. 3C); For upper respiratory tract symptoms (2 symptoms) were coryza and catarrh (Fig. 3 D); For gastrointestinal symptoms (1 symptom) was emesis (Fig. 3 E). Other symptoms (Fig. 3 F).

A)

Targets	Uniprot ID	Molecular Weight	General Function	Specific Function
ESR1	P03372	66215.45 Da	Zinc ion binding	Nuclear hormone receptor, AP-1, Sps, NF-κB
ESR2	P10275	98987.9 Da	Zinc ion binding	Steroid hormone receptors
AR	Q92731	59215.765 Da	Zinc ion binding	Nuclear hormone receptors
PPARG	P37231	57619.58 Da	Zinc ion binding	Nuclear receptor
TRPV3	Q8NET8	90635.115 Da	Calcium channel activity	Putative recepor-activated no-selective Ca2+ channel

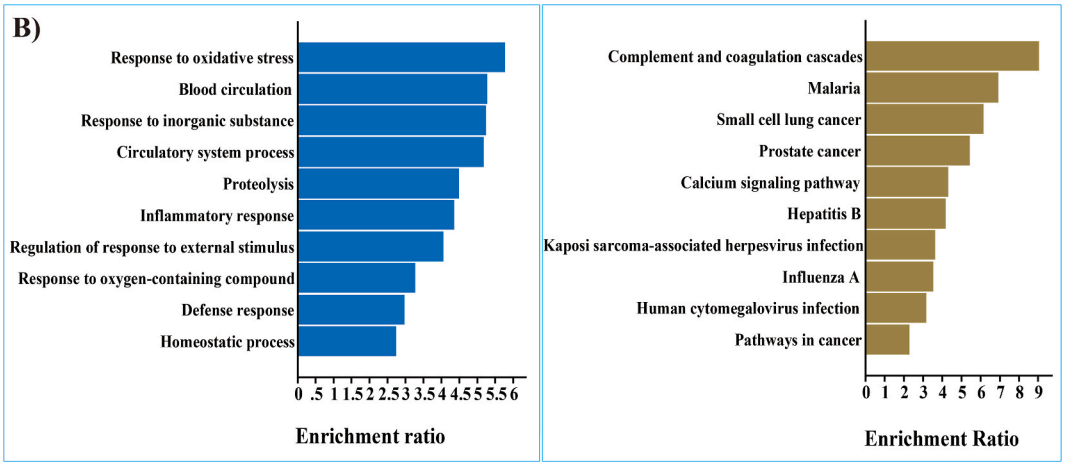

Fig. 2. Functional characterization of eugenol targets collected form T3DB database, HEARB and SymMap, 292 out of 295 targets involved in the enrichment. (A) T3DB targets. (B) Gene ontology analysis. (C) Kyoto Encyclopedia of Genes and Genomes (KEGG) pathway analysis. The results of gene over representation analysis (ORA) were depicted by bar charts, and enriched items were ranked by enrichment ratio, and the adjusted P value was lower than 0.05.

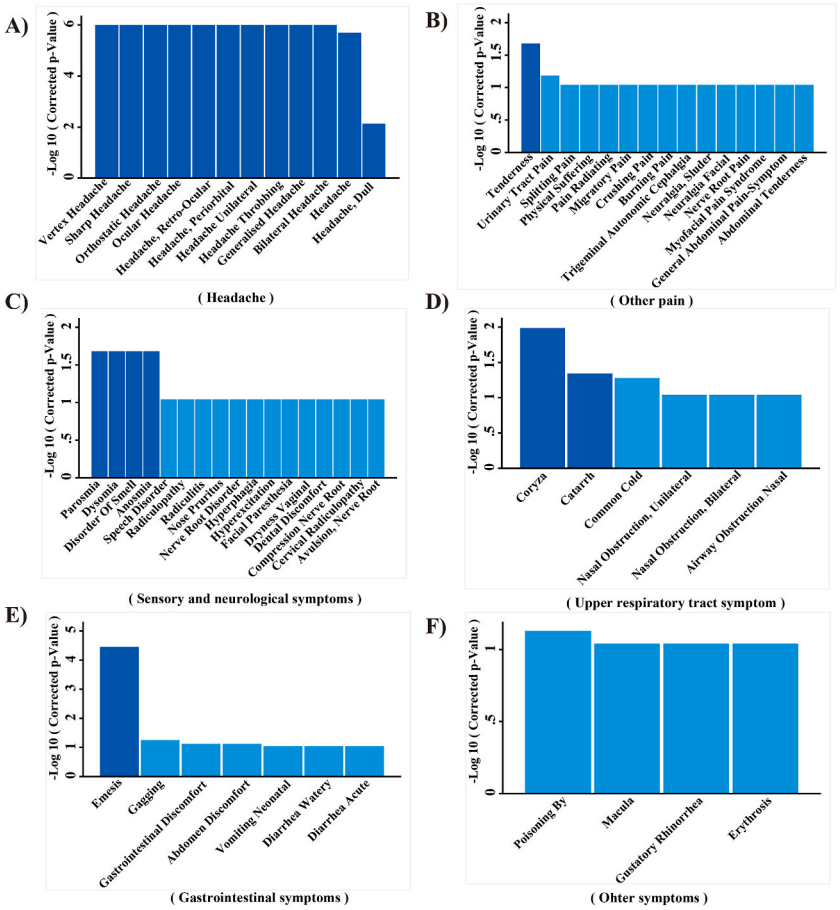

Fig. 3. Correlation of eugenol and clinical symptoms with six classification. (A) Headache. (B) Other pain. (C) Sensory and neurological symptoms. (D) Upper respiratory tract symptoms. (E) Gastrointestinal symptoms. (F) Other symptoms. Bar charts with dark blue denote P value < 0.05, and bar charts with light blue denote a P value > 0.05.

3.4. Identical core targets of eugenol and SARS-CoV-2 antigens

Human protein atlas collected 333 SARS-CoV-2 interacting human proteins based on transcriptomics and antibody-based proteomics [40]. The 333 proteins intersected with 295 eugenol targets, and six unique targets, including PLAT, HMOX1, NUP88, CTSL, ITGB1 and TMPRSS 2 were identified (Supplemental Table 5). The six targets were confirmed the proteases contributing to SARS-CoV-2 entry as TMPRSS2 and CTS L [40,82,83], or COVID-19 severity as PLAT, HMOX1, NUP88 and ITGB1 [84–89] (Fig. 4).

3.5. Contribution of eugenol targets in immune response signaling of COVID-19 cases

Eugenol targets matched to the single-Cell RNA sequencing dataset of Zhang et al., and the integrative analyses were performed in Metascape platform. Statistics of gene list involves 295 eugenol targets and the transcribed genes in immune cells (47 genes in Monocytes, 45 genes in nature killer cells, 81 genes in B- lymphocyte and 79 genes in T-lymphocytes) of severe COVID-19 cases (Fig. 5 A). The summarized results indicated that eugenol targets highly enriched in the pathways of neutrophil deregulation and cytokine signaling in immune system (Fig. 5 B). The results of BPs enrichment indicated eugenol targets extensively participated in multiple biological process and immune system process (Fig. 5C). Furthermore, the results of disease enrichment and the enrichment for specific organism or cell lines represented that eugenol can impact the processes of multiple human diseases, and poses biological actions on various organism and cell lines (Fig. 5 D and Fig. 5 E). The results of merged PPI network implicated that eugenol targets may play an important role in the hub pathways of COVID-19, including cellular response to stress, cellular response to the stimuli and cytokine singling in immune system (Fig. 5 F).

3.6. Eugenol induced transcription change verified by analyzing GSE171360

There is lack of genomics data about eugenol induced transcription change in animal models or cell lines. Therefore, the current

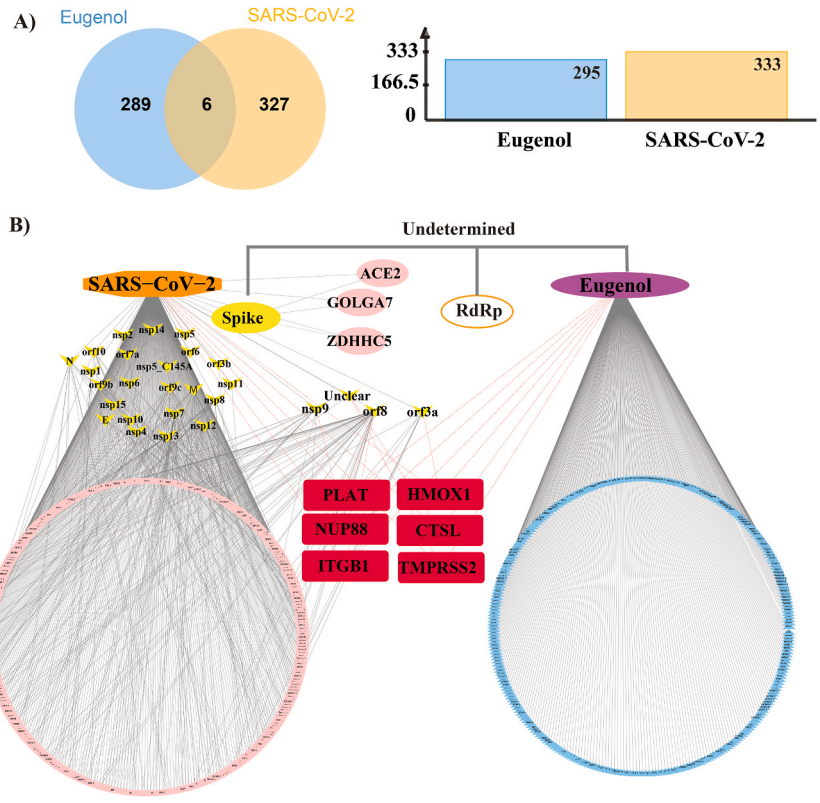

Fig. 4. Intersecting genes of eugenol targets and SARS-CoV-2 antigens. (A) Venn diagram depicts intersecting genes of eugenol and SARS-CoV-2 antigens. (B) Cytoscape depicts the network of SARS-CoV-2 antigens, SARS-CoV-2 interacting genes and eugenol targets. A total of six intersecting genes, including PLAT, HMOX1, NUP88, CTSL, ITGB1 and TMPRSS2 were obtained.

study selected GSE171360, a HepaRGTM Cell based transcriptomic dataset as the external verification of single analysis above. Three dose-gradients (C1:156.25 μM; C2: 312.5 μM; C3: 625 μM) were chosen, and C0 (baseline gene expression) was set as the control (Fig. 6 A). Results of immune cell infiltration analyses indicated that the transcribed genes highly enriched in macrophage ($P = 0.03$) only at the dose of 625 μM, there was no significant enrichment of that at the dose of 156.25 μM or 312.5 μM. The results suggest that eugenol is macrophage selective immunomodulatory compound, which may play a role in regulating macrophage activity (Fig. 6B). Additionally, the screening results represented that eugenol application induced deferential expression of 3, 26, 72 genes (Log FC > 1; adjusted P value < 0.05) at the dose of 156.25 μM, 312.5 μM and 625 μM respectively (Supplemental Tables 6–8). There is no intersection of SARS-CoV-2 targets and differentially expressed gene by eugenol at a dose of 156.25 μM. However, 3 intersected genes, including human scavenger receptor class B type I (SCARB1), heme oxygenase 1 (HMOX1/HO-1) and differentiation factor 15 (GDF15) were obtained at the doses of 312.5 μM or 625 μM. SCARB1and GDF15 genes were confirmed the regulators of high-density lipoprotein (HDL) metabolism to our knowledge [90–92] (Fig. 6C and Fig. 7).

Furthermore, functional roles of differentially expressed genes by eugenol in immune signaling of severe COVID-19 cases were investigated in Metascape. The results indicated that differentially expressed genes by eugenol at a dose of 312.5 μM and 625 μM significantly enriched in the BPs, including response to stimulus, cellular process, immune system process, metabolic process, and positive regulation of biological process. Pathways included neutrophil deregulation and cytokine signaling in immune system. The results of merged PPI network implicated the hub pathways, including protein processing in endoplasmic reticulum, neutrophil degranulation and cellular response to stress or stimuli (Fig. 8 A-F and Fig. 9A–F). These results suggests eugenol plays important roles in strengthen of immunologic functions, regulating inflammatory reaction.

3.7. Gene set enrichment analysis (GSEA) of eugenol induced deferentially expressed genes form GSE171360

Gene set enrichment analysis (GSEA) was performed in WebGestalt. The results indicated that there is no significant enrichments for differentially expressed genes by eugenol at the doses of 156.25 μM and 312.5 μM. At the doses of 625 μM, 72 differential expressed genes significantly enriched in the BPs, including lipid localization (Fig. 10 A and Fig. 10 B1), and establishment of organelle localization (Fig. 10 A and Fig. 10 B2). MF included monooxygenase activity (Fig. 10 A and Fig. 10C1), iron ion binding (Fig. 10 A and Fig. 10C2), and organic acid binding (Fig. 10 A and Fig. 10C3). The KEGG pathway included PPAR pathway signaling (Fig. 10 A and Fig. 10 D). The disease enrichment involved fatty liver, hepatitis and hepatic steatosis (Fig. 10 A and Fig. 10 E1-E3). Drug enrichment

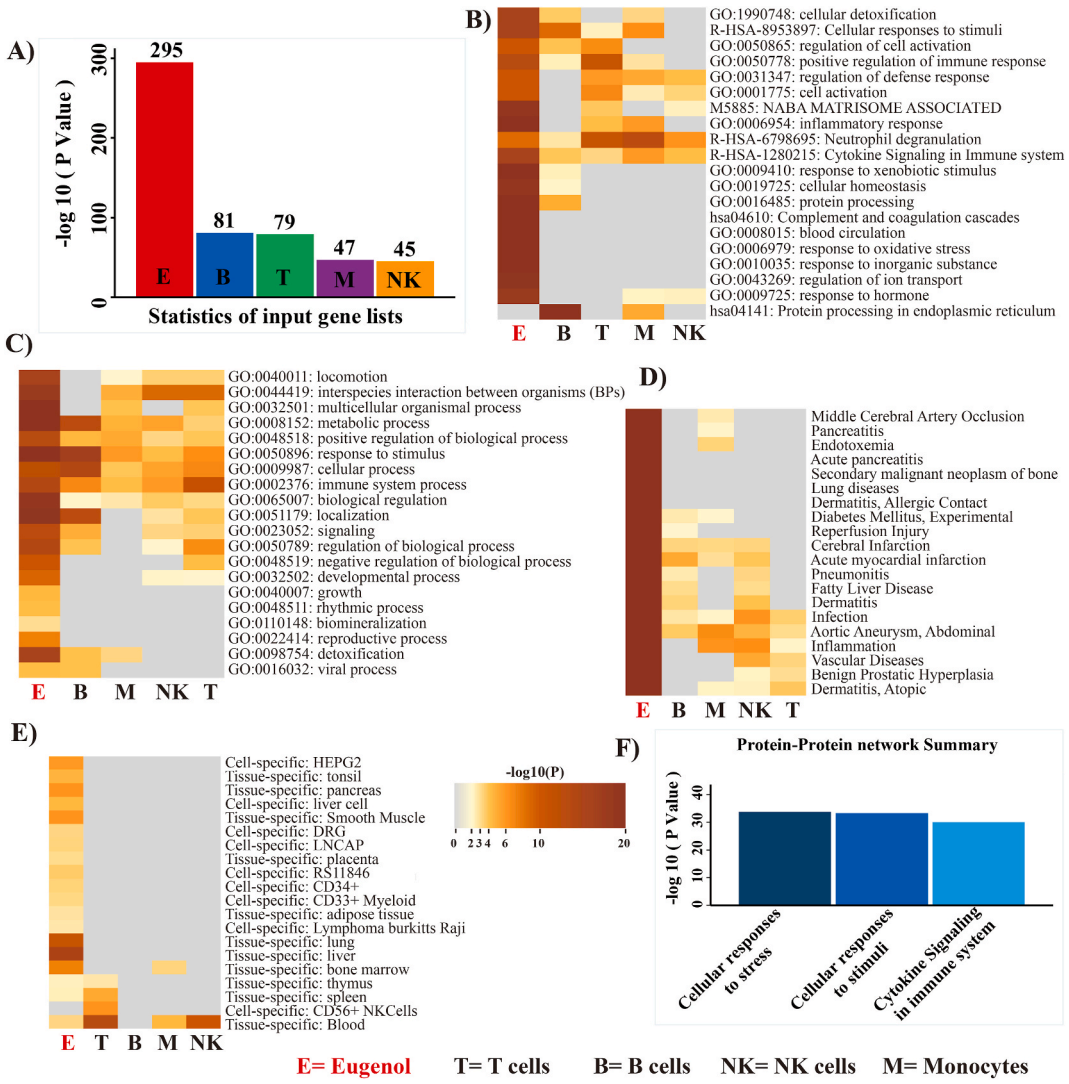

Fig. 5. Integrative analyses of the functional roles of 295 eugenol targets in transcriptomics of immune cells in COVID-19 cases. (A) Statistic input gene lists. (B) Heatmap of enriched terms across input gene lists, colored by P-values. (C) The top-level Gene Ontology biological processes. (D) Summary of enrichment analysis in DisGeNET. (E) Summary of enrichment analysis in PaGenBase. (F) Summary of Protein-Protein Interaction (PPI) enrichment analysis. Enriched terms were ranked with "Count" and "-log 10 (P-value)".

included central nervous system and nervous system (Fig. 10 A and Figure F1, F2).

3.8. Binding capacities of eugenol with the proteins of TLR-4/AP-1 axis and T cell receptor

Eugenol represented differential binding affinities with the TLR-4, JNK, NF-κB, AP-1 and T cell receptor (TCR) protein as a result of the formation of various hydrophilic and hydrophobic interactions. The pocket coordinates of active site _ x, y, z are listed in Table 1. Eugenol and TLR-4 formed two hydrophilic interactions, as TRP-256, ASP-209 and two Hydrogen bonds, as HIS-179, GLU-230 (Fig. 11 A). Eugenol and NF-κB formed one Hydrogen bond as DA17, and three hydrophilic interactions, including LYS218, PHE307 and DA17 (Fig. 11 B). Eugenol and JNK/MAPK formed seven hydrophilic interactions, as LEU206, ILE70, MET146, LEU206, ALA91, LEU148 and VAL196, while one Hydrogen bond as MET149 (Fig. 11C). Eugenol and AP-1 formed three hydrophilic interactions, including LEU71, ALA27 and PRO47, and two Hydrogen bond as THR48 and ALA27 (Fig. 11 D). Furthermore, eugenol and clone18 TCR formed five hydrophilic interactions, including MET48, ALA46, PRO46, VAL101 and ALA46, and three Hydrogen bond as ARG121, SER101 and PRO192 (Fig. 11 E). The binding energy of eugenol with TLR-4, NF-κB, JNK and AP-1 were listed in Table 2. These results showed high affinity of eugenol with the amino acids of these proteins, and further implicated that TLR-4/AP-1 axis and TCR were potential targets of eugenol.

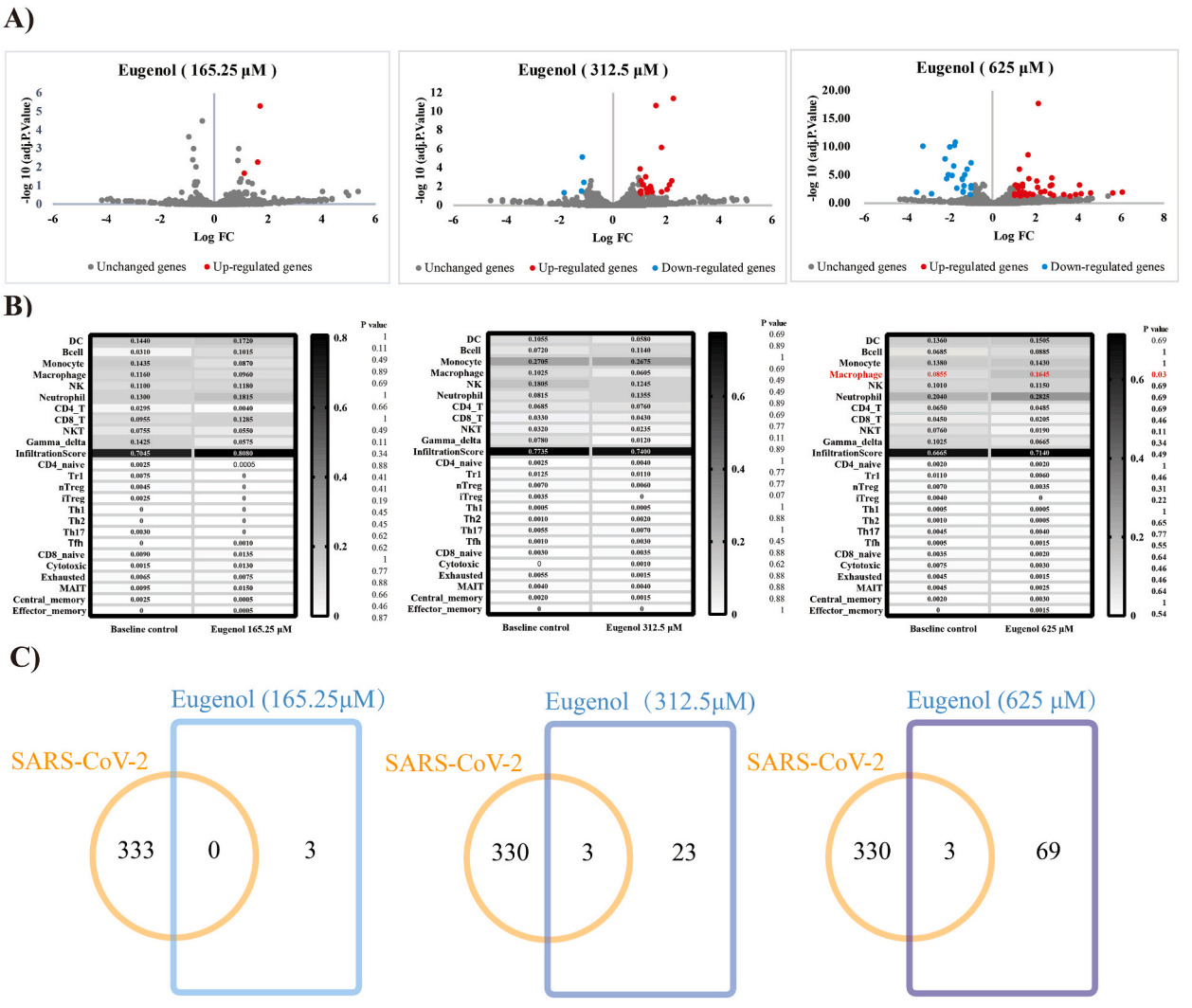

Fig. 6. External validation through analyzing GSE171360. Eugenol at the doses of 156.25 μM, 312.5 μM and 625 μM were selected for the screening and analyzing. Raw data were normalized with Log 2-counts per million, and parameters were set as Log 2 FC > 1 and adjusted P value < 0.05. (A) Volcano-plots represent differential gene expression induced by eugenol. (B) Immune cell infiltration analyses of transcriptional genes by eugenol. (C) Venn diagrams depict intersecting genes in eugenol/COVID-19. A P value < 0.05 indicates the statistical significance.

3.9. Binding capacity of eugenol to the SARS-CoV-2 spike protein-ACE2 complex and RdRp

We aimed at predicting the S protein-ACE2 complex without removing crystal structure of ACE2. For wild type S protein-ACE2 complex, one hydrogen bond between ASN-210 of complex and eugenol was observed. π-π interaction between VAL-209 and PRO-565, and the hydrophobic interaction between LEU-95 and eugenol were predicted (Fig. 12 A). The binding energy is −4.80 kcal/mol. For Omicron mutant S protein-ACE2 complex, the eugenol molecule forms two hydrogen bonds with the amino acid residue ASN-33 and GLN-96 respectively. Eugenol molecule forms π-π interaction with amino acid residue PRO-389, and the hydrophobic interaction is generated between amino acid residue PRO-389 and eugenol (Fig. 12 B). The binding energy is −4.3 kcal/mol. For SARS-CoV-2 RdRp without identification of finger subdomain, the two hydrogen bonds were predicted, as eugenol molecule forms hydrogen bond with the amino acid residue A-11 and ILE-589 respectively. Eugenol molecule forms π-π interaction with the amino acid residue PHE-812, whereas the hydrophobic interaction is generated between the amino acid residue ILE-589 and the eugenol (Fig. 12C). The binding energy is −5.42 kcal/mol. The pocket coordinates of active site _ x, y, z and interacting amino acids in the calculation were listed in Table 3 and Table 4.

Typically, the results of molecular docking implicated a potential affinity association between eugenol and the SARS-CoV-2 Spike-ACE2 complex, and SARS-CoV-2 RdRp. Nevertheless, molecular docking makes only primary opinion, while the molecular dynamics simulation makes the final prediction. Therefore, a further molecular dynamics simulation was conducted.

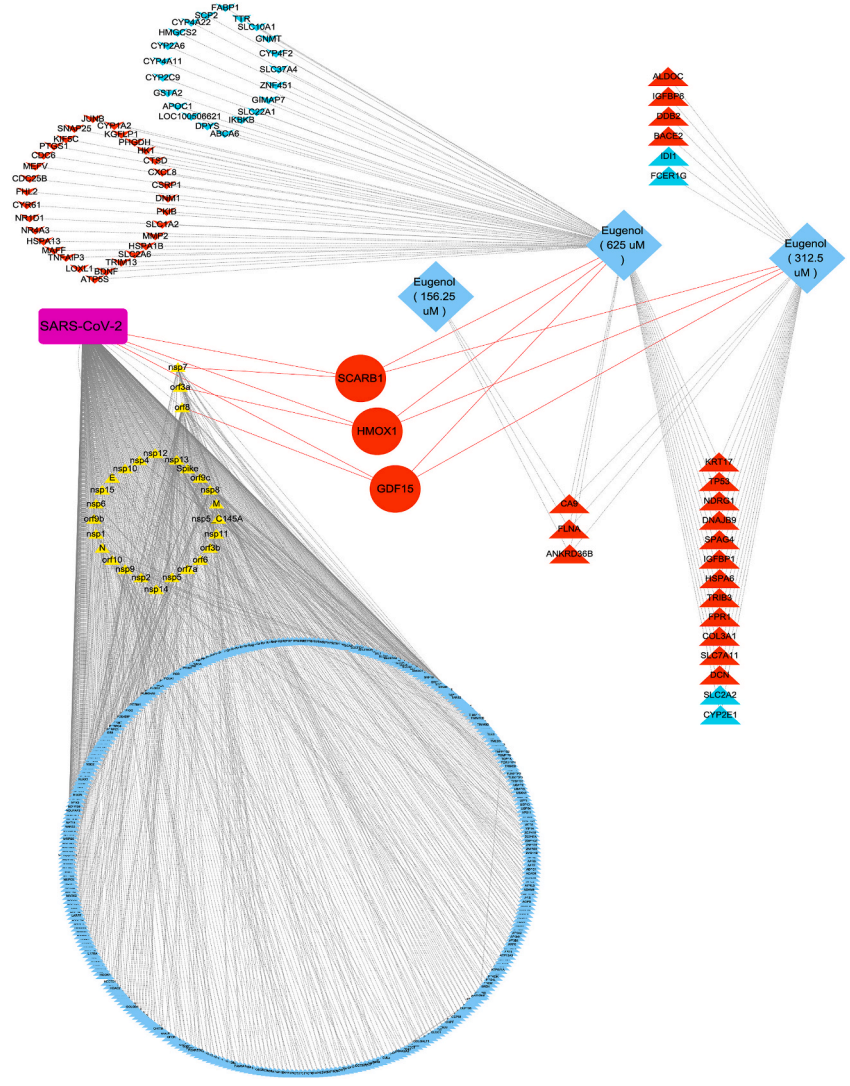

Fig. 7. Intersecting genes of differentially expressed genes by eugenol and COVID-19. Cytoscape depicts the network of SARS-CoV-2 antigens, SARS-CoV-2 interacting genes and eugenol induced differentially expressed genes. Yellow triangles demotes the SARS-CoV-2 antigens, Red triangles demote up-regulated genes by eugenol at corresponding doses, light blue triangles demote down-regulated genes by eugenol at corresponding doses, red ellipses denote the three interesting genes, including SCARB1, HMOX1 and GDF 15.

3.10. Molecular dynamics simulation of eugenol and SARS-CoV-2 spike protein-ACE2 complex without removing ACE2, and nonfinger subdomain of SARS-CoV-2 RdRp(100ns)

We performed molecular dynamics simulation of molecular conformation by 100 ns after molecular docking, then, small protein complexes in each molecular dynamics trajectory was analyzed with RMSD method, the results manifested that four RMSD reached to smooth and steady status. The complex and small molecules in molecular dynamics trajectory with 20–100 ns was in stable binding state. Therefore, we can sample and analyze the trajectories of 20–100ns (Fig. 13 A). Furthermore, we performed RMSF analyses to the proteins in the stabile trajectories. Compared with the RMSF value of SARS-CoV-2 RdRp-molnupiravir complex, the better RMSF value of SARS-CoV-2 RdRp-Eugenol complex was observed. The result suggested that the binding stabilization of eugenol to SARS-CoV-2 RdRp is more intension than that of molnupiravir. Identically, binding stabilization of eugenol to SARS-CoV-2 omicron spike protein-ACE2 complex is more intension than that of nilotinib (Fig. 13 B and Fig. 13C).

Furthermore, binding patterns of each complex before MD and after MD were obtained, and superimposition comparison and docking were visualized (Fig. 14 A, B for RdRp and Fig. 15 A, B for Omicron Spike-ACE2 complex). The results showed that there was little difference of binding position of eugenol or controls before and after simulation, which implicated that eugenol had bound to the corresponding pockets.

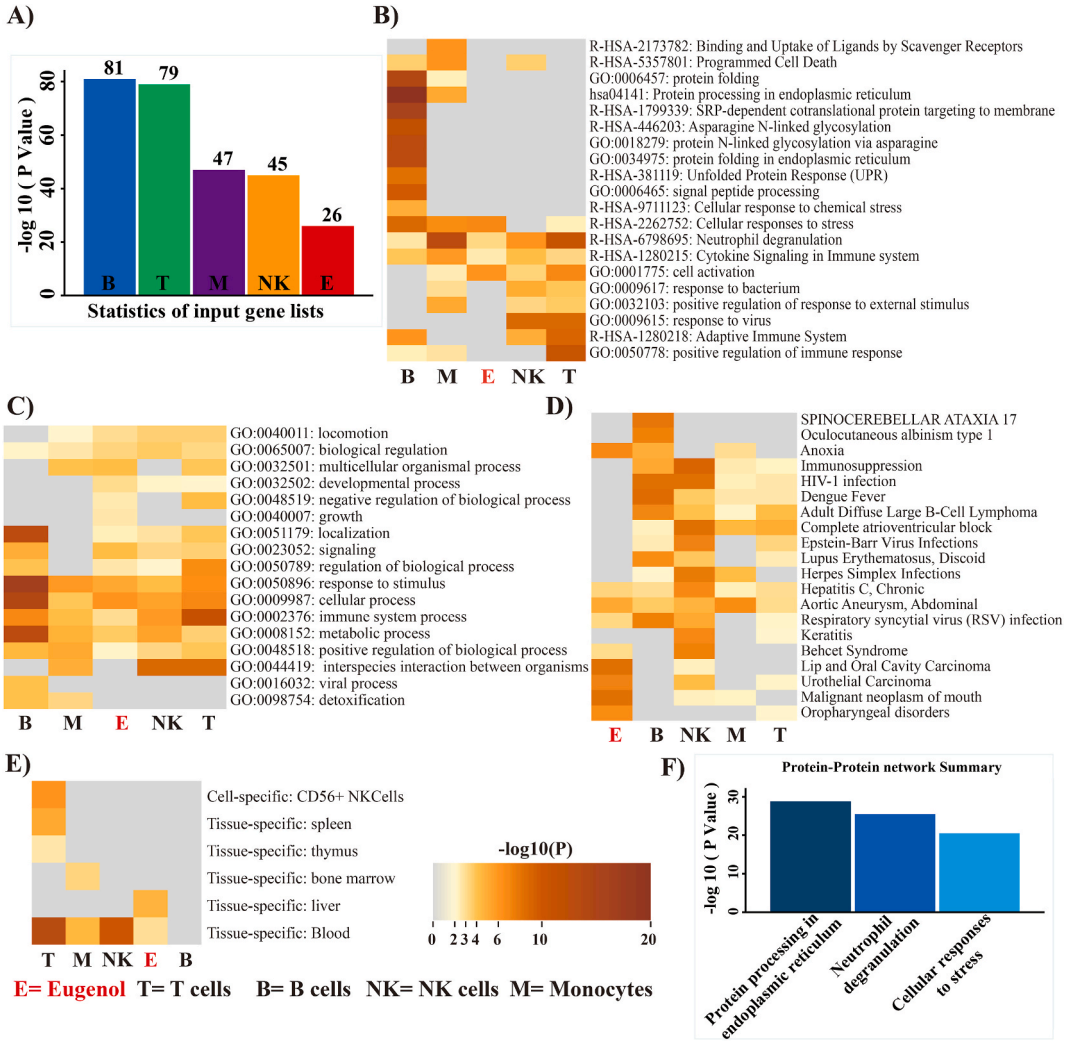

Fig. 8. Integrative analyses of the functional roles of 26 differentially expressed genes by eugenol (312.5 μM) in transcriptomics of immune cells in COVID-19 cases. (A) Statistic input gene lists. (B) Heatmap of enriched terms across input gene lists, colored by P-values. (C) The top-level Gene Ontology biological processes. (D) Summary of enrichment analysis in DisGeNET. (E) Summary of enrichment analysis in PaGenBase. (F) Summary of Protein-Protein Interaction (PPI) enrichment analysis. Enriched terms were ranked with "Count" and "-log 10 (P-value)".

3.11. Free energy calculations and residue decomposition between eugenol and SARS-CoV-2 omicron Spike-ACE2 complex, and SARS-CoV-2 RdRp

MMGBSA model was used to calculate the free energy calculations and residue decomposition of protein-small molecule complex, including SARS-CoV-2 RdRp-molnupiravir, SARS-CoV-2 RdRp-Eugenol, SARS-CoV-2 Omicron Spike-ACE2 complex-nilotinib and SARS-CoV-2 Omicron Spike protein-ACE2 complex-Eugenol. The results represent that the binding free energy were -23.15 ± 2.072, -24.93 ± 4.04, -23.016 ± 1.28, -27.31 ± 0.93 respectively, suggested that eugenol has the advantage of binding to the two SARS-CoV-2 virulence domains (Table 5 and Table 6). Meanwhile, in the interaction of RdRp-eugenol complex, SER-592 and LYS-593 more contributed to the binding free energy (Fig. 16 A, B and Table 7). In the interaction of Omicron Spike_protein-ACE2-eugenol complex, Pro389 has more contribution to the binding free energy (Fig. 16C, D and Table 7). These simulated results together with molecular docking analysis above implicated that eugenol might modify the structure of SARS-CoV-2 Omicron Spike-ACE2 complex, aiming at the region of ACE2, and RdRp, which may provide evidence for the subsequent investigation of structural modification of SARS-CoV-2 Omicron Spike-ACE2 complex by eugenol. However, the results were limited due to 100ns simulation and Spike protein was not estimated individually, as removing ACE2. Therefore, the following simulation with 200ns were performed, SARS-CoV-2/Omicron was set as the independent object, and a recommended finger subdomain of SARS-CoV-2 RdRp were used in simulation [56].

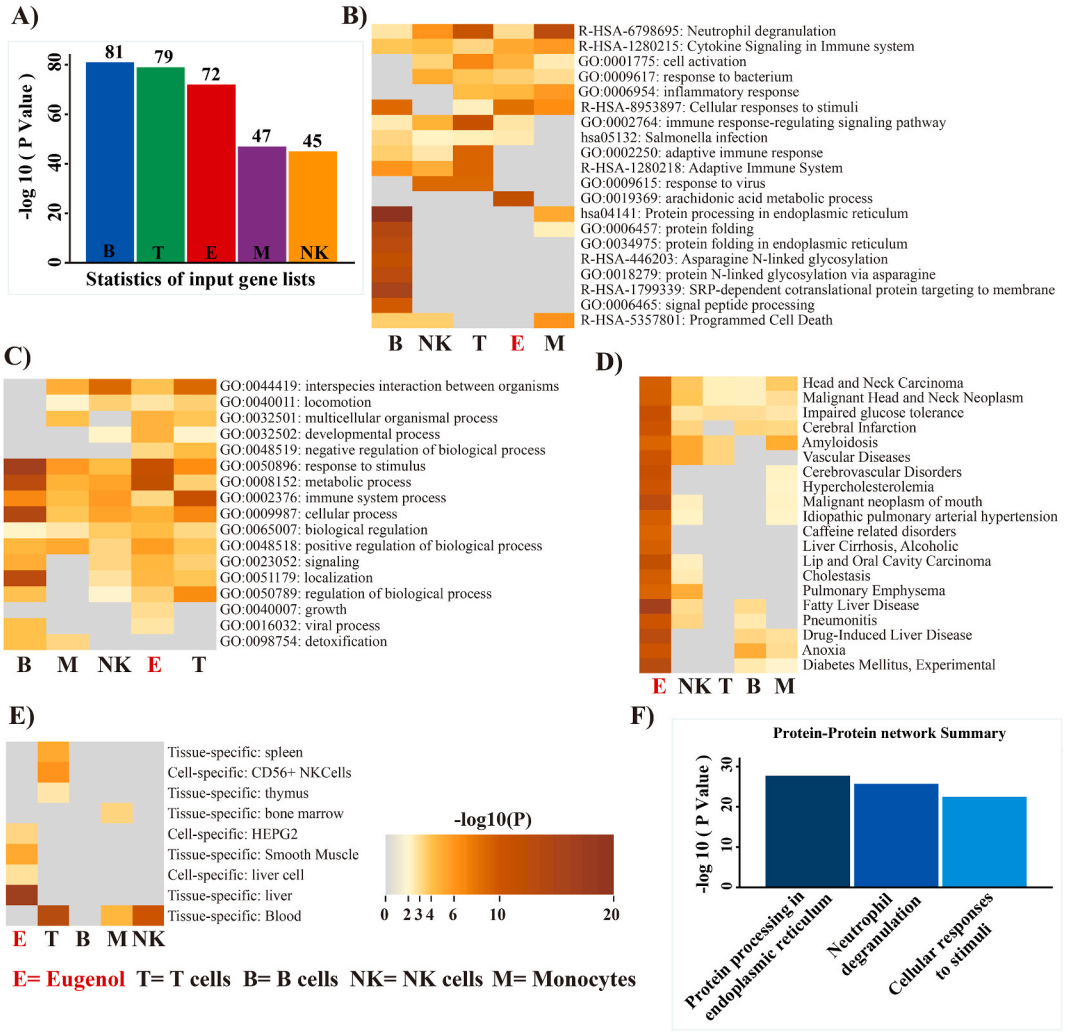

Fig. 9. Integrative analyses the functional roles of 72 differential expressed genes by eugenol (625 μM) in transcriptomics of immune cells in COVID cases. (A) Statistic input gene lists. (B) Heatmap of enriched terms across input gene lists, colored by P-values. (C) The top-level Gene Ontology biological processes. (D) Summary of enrichment analysis in DisGeNET. (E) Summary of enrichment analysis in PaGenBase. (F) Summary of Protein-Protein Interaction (PPI) enrichment analysis. Enriched terms were ranked with "Count" and "-log 10 (P-value)".

3.12. Binding capacity and stability of eugenol to SARS-CoV-2 Spike_RBD alone and finger subdomain of SARS-CoV-2 RdRp

In order to estimate the binding probability of eugenol to SARS-CoV-2 Spike_RBD alone, the human ACE2 was removed. Fig. 17A showed the eugenol bound to the surface of wt_spike protein interacting with ACE2 (−4.5 kcal/mol), hydrogen bounds were observed between eugenol and ASN-501, GLY-496 of S protein. Hydrophobic interactions were observed between eugenol and TYR-453, TYR-495 of S protein. Hydrogen bound is one of the most intensive noncovalent bonds known. Therefore, ASN-501 and GLY-496 contributed to the binding stability. Fig. 17B showed the eugenol bound to the surface of Omicron mutant Spike protein interacting with ACE2(−4.6 kcal/mol), eugenol generated a hydrogen bound to ARG-403 of Omicron mutant Spike protein_RBD, while hydrophobic interactions were observed between eugenol and TYR-453 of Omicron Spike protein_RBD. Similarly, ARG-403 contributed to the binding stability. Fig. 17C showed the eugenol bound to the finger subdomain of SARS-CoV-2 RdRp (−4.6 kcal/mol), two hydrogen bounds were generated between eugenol and ARG-553, ARG-624 of RdRp, nevertheless, no hydrophobic interactions were observed. ARG-553 and ARG-624 contributed to the binding stability of eugenol to finger subdomain of SARS-CoV-2 RdRp. The pocket coordinates of active site _ x, y, z in the calculation were listed in Table 8.

3.13. Molecular dynamics simulation of eugenol and SARS-CoV-2 spike RBD alone, and RdRp finger subdomain (200ns)

In order to estimate the interaction of eugenol to SARS-CoV-2 spike RBD alone, disregarding the hACE2, molecular dynamics simulation with 200ns was performed in addition to the results above. RMSD and RMSF can reflect the movement process of the

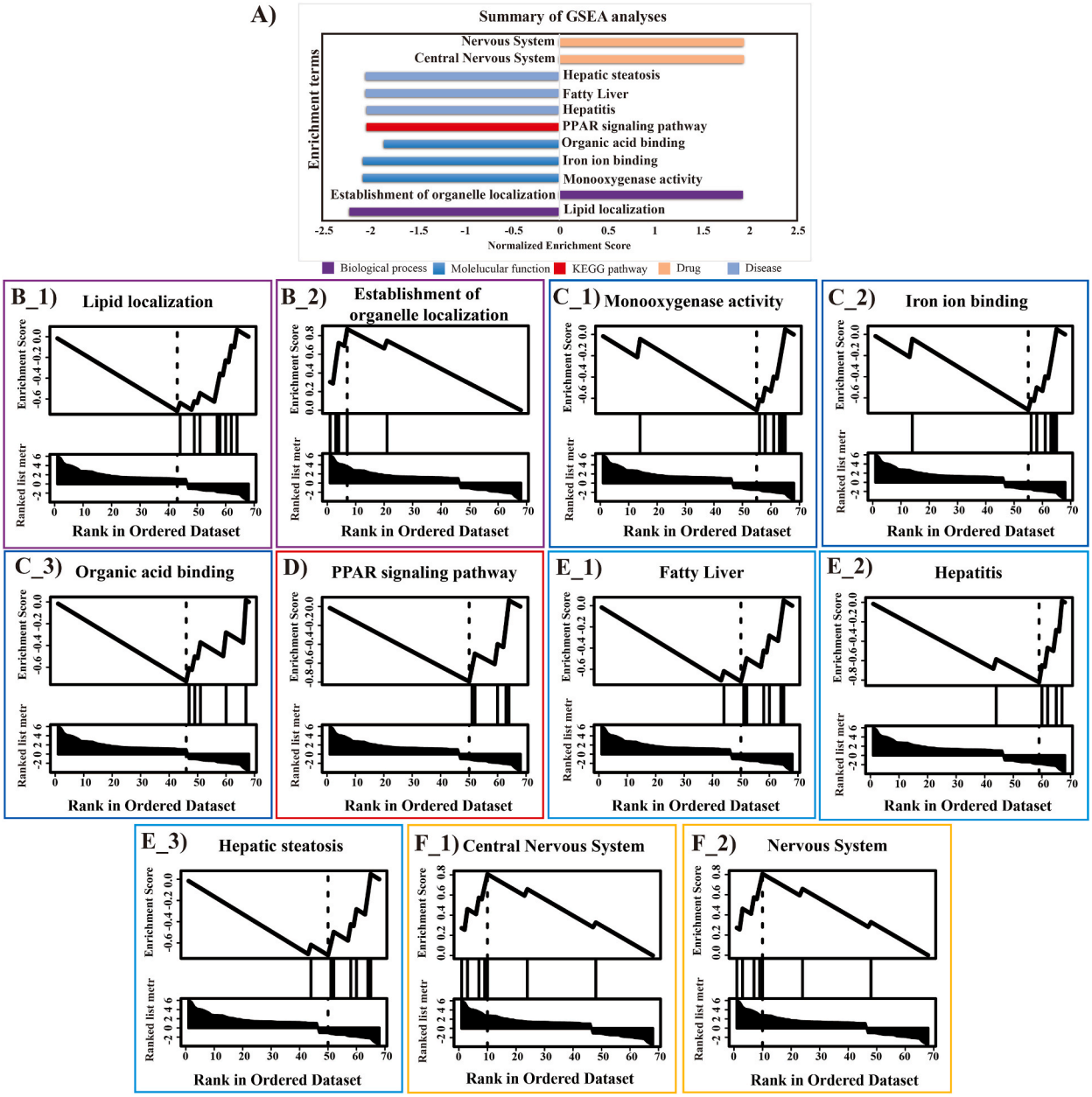

Fig. 10. Functional roles of eugenol induced deferentially expressed genes calculated with GSEA. The significant enrichments obtained from eugenol at a dose of 625 μM. (A) Summary of GSEA results. (B) Biological process. (C) Molecular function. (D) KEGG pathway. (F) Disease. (G) Pharmacological action.

Table 1
Molecular docking coordinates of eugenol with the human the proteins of TLR-4/AP-1 axis and TCR.

Proteins	x center	y center	z center	size_x	size_y	size_z
TLR-4	22.55	5.13	32.02	125	125	125
clone18 TCR	6.247000	−17.680500	6.740500	14.844000	15.252999	17.819000
NF-κB	68.365997	30.267501	25.716499	14.501999	16.655001	17.465000
JNK/MAPK	−0.406000	−1.293000	−29.791501	16.020000	15.084000	17.829000
AP-1	−121.043503	27.370000	15.220000	12.598999	16.822001	18.560000

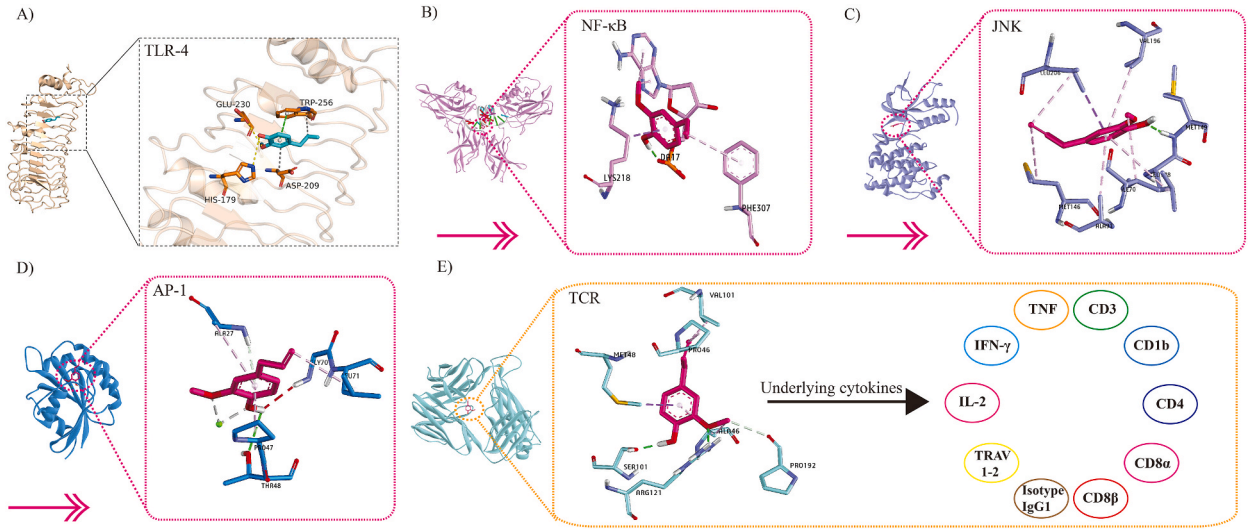

Fig. 11. Molecular docking analysis indicates high-affinity association between eugenol and TLR-4/NF-κB/JNK(MAPK)/AP-1 axis and T cell receptor. (A) Structural interaction of eugenol with TLR-4 (PDB ID: 2z63). (B) Structural interaction of eugenol with NF-κB (PDB ID:1le5). (C) Structural interaction of eugenol with JNK/MAPK (PDB ID: 30xi). (D) Structural interaction of eugenol with AP-1(PDB ID: 4hmy). (E) Structural interaction of eugenol with TCR(PDB ID: 4g8e).

Table 2
Binding energy and interacting amino acids of eugenol with the human the proteins of TLR-4/AP-1 axis and TCR.

Proteins	PDB code	Chemical	Pubchem code	Binding energy (kcal•mol^{-1})	Interactions	Category
TLR-4	2Z65	Eugenol	3314	−5.1 kcal/mol	TRP-256, ASP-209	Hydrophobic interactions
					HIS-179,GLU-230	Hydrogen bonds
					TRP-256	Pi stacks
clone18 TCR	4g8e	Eugenol	3314	−6.98 kcal/mol	ARG121, SER101, PRO192	Hydrogen Bond
					MET48, ALA46, PRO46, VAL101, ALA46	Hydrophobic interactions
NF-κB	1le5	Eugenol	3314	−5.61 kcal/mol	DA17:OP2	Hydrogen bonds
					LYS218, PHE307, DA17	Hydrophobic interactions
JNK/MAPK	30xi	Eugenol	3314	−7.06 kcal/mol	MET149	Hydrogen bonds
					LEU206, ILE70, MET146, LEU206, ALA91, LEU148, VAL196	Hydrophobic interactions
AP-1	4hmy	Eugenol	3314	−6.38 kcal/mol	THR48, ALA27	Hydrogen Bonds
					LEU71, ALA27, PRO47	Hydrophobic interactions
					MG1002	Other (Metal-Acceptor)

complex, higher RMSD value and violent fluctuation as higher RMSF value implicate unstable movement of the complex. In the current results, RBD_WT/Eugenol complex manifested higher RMSD and RMSF values than RBD_WT/Nilotinib. This means RBD_WT/Eugenol was less well than RBD_WT/Nilotinib (Fig. 18A). In the RBD_Omicron system, either RBD_Omicron/eugenol or RBD_Omicron/nilotinib system were stable in middle-later simulation phase, this implicated that the two system both can exist steadily (Fig. 18 B). For RdRp finger subdomain of SARS-CoV-2, RMSD value of Eugenol/RdRp complex outdistanced molnupiravir/RdRp complex. This implicated Eugenol/RdRp complex is more stable and effective than molnupiravir in these aspects (Fig. 18C). Furthermore, RMSF also reflected the protein flexibility during the process of molecular dynamics simulation. Generally, protein flexibility is changed and enzyme activity is generated when small molecule drug combined to target protein. There were no significant differences of RMSF values for eugenol and two positive control, molnupiravir and nilotinib (Table 9). These aspects means effects of eugenol on protein flexibility of SARS-CoV-2 were the same as the two positive controls, eugenol might exert similar biological actions as molnupiravir and nilotinib (Fig. 18D–F).

MM-GBSA method was used to calculate the binding energy of complexes, which provided more precise the binding efficacy of small molecules and target proteins, the results implicated that the free energy of RBD-wt/Eugenol, RBD-wt/Nilotinib, RDRP/Eugenol, RDRP/molnupiravir, RBD-Omicron/Eugenol, RBD-Omicron/Nilotinib were −8.1363, −23.1307, −16.9318, −9.5256, −10.5605,

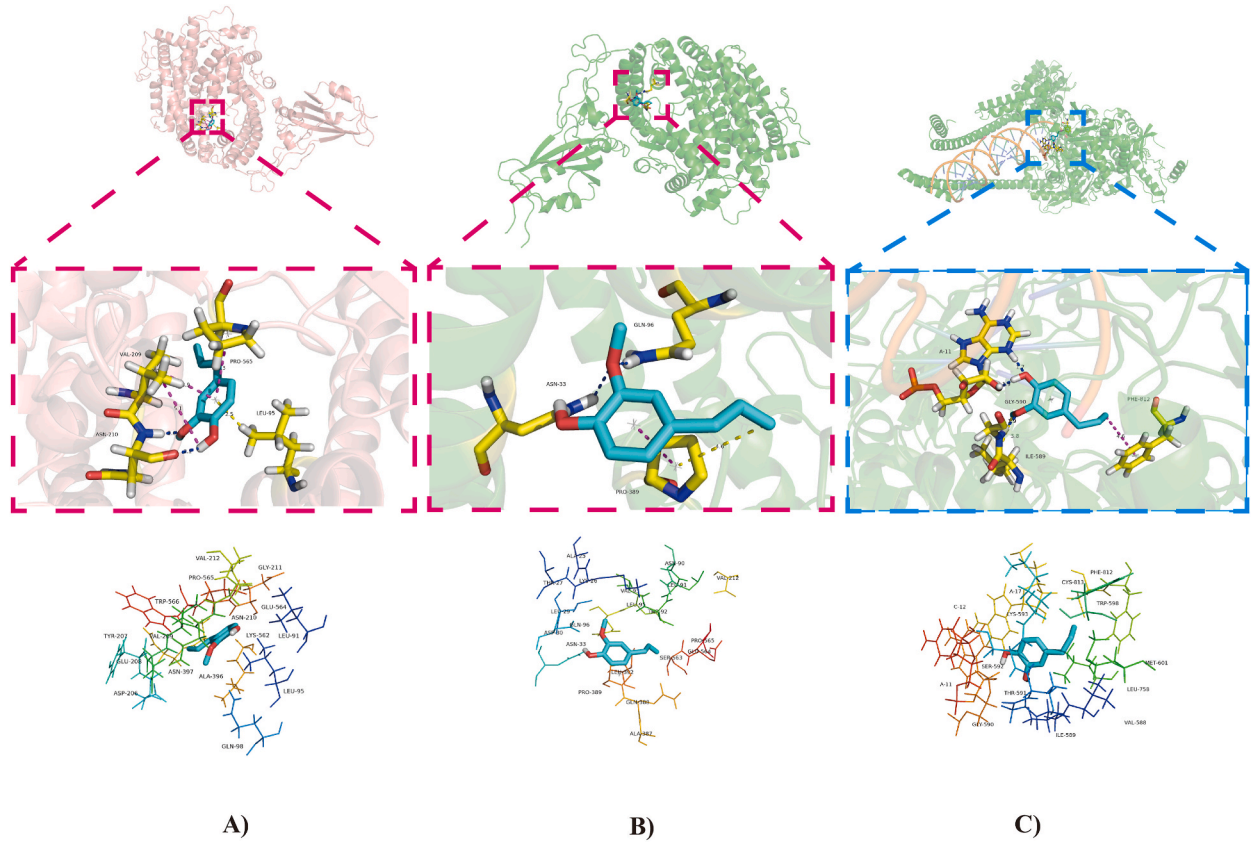

Fig. 12. Molecular docking analysis indicates high-affinity association between eugenol and the pathogenic components of SARS-CoV-2. (A) Structural interaction of eugenol with earlier SARS-CoV-2 spike protein in complex with human ACE2 (PDB ID: 6M0J). (B) Structural interaction of eugenol with SARS-CoV-2 Omicron spike protein in complex with human ACE2 (PDB ID: 7T9L). (C) Structural interaction of eugenol with SARS-CoV-2 replicating SARS-CoV-2 polymerase (PDB ID: 6YYT), the blue dotted line demotes the hydrogen bond, pink dotted line indicates the π-π interaction of molecules, and yellow dotted line demotes the hydrophobic interaction.

Table 3
The coordinates of grid box for the SARS-CoV-2/Omicron spike protein-ACE2 complex, RdRp.

Proteins	x center	y center	z center
SARS-CoV-2 Spike-ACE2 complex (6M0J)	−20.499923	35.220462	−15.917385
SARS-CoV-2 Omicron Spike-ACE2 complex (7T9L)	217.362	178.068	259.800
SARS-CoV-2 RNA dependent RNA Polymerase (6YYT)	84.881	92.002	99.408

Table 4
Molecular docking results of eugenol with SARSCoV-2/Omicron spike protein-ACE2 complex, RdRp.

Proteins	Chemical	Interacting residues	Type of interaction bond	Binding energy (kcal•mol^{-1})
6M0J (Complex)	Eugenol	ASN-210 VAL-209; PRO-565 LEU-95	hydrogen bond π-π interaction hydrophobic interaction	−4.80 kcal/mol
7T9L (Complex)	Eugenol	ASN-33; GLN-96 PRO-389 PRO-389	hydrogen bond π-π interaction hydrophobic interaction	−4.3 kcal/mol
6YYT (Complex)	Eugenol	A-11; ILE-589 PHE-812 ILE-589	hydrogen bond π-π interaction hydrophobic interaction	−5.42 kcal/mol

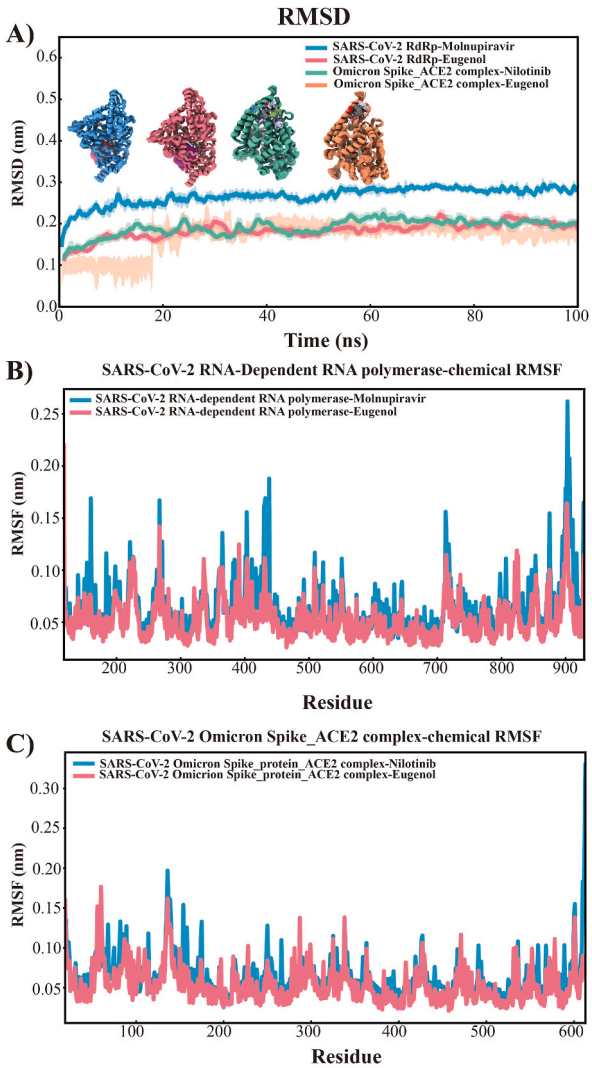

Fig. 13. Molecular dynamics simulation (100ns). (A) Trajectory RMSD analysis with 100ns using Gromacs2021.3 RSMF analysis for stable trajectory. (B) Comparison between SARS-CoV-2 RdRp-molnupiravir complex and SARS-CoV-2 RdRp-eugenol complex. (C) Comparison between SARS-CoV-2 omicron spike-ACE2 complex-nilotinib and SARS-CoV-2 omicron spike-ACE2 complex-eugenol.

−23.0234 kcal/mol respectively (Table 10). The results implicated that eugenol had a higher affinity with finger subdomain of SARS-CoV-2 RdRp than molnupiravir, whereas, these results were accorded to the finding of simulation with 100ns. Furthermore, referring to the results of energy decomposition, Van der waals energy and electrostatic energy were considered the major contributors. Meanwhile, binding patterns of each complex before MD and after MD were obtained, and superimposition comparison was performed. Significantly, there is little difference of binding position of eugenol or controls before and after simulation, which implicated that eugenol had bound to the corresponding pockets (Fig. 19A–F). Due to little change in the position of Eugenol/RBD-wt, Eugenol/RdRp, Eugenol/RBD-Omicron complex before/after simulation, we considered that some docking amino acids might possess important effects on SARS-CoV-2 invasion and proliferation (Table 11).

3.14. Sequence discrepancy between RBD_WT and RBD_Omicron of SARS-CoV-2 spike

The result of sequence alignment showed the identity of RBD_WT and RBD_Omicron of SARS-CoV-2 was 92.27%, there were frequent mutations of amino acids in RBD_Omicron of SARS-CoV-2 spike. Importantly, more frequent mutations were observed in the active sequence of Omicron S protein RBD which interacted with hACE2, as AG … YQ (AGSTPCNGVEGFNCYFPLQSYGFQPTNGV-GYQ. Therefore, the mutations of SARS-CoV-2 lead to the change of interacting pattern of S protein RBD with hACE2 (Fig. 20).

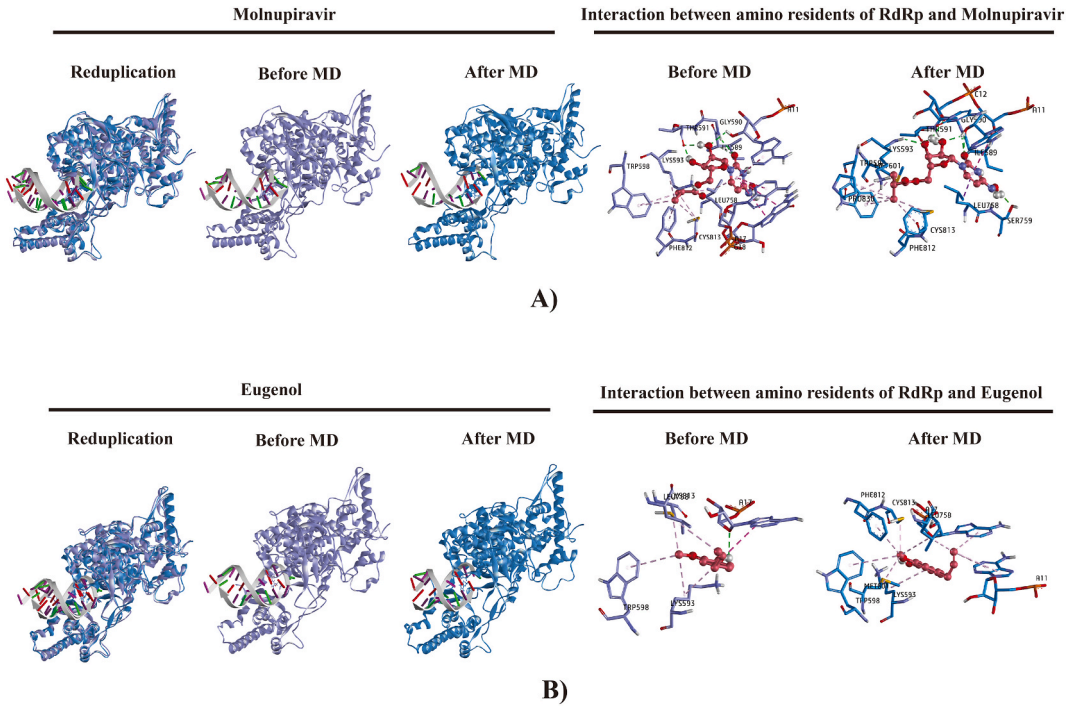

Fig. 14. Conformational change of SARS-CoV-2 RdRp-eugenol complex before MD and after MD. (A) SARS-CoV-2 RdRp-molnupiravir complex (Control). (B) SARS-CoV-2 RdRp-eugenol complex.

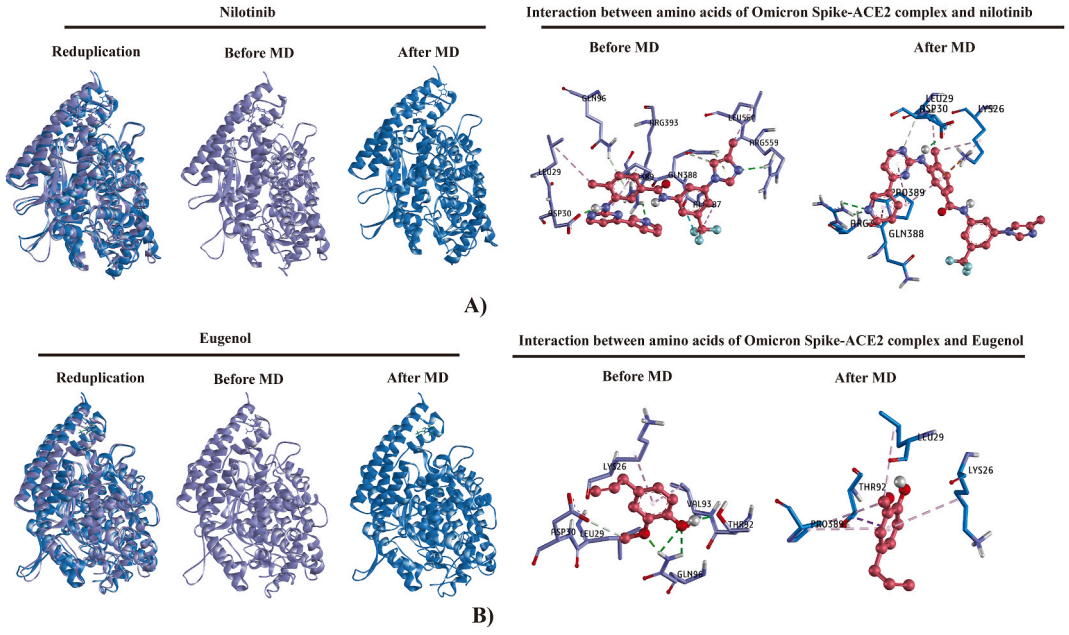

Fig. 15. Conformational change of SARS-CoV-2 Omicron Spike-ACE2 complex before MD and after MD. (A) SARS-CoV-2 Spike-ACE2 complex-nilotinib (Control). (B) SARS-CoV-2 Spike-ACE2 complex-eugenol.

3.15. Comparison of physicochemical properties of chemicals

As SARS-CoV-2 infection leads to neuronal damage, small molecule drugs with activity of blood-brain barrier (BBB) permeant are essential for neuron protection [93,94]. The aiming chemical, eugenol (164.20 g/mol) has a lower molecular weight than molnupiravir (329.31 g/mol) and nilotinib (529.52 g/mol). The lipophilicity of eugenol is higher than molnupiravir and lower than nilotinib.

Table 5
Free energy calculations of SARS-CoV-2 RdRp-Eugenol complex, comparing with SARS-CoV-2 RdRp-Molnupiravir complex.

Energy Component	Polymerase-Molnupiravir		Polymerase-Eugenol	
	Average	SD (Prop.)	Average	SD (Prop.)
VDWAALS	−23.2712	0.535132	−33.2167	0.480432
EEL	−15.9719	1.821813	−6.86507	3.937915
EGB	19.06847	0.830386	19.03201	0.774748
ESURF	−2.97655	0.010182	−3.8803	0.006841
GGAS	−39.2431	1.898781	−40.0818	3.967114
GSOLV	16.09192	0.830448	15.15171	0.774778
TOTAL	**−23.1512**	**2.072441**	**−24.93**	**4.042063**

Table 6
Free energy calculations of Spike_protein-ACE2 complex-Eugenol, comparing with Spike_protein-ACE2 complex-Nilotinib.

Energy Component	Spike_protein-Nilotinib		Spike_protein-Eugenol	
	Average	SD (Prop.)	Average	SD (Prop.)
VDWAALS	−17.196794	0.405644	−38.0702	0.881745
EEL	−11.9901885	1.199514	−17.9769	0.17159
EGB	13.835786	0.151878	33.11289	0.242749
ESURF	−7.664767686	0.021543	−4.37811	0.014622
GGAS	−29.1869825	1.266247	−56.0471	0.898286
GSOLV	6.171018314	0.153398	28.73478	0.243189
TOTAL	**−23.01596419**	**1.275504**	**−27.3123**	**0.930622**

Eugenol and molnupiravir were classified as the soluble chemicals in water, nilotinib as the innsoluble chemical. GI absorption of eugenol is better than molnupiravir and nilotinib, more importantly, eugenol can pass through the blood-brain barrier (BBB), whereas molnupiravir and nilotinib cannot. Summarized physicochemical properties of chemicals were listed in Supplementary Table 9. These results implicated that eugenol has good physicochemical properties.

3.16. Aberration and toxic properties of eugenol, molnupiravir and nilotinib

The results manifested that the predicted LD50 for eugenol was 1930 mg/kg (Fig. 21 A), with 100% prediction accuracy, while the predicted LD50 for molnupiravir and nilotinib were 826 mg/kg and 800 mg/kg respectively (Fig. 21B and C). Nevertheless, the prediction accuracy of LD50 for the two chemicals were relatively low, as 69.26% and 54.26%. A further toxicity model reports manifested that eugenol was not associated with significant aberration and toxic properties in spite of slight effect on the liver (67%). Molnupiravir was predicted to be associated with hepatotoxicity (56%), and low affinity to carcinogenicity (50%) and mutagenicity (53%). Nilotinib was predicted to be associated with hepatotoxicity (82%) and carcinogenicity (53%), immunotoxicity (98%) (Fig. 21D). Taken these results, eugenol is considered as safe chemical, the calculated results for molnupiravir and nilotinib were undetermined due to the limited prediction percentage. Immunotoxicity and hepatotoxicity with higher prediction percentage should be attached importance to nilotinib.

4. Discussion

Development of COVID drugs have two major aspects, the immune regulatory effects of the drug or as an inhibitor of the virus. In response to unceasing variation of SARS-CoV-2, investigating more pan-corona antiviral reagents are essential. This work comprehensively studied the interaction of eugenol to major targets of inflammatory activation, and the binding potential of eugenol to the virus. In single analysis/network pharmacology, the results suggest that eugenol can target multiple core genes for SARS-CoV-2 entry, which is beneficial for contracting immunopathological injury, regulating macrophage activity and cytokine signaling. Further genomics validation were applied to analyze GSE171360, the methods involved screening different genes, immune infiltration analysis and GSEA analyses. The results implicated eugenol can impact multiple biological processes and the pathway relating to lipid metabolism and neuroinvasion of SARS-CoV-2. Eugenol also increased the transcription of antioxidant HMOX1, SCARB1 and GDF15, which were identified important regulator of inflammation, macrophage activity, and served as a hub gene of COVID-19 according to the literatures [85,86]. The author further found that eugenol interacted with human TCR, TLR-4 and three downstream molecules (NF-κB, JNK and AP-1). NF-κB, JNK/MAPK and AP-1were confirmed the upstream signaling of human TLR-4, which contributes to the mechanism of regulating and facilitating the inflammatory cytokine production. Activation of human TLR-4/AP-1 axis promoted the release of interleukin-1β (IL-1β), interleukin-6 (IL-6), and tumor necrosis factor-α (TNF-α) [52]. Furthermore, the molecular dynamics simulation revealed that the binding capacity and stability of eugenol to SARS-CoV-2 RdRp and its finger subdomain, and the modificatory action of eugenol on SARS-CoV-2 Omicron Spike-ACE2 complex, were no less favorable than two positive controls, molnupiravir and nilotinib. The binding capacity and stability of eugenol to SARS-CoV-2/Omicron Spike RBD alone was less than nilotinib. Eugenol was predicted with lower cytotoxicity compared to molnupiravir and nilotinib, and it can pass through the BBB.

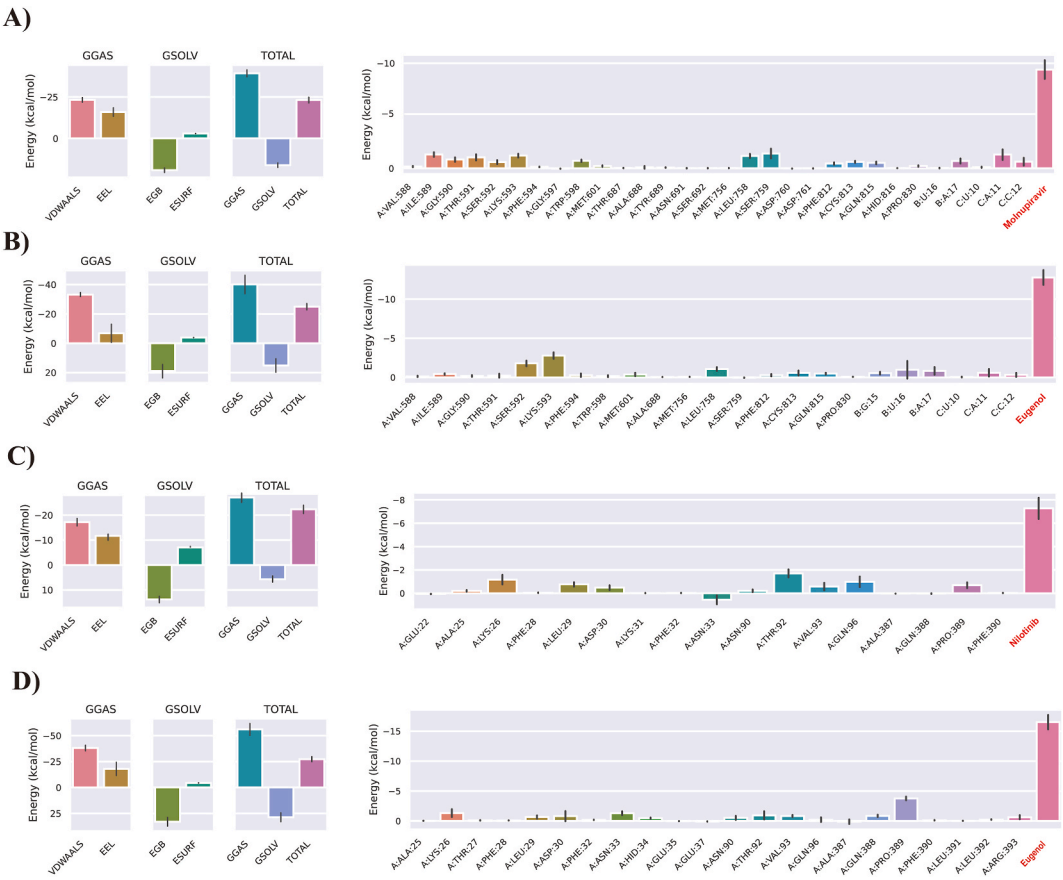

Fig. 16. Free energy calculations and residue decomposition employing the MM-GBSA method. The energy set, including VDWAALS, EEL, EGB, ESURF, GGAS and GSOLV, were estimated. (A) Comparison between SARS-CoV-2 RNA dependent RNA polymerase-molnupiravir complex and SARS-CoV-2 RNA dependent RNA polymerase-eugenol complex. (B) Comparison between SARS-CoV-2 Omicron spike-ACE2 complex-nilotinib and SARS-CoV-2 Omicron spike-ACE2 complex-eugenol. Units of energy are defined as kacl/mol. SER-592 and LYS-593 poses more contributions of binding free energy in SARS-CoV-2 RNA dependent RNA polymerase-eugenol interactions, whereas, Pro389 poses more contributions of binding free energy in SARS-CoV-2 Omicron spike-ACE2 complex -eugenol interactions.

Table 7
Interacting amino acids of small molecular eugenol and SARS-CoV-2.

System	hydrophobic_interactions	Hydrogen_bonds
SRS-CoV-2 RdRp-Eugenol	A17, A11, LYS593, CYS813, LEU758, TRP598, PHE812, MET 601	LYS 593, A17: O4′
SARS-CoV-2 Omicron Spike-ACE2 complex-Eugenol	PRO389, LEU29, LYS26, VAL93	GLN96, THR92: OG1, ASP30:OD1

The chemical eugenol (4-allyl-2-methoxyphenol, C10H12O2) as the major volatile, biologically active component of clove oil, has been widely used in food, cosmetics and pharmaceuticals. Eugenol was recognized as a safe chemical without DNA strand break activity and had not listed as environmental pollutant [95]. Generally, eugenol avoids mosquito bites, survives the test of time in dental medicine [96,97]. Recent studies confirmed that eugenol significantly inhibited a variety of bacteria, including proliferating pathogenic fungi, staphylococcus aureus, shigella, mycobacterium tuberculosis, bacillus proteus and escherichia coli [35]. Hereof, eugenol and its derivatives are the source of Isoniazid [98]. Historically, eugenol exerts anesthetic activity, acts as a positive allosteric modulators of the γ-aminobutyric acid (GABA)-A receptor, and possesses neuroprotective and radio-protective effects in experimental models [99–102]. Eugenol also attenuated TiO2 nanoparticles-induced DNA damage and H2O2-mediated oxidative stress in HUVECs [103,104]. An aspirin-eugenol eater (AEE) reducedformation of thrombosis in a rat tail thrombosis model [105]. In vivo studies revealed that eugenol generated various biological effects including anti-oxidant, anti-mutagenic, anti-genotoxic and anti-cancer capacities [106–109]. Therefore, eugenol was recommended to clinicians for treating inflammatory diseases and some chronic diseases [109,110] (Therapeutic effects of eugenol was listed in Fig. 22 according to the literature).

SARS-CoV-2 infection cause a series of immune-mediated complications and neurologic sequela, including systemic inflammatory

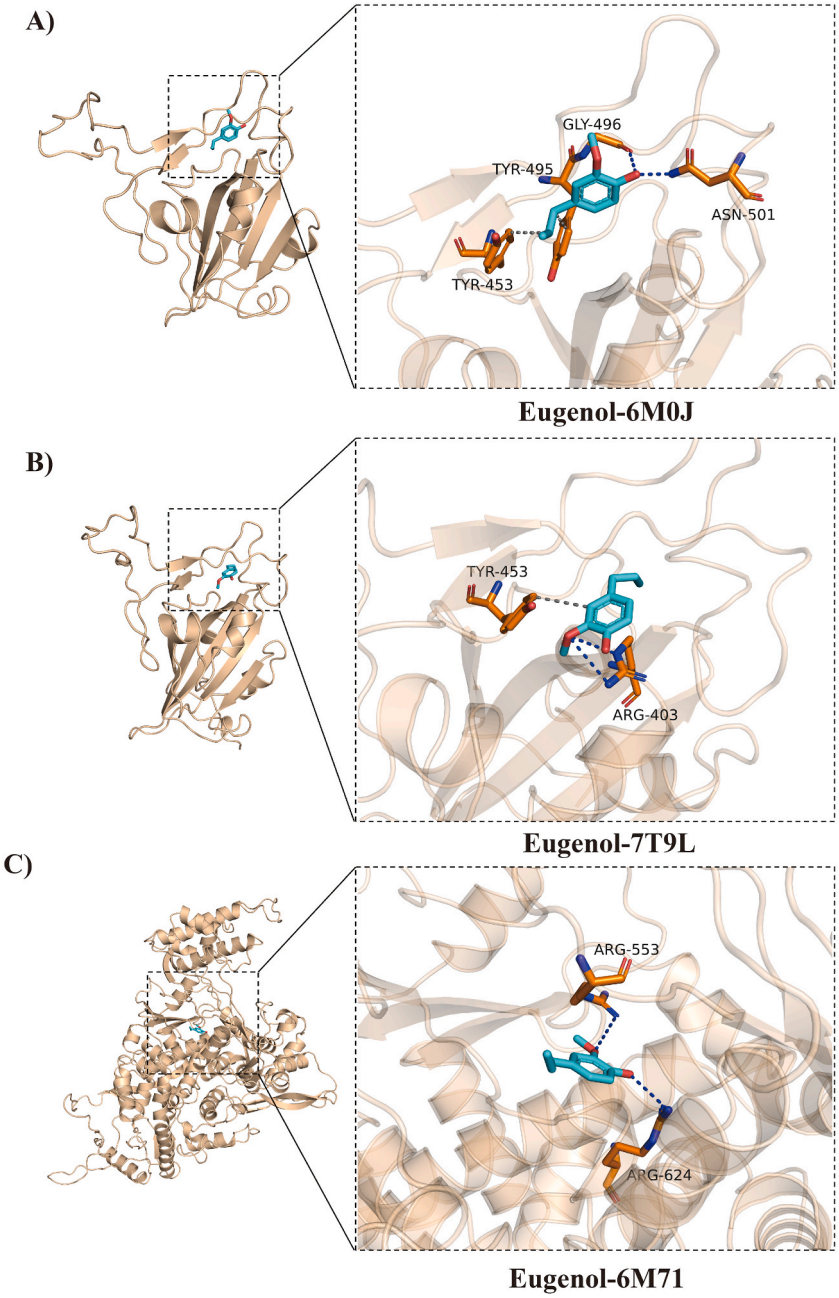

Fig. 17. Molecular docking analysis indicates moderate-affinity association between eugenol and SARS-CoV-2 Spike_RBD and finger subdomain of SARS-CoV-2 RdRp.(A) Structural interaction of eugenol with SARS-CoV-2 wild type Spike RBD (6M0J), removing human ACE2.(B) Structural interaction of eugenol with SARS-CoV-2 Omicron mutant Spike RBD (7T9L), removing human ACE2.(C) Structural interaction of eugenol with finger subdomain of SARS-CoV-2 RdRp (6M71).

Table 8
Molecular docking coordinates of eugenol with SARS-CoV-2 wild type/Omicron Spike RBD and finger subdomain of RdRp.

Proteins	x center	y center	z center	size_x	size_y	size_z
Wild type Spike RBD without ACE2 (6M0J)	−34.13	28.75	8.17	25	25	25
Omicron Spike RBD without ACE2 (7T9L)	228.32	173.83	256.78	25	25	25
Finger subdomain of RdRp (6M71)	122.01	115.50	133.25	22.5	22.5	22.5

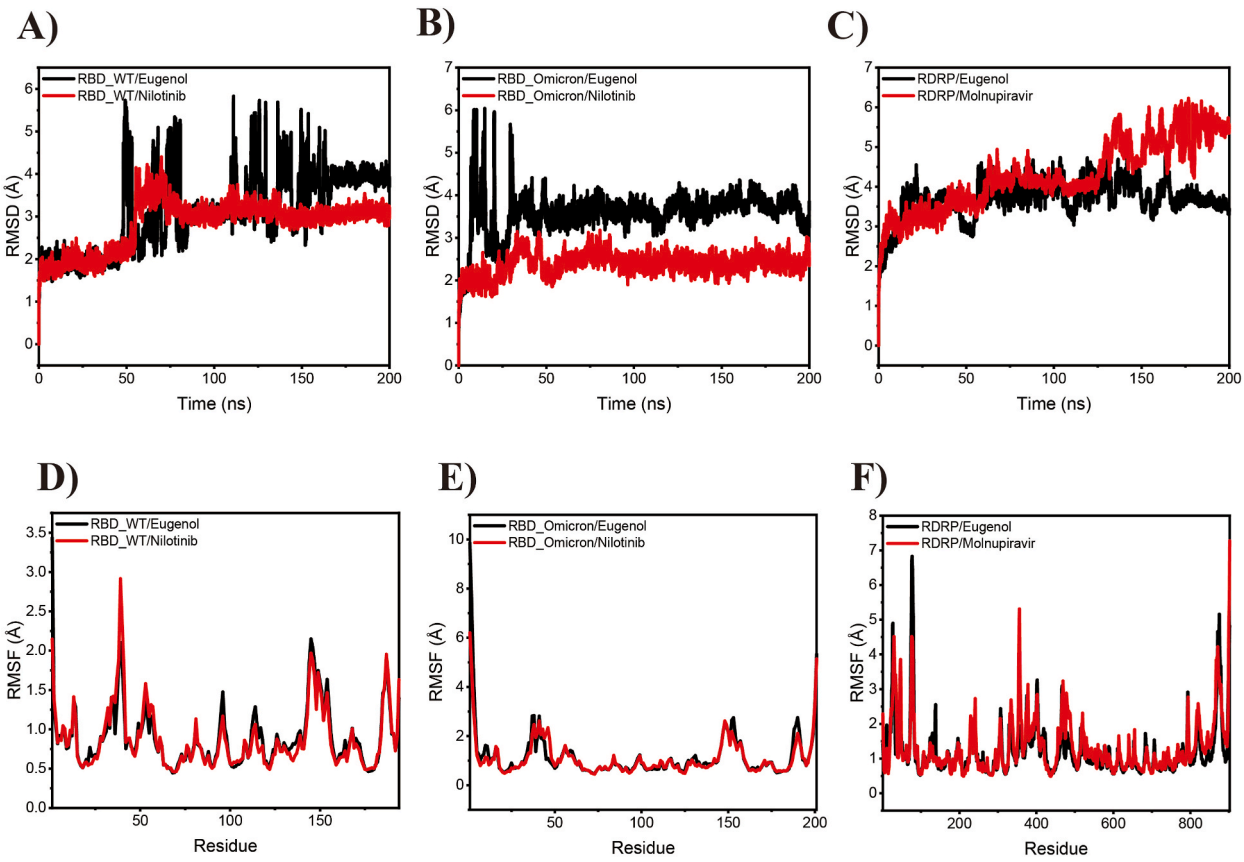

Fig. 18. Trajectory RMSD and RMSF analysis indicated eugenol exerted similar biological activity as two positive controls, and eugenol-SARS-CoV-2 RdRp presented better stability as molnupiravir. The stability of eugenol-SARS-CoV-2 wt/Omicron mutant Spike RBD complex was less stability than nilotinib. (A) RMSD of eugenol/nilotinib- SARS-CoV-2 wt Spike RBD complex (200ns). (B) RMSD of eugenol/nilotinib-SARS-CoV-2 Omicron mutant Spike RBD complex (200ns). (C) RMSD of eugenol/molnupiravir- SARS-CoV-2 RdRp complex (200ns). (D) RMSF of eugenol/nilotinib- SARS-CoV-2 wt Spike RBD complex. (E)RMSF of eugenol/nilotinib-SARS-CoV-2 Omicron mutant Spike RBD complex. (F) RMSF of eugenol/molnupiravir-SARS-CoV-2 RdRp complex.

Table 9
Molecular dynamics simulation (200ns) with RMSD and RMSF methods.

Complex	RMSD value (Mean)	RMSF value (Mean)
6M0J_RBD_wt-Eugenol	3.10976	0.90172
6M0J_RBD_wt-Nilotinib	2.8265	0.88501
7T9L_RBD_mut-Eugenol	3.69205	1.20363
7T9L_RBD_mut-Nilotinib	4.27111	1.31275
6M71_RdRp-Eugenol	3.5666	1.17827
6M71_RdRp-Molnupiravir	2.3788	1.10242

disease, stroke, thromboembolism and Alzheimer's-like brain injury in the cases infected by earlier virus strains, which are strongly correlated with the prognosis of patients to our best knowledge [111–115]. Risks of death, hospitalization and sequelae in various organs further soared after repeated infection in the acute and postacute phase [116]. Notably, there is a portion of patients recovering from earlier SARS-CoV-2 infection along with Long-COVID, including dyspnea, loss of taste and smell, mental abnormality [2,117]. Previous studies confirmed that SARS-CoV-2 infection led to DNA damage of cardiac tissues, vascular endothelial inflammatory, and microvascular disease, while individuals are at a high risk of the incident cardiovascular disease after COVID-19 [118–121]. In peripheral circulating blood, heparin as a potential receptor of SARS-CoV-2 spike protein exerts undefined effects [122]. Although, the effects of SARS-CoV-2 on function of coagulation and anticoagulation have not been fully understood, at least, along with cardiovascular damage, SARS-CoV-2 infection may increase the risk of thrombogenesis, and the risk likely persist in the future, especially in hospitalized patients with heart failure or stroke [123]. Furtherly, immune functional change post SARS-CoV-2 infection have not yet been fully explained, SARS-CoV-2 infection caused sustained transcriptional changes of myeloid and T cell, and infection elicited more severe damage to organs such as lung, kidney and impacted the olfactory bulb and olfactory epithelium than the those by influenza A

Table 10
Free energy calculations of SARS-CoV-2 wild type and Omicron mutant Spike_RBD-Eugenol, and the finger subdomain of SARS-CoV-2 RdRp-Eugenol, comparing with Nilotinib and Molnupiravir.

Complex system	VDW	EEL	EGB	ESURF	DELTA-GAS	DELTA-SOL	DELTATOT
RBD_WT-Eugenol	−10.686	−3.7435	8.0797	−1.7864	−14.4295	6.2932	**−8.1363**
RBD_WT-Nilotinib	−36.9626	−3.4302	21.6568	−4.3971	−40.3903	17.2597	**−23.1307**
RdRp finger subdomain-Eugenol	−20.1754	−4.2059	10.468	−3.0186	−24.3812	7.4494	**−16.9318**
RdRp-finger subdomain-Molnupiravir	−10.3971	−20.2175	23.183	−2.094	−30.6146	21.089	**−9.5256**
Omicron RBD_M-Eugenol	−14.9489	−10.0712	16.4989	−2.0393	−25.02	14.4596	**−10.5605**
Omicron RBD_M-Nilotinib	−34.9401	−15.5797	32.1134	−4.6175	−50.5193	27.4959	**−23.0234**

Foot note: VDW: van der Waals energy; EEL: electrostatic energy; EGB: electrostatic contribution to solvation; ESURF: non-polar contribution to solvation; DELTA-GAS: VDW + EEL; DELTA-SOL: EGB + ESURF; DELTA-TOT: binding free energy.

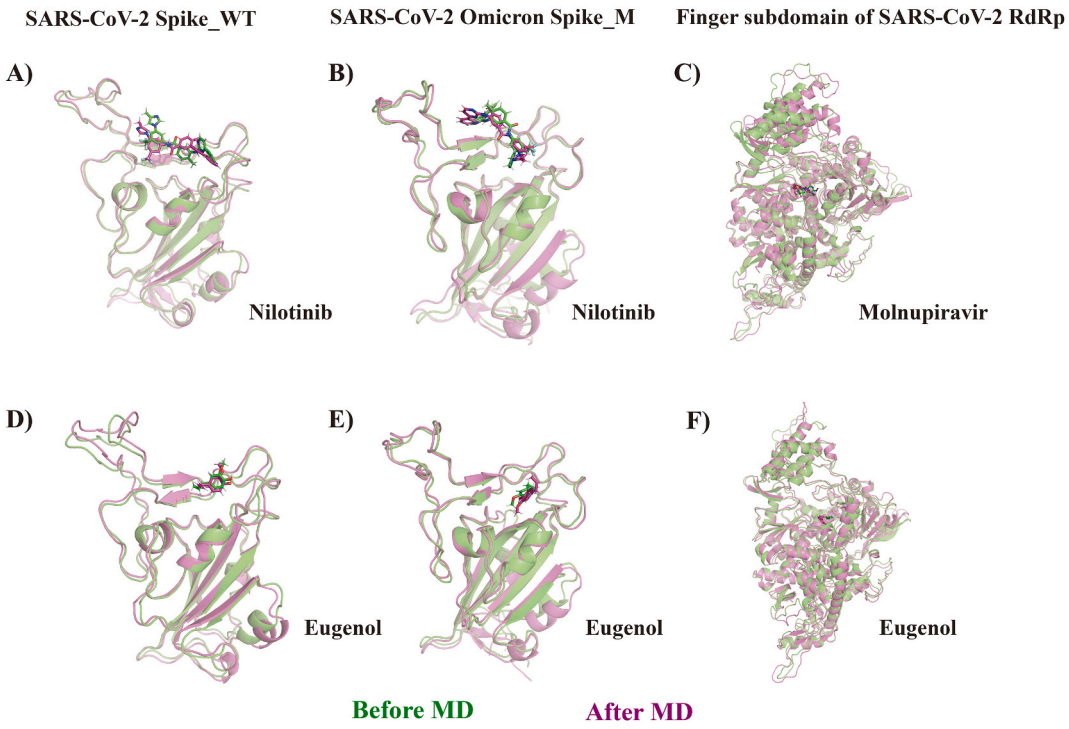

Fig. 19. Superimposition comparison of SARS-CoV-2 Spike RBD alone before MD and after MD. (A) SARS-CoV-2 Spike wild type RBD-nilotinib (Control). (B) SARS-CoV-2 Omicron mutant Spike RBD-nilotinib (Control). (C) Finger subdomain of SARS-CoV-2 RdRp-molnupiravir (Control). (D) SARS-CoV-2 Spike wild type RBD-Eugenol. (F) SARS-CoV-2 Omicron mutant Spike RBD-Eugenol. (F) Finger subdomain of SARS-CoV-2 RdRp-Eugenol.

Table 11
Interaction of small molecular eugenol and amino acids.

System	Hydrophobic_interactions	Hydrogen_bonds
SARS-CoV-2 RBD_WT-Eugenol	TYR-453,TYR-495	ASN-501,GLY-496
SARS-CoV-2 Omicron RBD_M-Eugenol	TYR-453	ARG-403
SARS-CoV-2 RdRp finger subdomain-Eugenol		ARG-553,ARG-624

virus infection [124]. Klein et al. found that long COVID is along with significant changes in leukocytes at > 400 days post infection [125]. Intrinsic Epstein-Barr virus reactivated by SARS-CoV-2 infection may be contribute to neurological symptoms of Long-COVID [126]. Meanwhile, multisystem inflammatory syndrome (MIS-C), acute hepatitis, and Omicron infection related unexplained abdominal pain needed to be operated (Fuji TV report), are potential infection related complications COVID-19 in Children [127]. Although Omicron variants like BA.1/BA.2 replicate more efficiently in human bronchus than that in the lung tissue, and the resultant symptoms and sequela may be not too serious, cumulative reinfection by viral variation though escape antibodies, and consequent effects to human body could not be neglected. Therapeutic drug with single target may be not enough for these infection-related

```
sq|RBD_WT       TNLCPFGEVFNATRFASVYAWNRKRISNCVADYSVLYNSASFSTFKCYGVSPTKLNDLCF   393
sq|RBD_Omicron  TNLCPFDEVFNATRFASVYAWNRKRISNCVADYSVLYNLAPFFTFKCYGVSPTKLNDLCF   393
                ******.******************************* * * ******************

sq|RBD_WT       TNVYADSFVIRGDEVRQIAPGQTGKIADYNYKLPDDFTGXVIAWNSNNLDSKVGGNYNYL   453
sq|RBD_Omicron  TNVYADSFVIRGDEVRQIAPGQTGNIADYNYKLPDDFTGXVIAWNSNKLDSKVSGNYNYL   453
                ************************:**********************:******.******

                                        Binding with ACE2 protein
sq|RBD_WT       YRLFRKSNLKPFERDISTEIYQAGSTPCNGVEGFNCYFPLQSYGFQPTNGVGYQPYRVVV   513
sq|RBD_Omicron  YRLFRKSNLKPFERDISTEIYQAGNKPCNGVAGFNCYFPLRSYSFRPTYGVGXQPYRVVV   513
                ************************..***** ********:**.*:** *** *******

sq|RBD_WT       LSFELLHAPATVCG-  527
sq|RBD_Omicron  LSFELLHAPATVCGP  528
                **************
```

Fig. 20. Sequence alignment Spike RBD of SARS-CoV-2 wild type and Omicron. The identity between the SARS-CoV-2_WT and Omicron was 92.27%. Red color and one dot denote the low similarity.

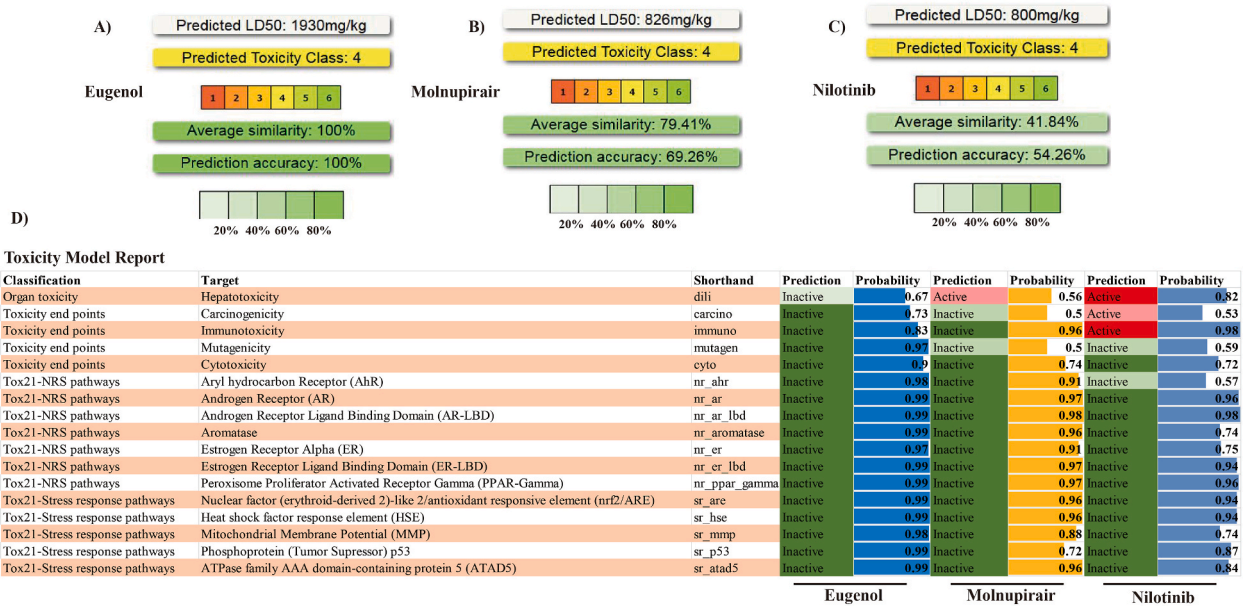

Toxicity Model Report

Classification	Target	Shorthand	Prediction	Probability	Prediction	Probability	Prediction	Probability
Organ toxicity	Hepatotoxicity	dili	Inactive	0.67	Active	0.56	Active	0.82
Toxicity end points	Carcinogenicity	carcino	Inactive	0.73	Inactive	0.5	Active	0.53
Toxicity end points	Immunotoxicity	immuno	Inactive	0.83	Inactive	0.96	Active	0.98
Toxicity end points	Mutagenicity	mutagen	Inactive	0.97	Inactive	0.5	Inactive	0.59
Toxicity end points	Cytotoxicity	cyto	Inactive	0.9	Inactive	0.74	Inactive	0.72
Tox21-NRS pathways	Aryl hydrocarbon Receptor (AhR)	nr_ahr	Inactive	0.98	Inactive	0.91	Inactive	0.57
Tox21-NRS pathways	Androgen Receptor (AR)	nr_ar	Inactive	0.99	Inactive	0.97	Inactive	0.96
Tox21-NRS pathways	Androgen Receptor Ligand Binding Domain (AR-LBD)	nr_ar_lbd	Inactive	0.99	Inactive	0.98	Inactive	0.98
Tox21-NRS pathways	Aromatase	nr_aromatase	Inactive	0.99	Inactive	0.96	Inactive	0.74
Tox21-NRS pathways	Estrogen Receptor Alpha (ER)	nr_er	Inactive	0.97	Inactive	0.91	Inactive	0.75
Tox21-NRS pathways	Estrogen Receptor Ligand Binding Domain (ER-LBD)	nr_er_lbd	Inactive	0.99	Inactive	0.97	Inactive	0.94
Tox21-NRS pathways	Peroxisome Proliferator Activated Receptor Gamma (PPAR-Gamma)	nr_ppar_gamma	Inactive	0.99	Inactive	0.97	Inactive	0.96
Tox21-Stress response pathways	Nuclear factor (erythroid-derived 2)-like 2/antioxidant responsive element (nrf2/ARE)	sr_are	Inactive	0.99	Inactive	0.96	Inactive	0.94
Tox21-Stress response pathways	Heat shock factor response element (HSE)	sr_hse	Inactive	0.99	Inactive	0.96	Inactive	0.94
Tox21-Stress response pathways	Mitochondrial Membrane Potential (MMP)	sr_mmp	Inactive	0.98	Inactive	0.88	Inactive	0.74
Tox21-Stress response pathways	Phosphoprotein (Tumor Supressor) p53	sr_p53	Inactive	0.99	Inactive	0.72	Inactive	0.87
Tox21-Stress response pathways	ATPase family AAA domain-containing protein 5 (ATAD5)	sr_atad5	Inactive	0.99	Inactive	0.96	Inactive	0.84
				Eugenol		Molnupirair		Nilotinib

Fig. 21. Pharmacokinetic properties, aberration and toxic properties of chemicals. (A) LD50 value of eugenol. (B) LD50 value of molnupiravir. (C) LD50 value of nilotinib. (D) Aberration and toxic properties of chemicals.

complications. In all, indefinite Omicron related sequelae still relies on long-term evaluation, pan-corona antiviral drugs, vaccines and efficient antibodies can provide reserves and guarantees for the unclear epidemic situation.

In the current study, by searching SymMap and HERB database, 295 eugenol related targets were identified. Then the gene enrichment analysis was performed. The results indicated that these target genes of eugenol highly enriched in the biological processes, pathways of human diseases and SARS-CoV-2 pathway (e.g. $Ca2^{+}$ signaling) [128], including complement and coagulation cascades, calcium signaling pathway, viral infection, and cancers. The SymMap symptoms manifested that eugenol was significantly associated to headache and pain, and some neurological symptoms, upper respiratory tract symptoms, and gastrointestinal symptoms. These calculated results are in line with the pharmacological action of eugenol and SARS-CoV-2 infection related clinical symptoms. Furthermore, 6 out of the 259 targets, including ITGB1, TMPRSS2, HMOX1, NUP88, CTSL and PLAT, were identified direct target proteins of SARS-CoV-2 antigens and eugenol. The six genes were confirmed to be strongly correlated to the SARS-CoV-2 invasion, lung inflammation, inflammatory response and vaccination related thrombosis pathway [40,82–89]. Furtherly, 259 eugenol targets were integrated with immune signaling of SARS-CoV-2 infected critical cases, eugenol targets enriched in cellular response to stress, cellular response to stimuli, and cytokine signaling. These results implicated that eugenol is a potential immunomodulator for the treatment of COVID-19. Nevertheless, although single analysis/network pharmacology above is helpful for identifying the pharmacological targets, biological function, clinical relations and therapeutic mechanisms of eugenol, transcriptional alteration in specific cell induced by eugenol remain to be disclosed.

Hence, in addition to single analysis above, omics analyses were conducted, based on GSE171360, dose-dependent differentially

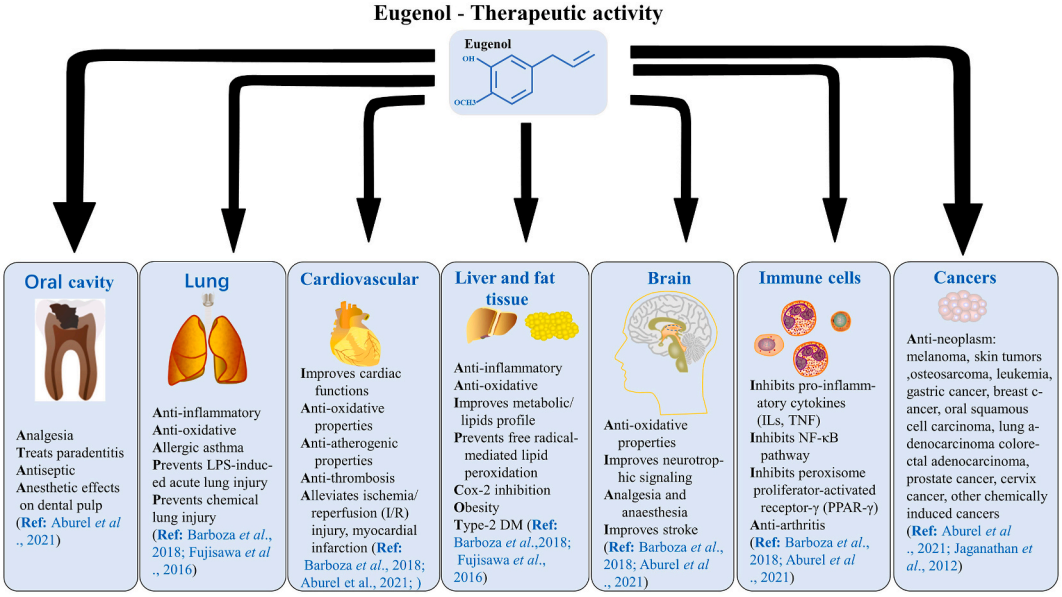

Fig. 22. A summary of anti-inflammatory properties and therapeutic potential of eugenol depending on the previous evidences.

expressed genes by eugenol were calculated. As a precautionary measure, three administrated doses within the considered safety range of eugenol application were selected, although eugenol was classified as a non-DNA damage-inducing chemical. The results showed that eugenol induced 3, 26, 72 differentially expressed genes with significance at the dose of 156.26 μM, 312.5 μM, 625 μM respectively. Identical genes regulated by eugenol and SARS-CoV-2 both are SCARB1, HMOX1 and GDF15. Accordingly, HMOX1 was identified in both single analysis and omics analyses, and eugenol can increase HMOX1 expression by 2 fold in HepaRGTM. The results of immune infiltration analysis showed that expressed genes induced by eugenol (625 μM) significantly enriched in macrophage, which indicated eugenol is a regulator of macrophage. Furthermore, GSEA analyses suggested these significant expressed genes induced by eugenol (625 μM) participated in the BPs and pathways, as lipid localization and PPAR signaling that is strongly associate to fatty liver, hepatitis and hepatic steatosis. Furthermore, in immune signaling of SARS-CoV-2 infected severe cases, differentially expressed genes identified by omics analyses indicate that eugenol effected the immune activities.

To undertake the omics analysis above, transcription of SCARB1, HMOX1 and GDF15 are closely associated with SARS-CoV-2 pathopoiesis. The SCARB1 protein is a plasma membrane receptor that mediates cholesterol transfer to and from HDL. Eugenol can increase the expression level of SCARB1, whereas the result contradicted with several limited studies [129–131]. These findings suggested that SCARB1 was a plausible receptor for hepatitis C virus (HCV) glycoprotein E2 and SARS-CoV2. Nevertheless, based on the consideration of the current study and literature, the core receptor for SARS-CoV-2 entry and pathopoiesia are ACE2, TMPRSS2 and TLR-4, eugenol was predicted to affect the binding of Spike protein to, or target these receptors, and there were also no evidence confirmed eugenol promoted the infection of HCV or SARS-CoV-2, while researches suggested that eugenol prevented the entry of HCV and SARS-CoV-2 [34,132,133]. Additionally, lipid envelope is the important component of SARS-CoV-2 and its variants that plays important role in viral infection process and neurological damage mediated by SARS-CoV-2 [134]. Lipid envelope promotes the transformation of initial infection to severe pneumonia. Targeting lipid metabolism may be a potential way for the treatment of COVDI-19 and its sequelae [134,135]. Several studies demonstrated that regulating glucose and HDL metabolism are available to reduce the mortality of COVID-19 [136–139]. Returning to our case study, eugenol can improve lipids profile, as it directly penetrates the lipid bilayer of liposomes, and exists on the surface, and is able to prevent free radical mediated lipid peroxidation [110]. Furthermore, eugenol elicited the transcription of GDF15 in the current study. GDF15 serves as a target and biomarker for diabetes and cardiovascular diseases, high expression of GDF15 improve insulin resistance, obesity, and type II diabetes [138]. GDF15 coordinates tolerance to inflammatory damage induced by the bacterial and viral infections, through regulation of triglyceride metabolism [140]. The findings suggested that eugenol has a wide range of biological functions, especially regulating lipid metabolism, lipid localization, PPAR pathway. These aspects of eugenol action may be beneficial for improving immunometabolism and attenuating COVID-19 related immunopathological injury.

HMOX1 was identified a hub gene in the current study, eugenol can up-regulate the expression of HMOX1. Various stresses stimuli, including pro-oxidants and pro-inflammatory mediators, can promote HMOX1 expression. High expression of HMOX1 possess immunity control action on many immune cells, especially macrophages. HMOX1 acts as an important immunoregulator in macrophage populations, HMOX1 transcription promotes macrophage polarization towards an anti-inflammatory 'M2-like' macrophage phenotype [85]. Characteristics of macrophage may present abnormal phagocytic function, reduced responsibility for viral clearance, impaired self-limiting pro-inflammatory action, and imbalance of phenotypic transformation in COVID-19 pathology [141,142]. This pattern of macrophage phenotype of SARS-CoV-2 infection may provide us reference, which the immunopathology represented pulmonary

proinflammatory, absence of wound-healing macrophages, and similar to SARS-CoV infection [143]. Eugenol promotes the wound healing to our best knowledge [97]. In the current study, transcribed genes induced by eugenol at a dose of 625 μM enriched in macrophages, the findings suggested that eugenol can regulate macrophages partially due to the HMOX1 transcription.

In the current study, the author used eugenol targets or eugenol induced transcription genes integrated to immune signaling of SARS-CoV-2 infected critical cases. The findings shows the identical pathway is cytokine signaling. The result implied eugenol may regulate cytokine signaling in immune system. As a supplement to the results above, the author considered that upstream signaling such as TLR-4/AP-1 axis and T lymphocyte receptor was confirmed major pathway facilitating inflammatory cytokine production/release and vascular endothelial damage induced by SARS-CoV-2 infection, while TLR-4/AP-1 signaling was commonly used to study the plant derived molecules for drug development [52,120]. Phenolic compound targeting PPAR and TLR4 signaling inhibited (S) protein-induced cytotoxicity and inflammation [144]. In the current study, binding capacities of eugenol to human TLR-4 and its molecules were investigated. The obtained results indicated that eugenol exerted effective binding capacity to TLR-4/AP-1 and TCR molecules.

There was slight discrepancy of eugenol targets for network pharmacology analyses and omics analyses. The author considered several factors may effect the differential results. (1) The discrepancy is intrinsic limitation due to adopting different datasets and corresponding cell lines. (2) In omics analyses, three safe doses of eugenol with a non-DDI classification were selected. Although the last two administrated doses (1250/2500 μM) of eugenol may amplify the transcription of genes, the two doses may have a prone to DDI classification according to the literature [43].

An important mechanism for eugenol to exert anti-microbe effects is the direct inhibition of enzymes related to microbial replication. Eugenol was confirmed an effective inhibitor of a variety of viruses, including influenza A virus, herpes simplex virus type 1, herpes simplex virus 2 and ebola virus. It is also a potential antileishmaniasis agent through activation of the host immune system [145–148] (Anti-microbe effects of eugenol was listed in Fig. 23 according to the literature). Turgeon et al. implicated the efficacy of aerosolized chemicals (eugenol) to reduce viral loads in the air through airborne phage models, and limited data could be referred to before their novel investigation [149]. This research provided us new prospect on the strategy of reducing viral load through droplets/aerosols. These evidences, together with the result of Paidi et al. which implicated eugenol has latent capability against multiple viruses [34]. In addition to their work, using molecular docking analyses, favorite binding capacities of eugenol with SARS-CoV-2 Spike-ACE2 complex and RdRp were determined, implicating that eugenol may be a potential modulator of SARS-CoV-2 Spike-ACE2 complex and act as a potential factor influencing viral transcription. However, molecular docking analysis depends on the recognition between molecules and the match of spatial conformation, and the results were limited by computing abilities and accuracy.

Therefore, the interactions of eugenol and SARS-CoV-2 Spike-ACE2 complex were further calculated with molecular dynamic simulation with 100ns. Nilotinib and molnupiravir were selected as positive controls of current analyses. Several kinase inhibitory agents as nilotinib, were suggested from the point of anti-fibrosis and intervention of the binding of Spike-ACE2 [55,150]. Based on molecular dynamics study, nilotinib was estimated an efficient compound to interfere, destabilize the metastable, perfusion complex of

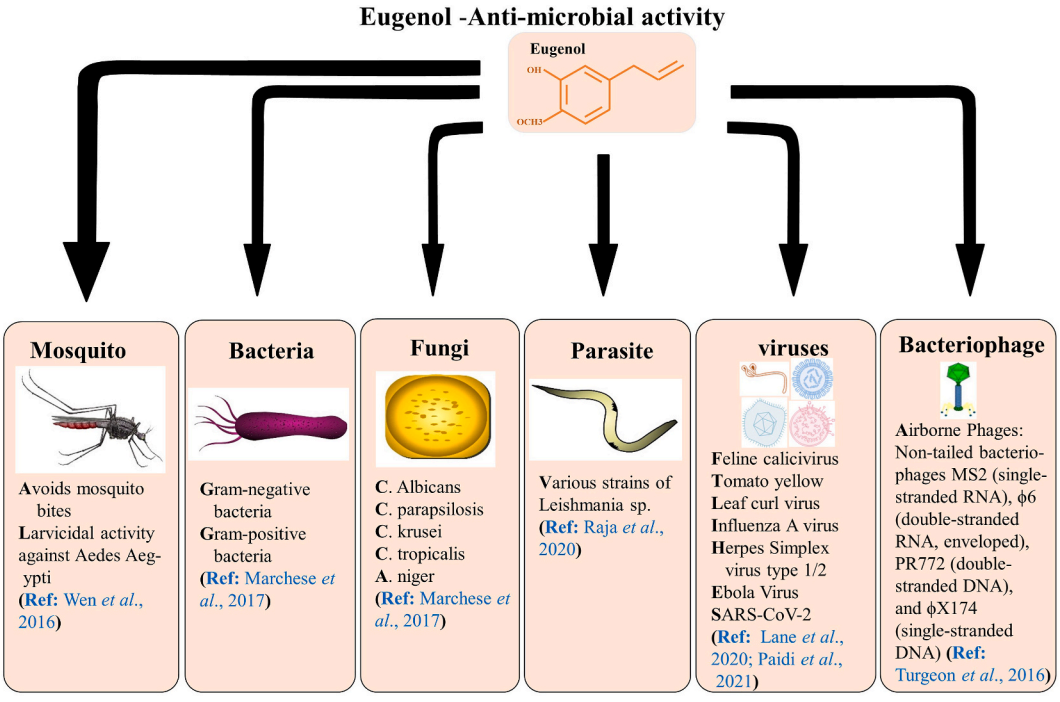

Fig. 23. A summary of antimicrobial activity depending on the previous evidences.

SARS-CoV-2 spike RBD-ACE2 [55]. Meanwhile, molnupiravir is orally active RdRp inhibitor of SARS-CoV-2, the interactions between molnupiravir and RdRp were investigated with molecular dynamic simulation [25,56–59]. Hence, the two inhibitors were used as the positive controls of eugenol. The statistic results suggested that the binding stability and capacity of eugenol to RdRp and SARS-CoV-2 Omicron Spike-ACE2 complex are no less favorable than molnupiravir and nilotinib. These results suggested that eugenol interacted with Spike-ACE2 complex, and it may modify the complex. Nevertheless, this part of simulation aimed at the whole binding complex, the interaction of eugenol with SARS-CoV2 Spike RBD were not estimated independently, therefore, a further simulation with 200ns was performed on the interaction of eugenol and SARS-CoV-2/Omicron Spike RBD individually. Meanwhile, an additional finger subdomain of SARS-CoV-2 RdRp, which was confirmed the important substructure for viral proliferation, was selected for simulation. The results suggested that binding stability and capacity of eugenol to finger subdomain of SARS-CoV-2 RdRp was no less than molnupiravir, whereas the result was consistent with the simulation with 100 ns, although there was a discrepancy in interacting amino acids due to different crystal structures we selected, and different docking domain. Furthermore, the binding capacity and stability of eugenol to wild type/Omicron Spike RBD were less than nilotinib. Therefore, the major mechanisms of anti- SARS-CoV-2 activity of eugenol were considered to be anti-inflammatory and imbibition of viral proliferation. Taken these results, eugenol may be valuable for developing drugs and therapeutic supplementation against COVID-19.

Eugenol as a small biological molecule, has higher bioactivity and cell membrane permeability/lipophilicity than some natural high molecular weight polyphenols, which the reduced absorption of some polyphenols and more complicated in vivo dynamics process limit their practical use [151]. Comparatively simple molecular components implicate more vivacious molecular activity, while this means more links between the chemical and bio-process, for this reason, indications and contraindications of eugenol attracted considerable attention. Several studies have emphasized the potential cytotoxicity of eugenol to oral cavity fibroblasts. However, most of these results obtained from the investigation of a zinc oxide-eugenol (ZOE) paste in animal-based cell models, and there was discrepancy of those results obtained in human cells. Meanwhile, the results obtained from the study of fibroblasts of animal fibroblasts manifested more sensitivity to eugenol's toxic effects as compared to primary human cell lines. Hence, human study might provide more reasonable basis. Besides, local cytotoxic reactions were more likely elicited by the mixing materials in dental procedure, technically or environmentally, not by eugenol. Either the time-dependent evolution of cytotoxicity or dose-dependency of cytotoxicity should be equally addressed in the future. Some investigations suggested that eugenol with reference high concentrations ($\geq$3 mmol/L) indicated toxic prone to oral mucosal fibroblasts, while a inhibitory effect of eugenol on lipid peroxidation was described at lower concentrations ($<$1 mmol/L) [95]. Martinez-Herrera et al. suggested that eugenol applied in low concentration (13 μM) excreted anti-inflammatory effect in dental pulp fibroblasts through inhibiting lipopolysaccharide (LPS) induced TNF-α transcription NF-κB signaling [152].

The World Health Organization (WHO) and Food and Agriculture Organization (FAO) permit the daily consumption of eugenol of 2.5 mg/kg body weight for humans. Besides, the (U.S.) Food and Drug Administration (FDA) stated eugenol was considered as non-carcinogenic/non-mutagenic [107]. Low concentrations of eugenol for rational application have not been linked to definite liver injury. Cytotoxic effects of eugenol are associated with the initial level of intracellular glutathione and ATP in hepatocytes [97,153]. Therefore, the major responsibility for the hepatotoxicity was overdose [154]. Furthermore, allergic responses triggered by eugenol application were reported in isolated cases. However, no severe allergic reaction like anaphylactic shock were confirmed [97]. There was also no report of definite allergic asthma induced by eugenol. Contrarily, eugenol exerted antiasthmatic effects in experimental

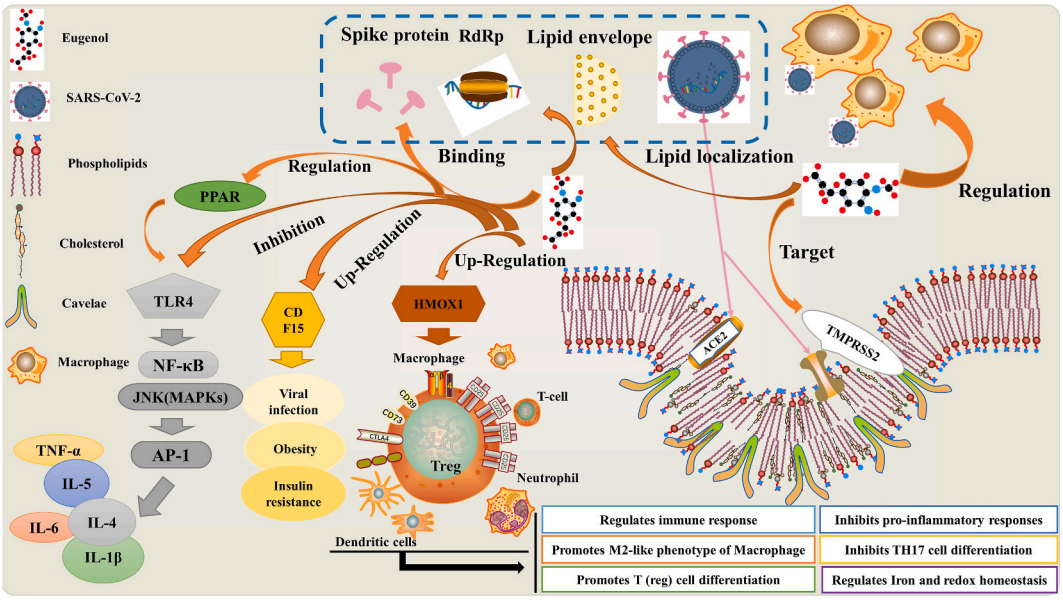

Fig. 24. Schematic representation of bioactivities of eugenol against SARS-CoV-2 based on current results.

allergic asthma [109]. Encouragingly, results from plasma pharmacokinetic and acute toxicity investigations indicated eugenol oleate is safe with an appreciable pharmacokinetic profile [148]. In the current study, eugenol was predicted with lower LD50 value, without significant cytotoxicity compared to nilotinib and molnupiravir. Importantly, eugenol can pass through the BBB, while nilotinib and molnupiravir cannot pass through BBB. Therefore, eugenol may have neuron protective effects against SARS-CoV-2 infection. Taken these above, eugenol is not recognized as an "ugly" chemical to the consensus of literature, instead, most consensus of the literature acknowledge beneficial effects of eugenol for antimicrobial activity, anti-inflammation and cancer in experimental models [97].

There are several limitations to the study. Firstly, the alternative omics datasets regarding eugenol induced genomic change in specific organ and cell line are limited. GSE171360 was selected in this study, and the cell line used in GSE171360 was HepaRGTM. HepaRGTM highly expresses transporters and metabolic enzymes, and this terminally differentiated hepatocellular carcinoma cells have facilitated numerous studies of uptake, metabolism, and disposition of drug candidates. Thereby it was extensively used as hepatic model in pharmaceutical, chemical and cosmetics industries. Generally, HepaRGTM can provide some valuable information, because SARS-CoV-2 induce hepatic impairment, patients with fatty liver, obesity and cancer more vulnerable, and there may be a close relationship between the SARS-CoV-2 superantigens and acute hepatitis [127,155–158]. Nevertheless, It is unclear that eugenol induced genomic change in other cell lines such as alveolar epithelial cell, cardiomyocytes, etc. Therefore, effects of eugenol on these cells remain to be determined. Secondly, it is unclear that eugenol induced genomic change in SARS-CoV-2 infected models. Therefore, further studies such as high-throughput sequencing are needed. Lastly, although the results of molecular dynamic simulation implicated that the binding stability and capacity of eugenol to the virulence sites and corresponding amino acids, this results are on the basis of molecular simulation, and the conclusions remain to be determined by further experimental investigation.

5. Conclusions

SARS-CoV-2 pandemic increased global financial burden, and continuous viral variation given the challenges to the developing COVID-19 vaccines and therapeutic drugs. In conclusion, the results of current study support the previous experimental study about the anti-COVID-19 effects of eugenol (Fig. 24 and Paidi et al.). Apart from the few evidence, the author further identified eugenol may play an important role in strengthen of immunologic functions, regulating inflammatory reaction and cytokine signaling. Eugenol is also a candidate natural reagent against Omicron SARS-CoV-2 transcription and pathopoiesia. Finally, inspired by the experimental results of Turgeon et al. [149], the author carefully gives an expectation/hypothesis that well-designed eugenol medicaments may be hopeful for reducing viral loads of droplets/aerosols environmentally.

Author contribution statement

Yang Liu, M.D.: Conceived and designed the experiments; Performed the experiments; Analyzed and interpreted the data; Contributed reagents, materials, analysis tools or data; Wrote the paper.

Funding statement

This research did not receive any specific grant from funding agencies in the public, commercial, or not-for-profit sectors.

Additional Information

URLs of Public datasets and online tools (free access) used in the current study were listed in the main text and supplementary tables, the raw data of molecular dynamics simulation are available for reasonable request. Due to huge reserves, please contact the corresponding author (Yangliu19830722@126.com)

Declaration of competing interest

The authors declare that they have no known competing financial interests or personal relationships that could have appeared to influence the work reported in this paper.

Acknowledgements

Thanks to the authors for providing the crystal structure of Omicron SARS-CoV-2 spike protein in Protein Data Bank (https://www.pdbus.org/), and to the providers of single-Cell RNA sequencing datasets and the developers of public databases/web tools involved in the current analyses.

Appendix A. Supplementary data

Supplementary data related to this article can be found at https://doi.org/10.1016/j.heliyon.2023.e13853.

References

[1] N. Barda, N. Dagan, C. Cohen, M.A. Hernán, M. Lipsitch, I.S. Kohane, B.Y. Reis, R.D. Balicer, Effectiveness of a third dose of the BNT162b2 mRNA COVID-19 vaccine for preventing severe outcomes in Israel: an observational study, Lancet 398 (10316) (2021) 2093–2100, https://doi.org/10.1016/S0140-6736(21)02249-2.

[2] C. Menni, A.M. Valdes, L. Polidori, M. Antonelli, S. Penamakuri, A. Nogal, P. Louca, A. May, J.C. Figueiredo, C. Hu, E. Molteni, L. Canas, M.F. Österdahl, M. Modat, C.H. Sudre, B. Fox, A. Hammers, J. Wolf, J. Capdevila, A.T. Chan, S.P. David, C.J. Steves, S. Ourselin, T.D. Spector, Symptom prevalence, duration, and risk of hospital admission in individuals infected with SARS-CoV-2 during periods of omicron and delta variant dominance: a prospective observational study from the ZOE COVID Study, Lancet 399 (10335) (2022) 1618–1624, https://doi.org/10.1016/S0140-6736(22)00327-0.

[3] M. Antonelli, J.C. Pujol, T.D. Spector, S. Ourselin, C.J. Steves, Risk of long COVID associated with delta versus omicron variants of SARS-CoV-2, Lancet 399 (10343) (2022) 2263–2264, https://doi.org/10.1016/S0140-6736(22)00941-2.

[4] M. Antonelli, R.S. Penfold, J. Merino, C.H. Sudre, E. Molteni, S. Berry, L.S. Canas, M.S. Graham, K. Klaser, M. Modat, B. Murray, E. Kerfoot, L. Chen, J. Deng, M.F. Österdahl, N.J. Cheetham, D.A. Drew, L.H. Nguyen, J.C. Pujol, C. Hu, S. Selvachandran, L. Polidori, A. May, J. Wolf, A.T. Chan, A. Hammers, E.L. Duncan, T.D. Spector, S. Ourselin, C.J. Steves, Risk factors and disease profile of post-vaccination SARS-CoV-2 infection in UK users of the COVID Symptom Study app: a prospective, community-based, nested, case-control study, Lancet Infect. Dis. 22 (1) (2022) 43–55, https://doi.org/10.1016/S1473-3099(21)00460-6.

[5] S. Kannan, P. Shaik Syed Ali, A. Sheeza, Omicron (B.1.1.529) - variant of concern - molecular profile and epidemiology: a mini review, Eur. Rev. Med. Pharmacol. Sci. 25 (24) (2021) 8019–8022, https://doi.org/10.26355/eurrev_202112_27653.

[6] T. Singhal, The emergence of omicron: challenging times are here again, Indian J. Pediatr. 89 (5) (2022) 490–496, https://doi.org/10.1007/s12098-022-04077-4.

[7] L. Yao, K.L. Zhu, X.L. Jiang, X.J. Wang, B.D. Zhan, H.X. Gao, X.Y. Geng, L.J. Duan, E.H. Dai, M.J. Ma, Omicron subvariants escape antibodies elicited by vaccination and BA.2.2 infection, Lancet Infect. Dis. 22 (8) (2022) 1116–1117, https://doi.org/10.1016/S1473-3099(22)00410-8.

[8] A. Tuekprakhon, R. Nutalai, A. Dijokaite-Guraliuc, D. Zhou, H.M. Ginn, et al., Antibody escape of SARS-CoV-2 Omicron BA.4 and BA.5 from vaccine and BA.1 serum, Cell 185 (14) (2022) 2422–2433.e13, https://doi.org/10.1016/j.cell.2022.06.005.

[9] N.P. Hachmann, J. Miller, A.Y. Collier, J.D. Ventura, J. Yu, M. Rowe, E.A. Bondzie, O. Powers, N. Surve, K. Hall, D.H. Barouch, Neutralization escape by SARS-CoV-2 omicron subvariants BA.2.12.1, BA.4, and BA.5, N. Engl. J. Med. 387 (1) (2022) 86–88, https://doi.org/10.1056/NEJMc2206576.

[10] E. Callaway, Will there be a COVID winter wave? What scientists say, Nature 610 (7931) (2022) 239–241, https://doi.org/10.1038/d41586-022-03157-x.

[11] P. Arora, A. Kempf, I. Nehlmeier, S.R. Schulz, H.M. Jäck, S. Pöhlmann, M. Hoffmann, Omicron sublineage BQ.1.1 resistance to monoclonal antibodies, Lancet Infect. Dis. 23 (1) (2023) 22–23, https://doi.org/10.1016/S1473-3099(22)00733-2.

[12] Y. Cao, A. Yisimayi, F. Jian, W. Song, T. Xiao, L. Wang, S. Du, J. Wang, Q. Li, X. Chen, Y. Yu, P. Wang, Z. Zhang, P. Liu, R. An, X. Hao, Y. Wang, J. Wang, R. Feng, H. Sun, L. Zhao, W. Zhang, D. Zhao, J. Zheng, L. Yu, C. Li, N. Zhang, R. Wang, X. Niu, S. Yang, X. Song, Y. Chai, Y. Hu, Y. Shi, L. Zheng, Z. Li, Q. Gu, F. Shao, W. Huang, R. Jin, Z. Shen, Y. Wang, X. Wang, J. Xiao, X.S. Xie, BA.2.12.1, BA.4 and BA.5 escape antibodies elicited by Omicron infection, Nature 608 (7923) (2022) 593–602, https://doi.org/10.1038/s41586-022-04980-y.

[13] C.J. Reynolds, C. Pade, J.M. Gibbons, A.D. Otter, K.M. Lin, et al., Immune boosting by B.1.1.529 (Omicron) depends on previous SARS-CoV-2 exposure, Science 377 (6603) (2022), eabq1841, https://doi.org/10.1126/science.abq1841.

[14] S. Lukassen, R.L. Chua, T. Trefzer, N.C. Kahn, M.A. Schneider, T. Muley, H. Winter, M. Meister, C. Veith, A.W. Boots, B.P. Hennig, M. Kreuter, C. Conrad, R. Eils, SARS-CoV-2 receptor ACE2 and TMPRSS2 are primarily expressed in bronchial transient secretory cells, EMBO J. 39 (10) (2020), e105114, https://doi.org/10.15252/embj.20105114.

[15] K.P.Y. Hui, J.C.W. Ho, M.C. Cheung, K.C. Ng, R.H.H. Ching, K.L. Lai, T.T. Kam, H. Gu, K.Y. Sit, M.K.Y. Hsin, T.W.K. Au, L.L.M. Poon, M. Peiris, J.M. Nicholls, M.C.W. Chan, SARS-CoV-2 Omicron variant replication in human bronchus and lung ex vivo, Nature 603 (7902) (2022) 715–720, https://doi.org/10.1038/s41586-022-04479-6.

[16] C.E. Hastie, D.J. Lowe, A. McAuley, A.J. Winter, N.L. Mills, C. Black, J.T. Scott, C.A. O'Donnell, D.N. Blane, S. Browne, T.R. Ibbotson, J.P. Pell, Outcomes among confirmed cases and a matched comparison group in the Long-COVID in Scotland study, Nat. Commun. 13 (1) (2022) 5663, https://doi.org/10.1038/s41467-022-33415-5.

[17] N. Wolter, W. Jassat, S. Walaza, R. Welch, H. Moultrie, M. Groome, D.G. Amoako, J. Everatt, J.N. Bhiman, C. Scheepers, N. Tebeila, N. Chiwandire, M. du Plessis, N. Govender, A. Ismail, A. Glass, K. Mlisana, W. Stevens, F.K. Treurnicht, Z. Makatini, N.Y. Hsiao, R. Parboosing, J. Wadula, H. Hussey, M.A. Davies, A. Boulle, A. von Gottberg, C. Cohen, Early assessment of the clinical severity of the SARS-CoV-2 omicron variant in South Africa: a data linkage study, Lancet 399 (10323) (2022) 437–446, https://doi.org/10.1016/S0140-6736(22)00017-4.

[18] J. Nealon, B.J. Cowling, Omicron severity: milder but not mild, Lancet 399 (10323) (2022) 412–413, https://doi.org/10.1016/S0140-6736(22)00056-3.

[19] J.S. Faust, C. Du, C. Liang, K.D. Mayes, B. Renton, K. Panthagani, H.M. Krumholz, Excess mortality in Massachusetts during the delta and omicron waves of COVID-19, JAMA 328 (1) (2022) 74–76, https://doi.org/10.1001/jama.2022.8045.

[20] Z. Strasser, A. Hadavand, S. Murphy, H. Estiri, SARS-CoV-2 Omicron Variant Is as Deadly as Previous Waves after Adjusting for Vaccinations, Demographics, and Comorbidities, 02, May 2022. PREPRINT (Version 1) available at: Research Square [10.21203/rs.3.rs-1601788/v1.

[21] D. Groff, A. Sun, A.E. Ssentongo, D.M. Ba, N. Parsons, G.R. Poudel, A. Lekoubou, J.S. Oh, J.E. Ericson, P. Ssentongo, V.M. Chinchilli, Short-term and long-term rates of postacute sequelae of SARS-CoV-2 infection: a systematic review, JAMA Netw. Open 4 (10) (2021), e2128568, https://doi.org/10.1001/jamanetworkopen.2021.28568.

[22] J.R.C. Pulliam, C. van Schalkwyk, N. Govender, A. von Gottberg, C. Cohen, M.J. Groome, J. Dushoff, K. Mlisana, H. Moultrie, Increased risk of SARS-CoV-2 reinfection associated with emergence of Omicron in South Africa, Science 376 (6593) (2022), eabn4947, https://doi.org/10.1126/science.abn4947.

[23] J. Schöley, J.M. Aburto, I. Kashnitsky, M.S. Kniffka, L. Zhang, H. Jaadla, J.B. Dowd, R. Kashyap, Life expectancy changes since COVID-19, Nat. Human Behav. 6 (12) (2022) 1649–1659, https://doi.org/10.1038/s41562-022-01450-3.

[24] E. Mahase, Covid-19: pfizer's paxlovid is 89% effective in patients at risk of serious illness, company reports, BMJ 375 (2021) n2713, https://doi.org/10.1136/bmj.n2713.

[25] M. Imran, M. Kumar Arora, S.M.B. Asdaq, S.A. Khan, S.I. Alaqel, M.K. Alshammari, M.M. Alshehri, A.S. Alshrari, A. Mateq Ali, A.M. Al-Shammeri, B. D. Alhazmi, A.A. Harshan, M.T. Alam, Abida, discovery, development, and patent trends on molnupiravir: a prospective oral treatment for COVID-19, Molecules 26 (19) (2021) 5795, https://doi.org/10.3390/molecules26195795.

[26] A.K. Singh, A. Singh, R. Singh, A. Misra, Molnupiravir in COVID-19: a systematic review of literature, Diabetes Metabol. Syndr. 15 (6) (2021), 102329, https://doi.org/10.1016/j.dsx.2021.102329.

[27] L. Vangeel, W. Chiu, S. De Jonghe, P. Maes, B. Slechten, J. Raymenants, E. André, P. Leyssen, J. Neyts, D. Jochmans, Remdesivir, Molnupiravir and Nirmatrelvir remain active against SARS-CoV-2 Omicron and other variants of concern, Antivir. Res. 198 (2022), 105252, https://doi.org/10.1016/j.antiviral.2022.105252.

[28] L.R. Fukumoto, G. Mazza, Assessing antioxidant and prooxidant activities of phenolic compounds, J. Agric. Food Chem. 48 (8) (2000) 3597–3604, https://doi.org/10.1021/jf000220w.

[29] P. Van Hung, Phenolic compounds of cereals and their antioxidant capacity, Crit. Rev. Food Sci. Nutr. 56 (1) (2016) 25–35, https://doi.org/10.1080/10408398.2012.708909.

[30] D. Lin, M. Xiao, J. Zhao, Z. Li, B. Xing, X. Li, M. Kong, L. Li, Q. Zhang, Y. Liu, H. Chen, W. Qin, H. Wu, S. Chen, An overview of plant phenolic compounds and their importance in human nutrition and management of type 2 diabetes, Molecules 21 (10) (2016) 1374, https://doi.org/10.3390/molecules21101374.

[31] H.M. Cho, T.K. Ha, L.H. Dang, H.T. Pham, V.O. Tran, J. Huh, J.P. An, W.K. Oh, Prenylated phenolic compounds from the leaves of Sabia limoniacea and their antiviral activities against porcine epidemic diarrhea virus, J. Nat. Prod. 82 (4) (2019) 702–713, https://doi.org/10.1021/acs.jnatprod.8b00435.

[32] D.W. Kim, K.H. Seo, M.J. Curtis-Long, K.Y. Oh, J.W. Oh, J.K. Cho, K.H. Lee, K.H. Park, Phenolic phytochemical displaying SARS-CoV papain-like protease inhibition from the seeds of Psoralea corylifolia, J. Enzym. Inhib. Med. Chem. 29 (1) (2014) 59–63, https://doi.org/10.3109/14756366.2012.753591.

[33] S. Jo, S. Kim, D.H. Shin, M.S. Kim, Inhibition of SARS-CoV 3CL protease by flavonoids, J. Enzym. Inhib. Med. Chem. 35 (1) (2020) 145–151, https://doi.org/10.1080/14756366.2019.1690480.
[34] R.K. Paidi, M. Jana, S. Raha, M. McKay, M. Sheinin, R.K. Mishra, K. Pahan, Eugenol, a component of holy basil (tulsi) and common spice clove, inhibits the interaction between SARS-CoV-2 spike S1 and ACE2 to induce therapeutic responses, J. Neuroimmune Pharmacol. 16 (4) (2021) 743–755, https://doi.org/10.1007/s11481-021-10028-1.
[35] A. Marchese, R. Barbieri, E. Coppo, I.E. Orhan, M. Daglia, S.F. Nabavi, M. Izadi, M. Abdollahi, S.M. Nabavi, M. Ajami, Antimicrobial activity of eugenol and essential oils containing eugenol: a mechanistic viewpoint, Crit. Rev. Microbiol. 43 (6) (2017) 668–689, https://doi.org/10.1080/1040841X.2017.1295225.
[36] S. Fang, L. Dong, L. Liu, J. Guo, L. Zhao, J. Zhang, D. Bu, X. Liu, P. Huo, W. Cao, Q. Dong, J. Wu, X. Zeng, Y. Wu, Y. Zhao, HERB: a high-throughput experiment- and reference-guided database of traditional Chinese medicine, Nucleic Acids Res. 49 (D1) (2021) D1197–D1206, https://doi.org/10.1093/nar/gkaa1063.
[37] Y. Wu, F. Zhang, K. Yang, S. Fang, D. Bu, H. Li, L. Sun, H. Hu, K. Gao, W. Wang, X. Zhou, Y. Zhao, J. Chen, SymMap: an integrative database of traditional Chinese medicine enhanced by symptom mapping, Nucleic Acids Res. 47 (D1) (2019) D1110–D1117, https://doi.org/10.1093/nar/gky1021.
[38] D. Wishart, D. Arndt, A. Pon, T. Sajed, A.C. Guo, Y. Djoumbou, C. Knox, M. Wilson, Y. Liang, J. Grant, Y. Liu, S.A. Goldansaz, S.M. Rappaport, T3DB, The toxic exposome database, Nucleic Acids Res. 43 (Database issue) (2015) D928–D934, https://doi.org/10.1093/nar/gku1004.
[39] E. Sjöstedt, W. Zhong, L. Fagerberg, M. Karlsson, N. Mitsios, et al., An atlas of the protein-coding genes in the human, pig, and mouse brain, Science 367 (6482) (2020), eaay5947, https://doi.org/10.1126/science.aay5947.
[40] D.E. Gordon, G.M. Jang, M. Bouhaddou, J. Xu, K. Obernier, et al., A SARS-CoV-2 protein interaction map reveals targets for drug repurposing, Nature 583 (7816) (2020) 459–468, https://doi.org/10.1038/s41586-020-2286-9.
[41] Y. Liao, J. Wang, E.J. Jaehnig, Z. Shi, B. Zhang, WebGestalt 2019: gene set analysis toolkit with revamped UIs and APIs, Nucleic Acids Res. 47 (W1) (2019) W199–W205, https://doi.org/10.1093/nar/gkz401.
[42] P. Bardou, J. Mariette, F. Escudié, C. Djemiel, C. Klopp, jvenn: an interactive Venn diagram viewer, BMC Bioinf. 15 (1) (2014) 293, https://doi.org/10.1186/1471-2105-15-293.
[43] J.K. Buick, A. Williams, M.J. Meier, C.D. Swartz, L. Recio, R. Gagné, S.S. Ferguson, B.P. Engelward, C.L. Yauk, A modern genotoxicity testing paradigm: integration of the high-throughput CometChip® and the TGx-DDI transcriptomic biomarker in human HepaRG™ cell cultures, Front. Public Health 9 (2021), 694834, https://doi.org/10.3389/fpubh.2021.694834.
[44] G. Zhou, O. Soufan, J. Ewald, R.E.W. Hancock, N. Basu, J. Xia, NetworkAnalyst 3.0: a visual analytics platform for comprehensive gene expression profiling and meta-analysis, Nucleic Acids Res. 47 (W1) (2019) W234–W241, https://doi.org/10.1093/nar/gkz240.
[45] Y.R. Miao, M. Xia, M. Luo, T. Luo, M. Yang, A.Y. Guo, ImmuCellAI-mouse: a tool for comprehensive prediction of mouse immune cell abundance and immune microenvironment depiction, Bioinformatics 38 (3) (2022) 785–791, https://doi.org/10.1093/bioinformatics/btab711.
[46] J.Y. Zhang, X.M. Wang, X. Xing, Z. Xu, C. Zhang, J.W. Song, X. Fan, P. Xia, J.L. Fu, S.Y. Wang, R.N. Xu, X.P. Dai, L. Shi, L. Huang, T.J. Jiang, M. Shi, Y. Zhang, A. Zumla, M. Maeurer, F. Bai, F.S. Wang, Single-cell landscape of immunological responses in patients with COVID-19, Nat. Immunol. 21 (9) (2020) 1107–1118, https://doi.org/10.1038/s41590-020-0762-x.
[47] Y. Zhou, B. Zhou, L. Pache, M. Chang, A.H. Khodabakhshi, O. Tanaseichuk, C. Benner, S.K. Chanda, Metascape provides a biologist-oriented resource for the analysis of systems-level datasets, Nat. Commun. 10 (1) (2019) 1523, https://doi.org/10.1038/s41467-019-09234-6.
[48] Y. Wang, S.H. Bryant, T. Cheng, J. Wang, A. Gindulyte, B.A. Shoemaker, P.A. Thiessen, S. He, J. Zhang, PubChem BioAssay: 2017 update, Nucleic Acids Res. 45 (D1) (2017) D955–D963, https://doi.org/10.1093/nar/gkw1118.
[49] J. Lan, J. Ge, J. Yu, S. Shan, H. Zhou, S. Fan, Q. Zhang, X. Shi, Q. Wang, L. Zhang, X. Wang, Structure of the SARS-CoV-2 spike receptor-binding domain bound to the ACE2 receptor, Nature 581 (7807) (2020) 215–220, https://doi.org/10.1038/s41586-020-2180-5.
[50] H.S. Hillen, G. Kokic, L. Farnung, C. Dienemann, D. Tegunov, P. Cramer, Structure of replicating SARS-CoV-2 polymerase, Nature 584 (7819) (2020) 154–156, https://doi.org/10.1038/s41586-020-2368-8.
[51] D. Mannar, J.W. Saville, X. Zhu, S.S. Srivastava, A.M. Berezuk, K.S. Tuttle, A.C. Marquez, I. Sekirov, S. Subramaniam, SARS-CoV-2 Omicron variant: antibody evasion and cryo-EM structure of spike protein-ACE2 complex, Science 375 (6582) (2022) 760–764, https://doi.org/10.1126/science.abn7760, 10.1126/science.abn7760.
[52] A. Khan, S.U. Khan, A. Khan, B. Shal, S.U. Rehman, S.U. Rehman, T.T. Htar, S. Khan, S. Anwar, A. Alafnan, K.R. Rengasamy, Anti-inflammatory and anti-rheumatic potential of selective plant compounds by targeting TLR-4/AP-1 signaling: a comprehensive molecular docking and simulation approaches, Molecules 27 (13) (2022) 4319, https://doi.org/10.3390/molecules27134319.
[53] S. Mujwar, Computational repurposing of tamibarotene against triple mutant variant of SARS-CoV-2, Comput. Biol. Med. 136 (2021), 104748, https://doi.org/10.1016/j.compbiomed.2021.104748.
[54] K. Cameron, L. Rozano, M. Falasca, R.L. Mancera, Does the SARS-CoV-2 spike protein receptor binding domain interact effectively with the DPP4 (CD26) receptor? A molecular docking study, Int. J. Mol. Sci. 22 (13) (2021) 7001, https://doi.org/10.3390/ijms22137001.
[55] M. Razizadeh, M. Nikfar, Y. Liu, Small molecule therapeutics to destabilize the ACE2-RBD complex: a molecular dynamics study, Biophys. J. 120 (14) (2021) 2793–2804, https://doi.org/10.1016/j.bpj.2021.06.016.
[56] S.M. Patil, K.R. Maruthi, S.N. Bajpe, V.M. Vyshali, S. Sushmitha, C. Akhila, R. Ramu, Comparative molecular docking and simulation analysis of molnupiravir and remdesivir with SARS-CoV-2 RNA dependent RNA polymerase (RdRp), Bioinformation 17 (11) (2021) 932–939, https://doi.org/10.6026/97320630017932.
[57] S. Wan, A.P. Bhati, A.D. Wade, D. Alfè, P.V. Coveney, Thermodynamic and structural insights into the repurposing of drugs that bind to SARS-CoV-2 main protease, Mol Syst Des Eng 7 (2) (2021) 123–131, https://doi.org/10.1039/d1me00124h.
[58] P. Priya, A. Basit, P. Bandyopadhyay, A strategy to optimize the peptide-based inhibitors against different mutants of the spike protein of SARS-CoV-2, J. Biomol. Struct. Dyn. 26 (2022) 1–12, https://doi.org/10.1080/07391102.2022.2103587.
[59] B. Shahbazi, L. Mafakher, L. Teimoori-Toolabi, Different compounds against Angiotensin-Converting Enzyme 2 (ACE2) receptor potentially containing the infectivity of SARS-CoV-2: an in silico study, J. Mol. Model. 28 (4) (2022) 82, https://doi.org/10.1007/s00894-022-05059-1.
[60] J. Wang, W. Wang, P.A. Kollman, D.A. Case, Automatic atom type and bond type perception in molecular mechanical calculations, J. Mol. Graph. Model. 25 (2) (2006) 247–260, https://doi.org/10.1016/j.jmgm.2005.12.005.
[61] H. Nguyen, J. Maier, H. Huang, V. Perrone, C. Simmerling, Folding simulations for proteins with diverse topologies are accessible in days with a physics-based force field and implicit solvent, J. Am. Chem. Soc. 136 (40) (2014) 13959–13962, https://doi.org/10.1021/ja5032776.
[62] M.J. Abraham, T. Murtola, R. Schulz, S. Páll, J.C. Smith, B. Hess, E. Lindahl, GROMACS: high performance molecular simulations through multi-level parallelism from laptops to supercomputers, SoftwareX, Volumes 1-2 19–25 (2015), https://doi.org/10.1016/j.softx.2015.06.001. ISSN 2352-7110.
[63] S. Genheden, U. Ryde, The MM/PBSA and MM/GBSA methods to estimate ligand-binding affinities, Expet Opin. Drug Discov. 10 (5) (2015) 449–461, https://doi.org/10.1517/17460441.2015.1032936.
[64] M.S. Valdés-Tresanco, M.E. Valdés-Tresanco, P.A. Valiente, E. Moreno, gmx_MMPBSA: a new tool to perform end-state free energy calculations with GROMACS, J. Chem. Theor. Comput. 17 (10) (2021) 6281–6291, https://doi.org/10.1021/acs.jctc.1c00645.
[65] O. Trott, A.J. Olson, AutoDock Vina, Improving the speed and accuracy of docking with a new scoring function, efficient optimization, and multithreading, J. Comput. Chem. 31 (2) (2010) 455–461, https://doi.org/10.1002/jcc.21334.
[66] P.A. Ravindranath, S. Forli, D.S. Goodsell, A.J. Olson, M.F. Sanner, AutoDockFR: advances in protein-ligand docking with explicitly specified binding site flexibility, PLoS Comput. Biol. 11 (12) (2015), e1004586, https://doi.org/10.1371/journal.pcbi.1004586.
[67] R. Salomon-Ferrer, D.A. Case, R.C. Walker, An overview of the Amber biomolecular simulation package, Wiley Interdiscip. Rev. Comput. Mol. Sci. 3 (2013) 198–210, https://doi.org/10.1002/wcms.1121.
[68] J. Wang, R.M. Wolf, J.W. Caldwell, P.A. Kollman, D.A. Case, Development and testing of a general amber force field, J. Comput. Chem. 25 (9) (2004) 1157–1174, https://doi.org/10.1002/jcc.20035.

[69] J.A. Maier, C. Martinez, K. Kasavajhala, L. Wickstrom, K.E. Hauser, C. Simmerling, ff14SB: improving the accuracy of protein side chain and backbone parameters from ff99SB, J. Chem. Theor. Comput. 11 (8) (2015) 3696–3713, https://doi.org/10.1021/acs.jctc.5b00255.

[70] P. Mark, L. Nilsson, Structure and dynamics of the TIP3P, SPC, and SPC/E water models at 298 K, J. Phys. Chem. 105 (43) (2001) 9954–9960, https://doi.org/10.1021/jp003020w.

[71] C. Sagui, T.A. Darden, Molecular dynamics simulations of biomolecules: long-range electrostatic effects, Annu. Rev. Biophys. Biomol. Struct. 28 (1999) 155–179, https://doi.org/10.1146/annurev.biophys.28.1.155.

[72] V. Kräutler, W.F. Van, Gunsteren, P.H. Hünenberger, A fast SHAKE algorithm to solve distance constraint equations for small molecules in molecular dynamics simulations, J. Comput. Chem. 22 (5) (2001) 501–508, https://doi.org/10.1002/1096-987X(20010415)22:5<501::AID-JCC1021>3.0.CO, 2-V.

[73] L. Larini, R. Mannella, D. Leporini, Langevin stabilization of molecular-dynamics simulations of polymers by means of quasisymplectic algorithms, J. Chem. Phys. 126 (10) (2007), 104101, https://doi.org/10.1063/1.2464095.

[74] G. Rastelli, A. Del Rio, G. Degliesposti, M. Sgobba, Fast and accurate predictions of binding free energies using MM-PBSA and MM-GBSA, J. Comput. Chem. 31 (4) (2010) 797–810, https://doi.org/10.1002/jcc.21372.

[75] T. Hou, J. Wang, Y. Li, W. Wang, Assessing the performance of the MM/PBSA and MM/GBSA methods. 1. The accuracy of binding free energy calculations based on molecular dynamics simulations, J. Chem. Inf. Model. 51 (1) (2011) 69–82, https://doi.org/10.1021/ci100275a.

[76] H. Nguyen, D.R. Roe, C. Simmerling, Improved generalized born solvent model parameters for protein simulations, J. Chem. Theor. Comput. 9 (4) (2013) 2020–2034, https://doi.org/10.1021/ct3010485.

[77] J. Weiser, P.S. Shenkin, W.C. Still, Approximate atomic surfaces from linear combinations of pairwise overlaps (LCPO), 19990130, J. Comput. Chem. 20 (2) (1999) 217–230, https://doi.org/10.1002/(SICI)1096-987X, 20:2<217::AID-JCC4>3.0.CO;2-A.

[78] J.P.G.L.M. Rodrigues, J.M.C. Teixeira, M. Trellet, A.M.J.J. Bonvin, pdb-tools: a swiss army knife for molecular structures, F1000Res, 2018. https://doi.org/10.12688/f1000research.17456.1, 7 1961.

[79] F. Sievers, A. Wilm, D. Dineen, T.J. Gibson, K. Karplus, W. Li, R. Lopez, H. McWilliam, M. Remmert, J. Söding, J.D. Thompson, D.G. Higgins, Fast, scalable generation of high-quality protein multiple sequence alignments using Clustal Omega, Mol. Syst. Biol. 7 (2011) 539, https://doi.org/10.1038/msb.2011.75.

[80] A. Daina, O. Michielin, V. Zoete, SwissADME: a free web tool to evaluate pharmacokinetics, drug-likeness and medicinal chemistry friendliness of small molecules, Sci. Rep. 7 (2017), 42717, https://doi.org/10.1038/srep42717.

[81] P. Banerjee, A.O. Eckert, A.K. Schrey, R. Preissner, ProTox-II: a webserver for the prediction of toxicity of chemicals, Nucleic Acids Res. 46 (W1) (2018) W257–W263, https://doi.org/10.1093/nar/gky318.

[82] F. Hikmet, L. Méar, Å. Edvinsson, P. Micke, M. Uhlén, C. Lindskog, The protein expression profile of ACE2 in human tissues, Mol. Syst. Biol. 16 (7) (2020), e9610, https://doi.org/10.15252/msb.20209610.

[83] M. Hoffmann, H. Kleine-Weber, S. Schroeder, N. Krüger, T. Herrler, S. Erichsen, T.S. Schiergens, G. Herrler, N.H. Wu, A. Nitsche, M.A. Müller, C. Drosten, S. Pöhlmann, SARS-CoV-2 cell entry depends on ACE2 and TMPRSS2 and is blocked by a clinically proven protease inhibitor, Cell 181 (2) (2020) 271–280.e8, https://doi.org/10.1016/j.cell.2020.02.052.

[84] R.L. Cho, C.C. Yang, H.C. Tseng, L.D. Hsiao, C.C. Lin, C.M. Yang, Haem oxygenase-1 up-regulation by rosiglitazone via ROS-dependent Nrf2-antioxidant response elements axis or PPARγ attenuates LPS-mediated lung inflammation, Br. J. Pharmacol. 175 (20) (2018) 3928–3946, https://doi.org/10.1111/bph.14465.

[85] N.K. Campbell, H.K. Fitzgerald, A. Dunne, Regulation of inflammation by the antioxidant haem oxygenase 1, Nat. Rev. Immunol. 21 (7) (2021) 411–425, https://doi.org/10.1038/s41577-020-00491-x.

[86] K. Huang, P. Zhang, Z. Zhang, J.Y. Youn, C. Wang, H. Zhang, H. Cai, Traditional Chinese Medicine (TCM) in the treatment of COVID-19 and other viral infections: efficacies and mechanisms, Pharmacol. Ther. 225 (2021), 107843, https://doi.org/10.1016/j.pharmthera.2021.107843.

[87] P.H. Guzzi, D. Mercatelli, C. Ceraolo, F.M. Giorgi, Master regulator analysis of the SARS-CoV-2/human interactome, J. Clin. Med. 9 (4) (2020) 982, https://doi.org/10.3390/jcm9040982.

[88] X. Nie, L. Qian, R. Sun, B. Huang, X. Dong, Q. Xiao, Q. Zhang, T. Lu, L. Yue, S. Chen, X. Li, Y. Sun, L. Li, L. Xu, Y. Li, M. Yang, Z. Xue, S. Liang, X. Ding, C. Yuan, L. Peng, W. Liu, X. Yi, M. Lyu, G. Xiao, X. Xu, W. Ge, J. He, J. Fan, J. Wu, M. Luo, X. Chang, H. Pan, X. Cai, J. Zhou, J. Yu, H. Gao, M. Xie, S. Wang, G. Ruan, H. Chen, H. Su, H. Mei, D. Luo, D. Zhao, F. Xu, Y. Li, Y. Zhu, J. Xia, Y. Hu, T. Guo, Multi-organ proteomic landscape of COVID-19 autopsies, Cell 184 (3) (2021) 775–791.e14, https://doi.org/10.1016/j.cell.2021.01.004.

[89] A.M. Thiebaut, I. Buendia, V. Ginet, E. Lemarchand, M.B. Boudjadja, et al., Thrombolysis by PLAT/tPA increases serum free IGF1 leading to a decrease of deleterious autophagy following brain ischemia, Autophagy 18 (6) (2022) 1297–1317, https://doi.org/10.1080/15548627.2021.1973339.

[90] K. Chrysovergis, X. Wang, J. Kosak, S.H. Lee, J.S. Kim, J.F. Foley, G. Travlos, S. Singh, S.J. Baek, T.E. Eling, NAG-1/GDF-15 prevents obesity by increasing thermogenesis, lipolysis and oxidative metabolism, Int. J. Obes. 38 (12) (2014) 1555–1564, https://doi.org/10.1038/ijo.2014.27.

[91] P. Zanoni, S.A. Khetarpal, D.B. Larach, W.F. Hancock-Cerutti, J.S. Millar Js, et al., Rare variant in scavenger receptor BI raises HDL cholesterol and increases risk of coronary heart disease, Science 351 (6278) (2016) 1166–1171, https://doi.org/10.1126/science.aad3517.

[92] A. Helgadottir, P. Sulem, G. Thorgeirsson, S. Gretarsdottir, G. Thorleifsson, B.Ö. Jensson, G.A. Arnadottir, I. Olafsson, G.I. Eyjolfsson, O. Sigurdardottir, U. Thorsteinsdottir, D.F. Gudbjartsson, H. Holm, K. Stefansson, Rare SCARB1 mutations associate with high-density lipoprotein cholesterol but not with coronary artery disease, Eur. Heart J. 39 (23) (2018) 2172–2178, https://doi.org/10.1093/eurheartj/ehy169.

[93] Y. Hou, C. Li, C. Yoon, O.W. Leung, S. You, X. Cui, J.F. Chan, D. Pei, H.H. Cheung, H. Chu, Enhanced replication of SARS-CoV-2 Omicron BA.2 in human forebrain and midbrain organoids, Signal Transduct. Targeted Ther. 7 (1) (2022) 381, https://doi.org/10.1038/s41392-022-01241-2.

[94] F. Crunfli, V.C. Carregari, F.P. Veras, L.S. Silva, M.H. Nogueira, et al., Morphological, cellular, and molecular basis of brain infection in COVID-19 patients, Proc. Natl. Acad. Sci. U. S. A. 119 (35) (2022), e2200960119, https://doi.org/10.1073/pnas.2200960119.

[95] J.H. Jeng, L.J. Hahn, F.J. Lu, Y.J. Wang, M.Y. Kuo, Eugenol triggers different pathobiological effects on human oral mucosal fibroblasts, J. Dent. Res. 73 (5) (1994) 1050–1055, https://doi.org/10.1177/00220345940730050601.

[96] Y. Wen, T. Ma, X. Chen, Z. Liu, C. Zhu, Y. Zhang, R. Strecker, G. Henderson, L.M. Hooper-Bùi, X. Chen, Z. Sun, X. Wen, C. Wang, Essential balm: a strong repellent against foraging and defending red imported fire ants (hymenoptera: formicidae), J. Econ. Entomol. 109 (4) (2016) 1827–1833, https://doi.org/10.1093/jee/tow130.

[97] O.M. Aburel, I.Z. Pavel, M.D. Dănilă, T. Lelcu, A. Roi, R. Lighezan, D.M. Muntean, L.C. Rusu, Pleiotropic effects of eugenol: the good, the bad, and the unknown, Oxid. Med. Cell. Longev. 2021 (2021), 3165159, https://doi.org/10.1155/2021/3165159.

[98] A.L. de Almeida, K.R. Caleffi-Ferracioli, R.B. de L. Scodro, V.P. Baldin, D.C. Montaholi, L.F. Spricigo, S.S. Nakamura-Vasconcelos, L.A. Hegeto, E.G. Sampiron, G.F. Costacurta, D.A. Dos S Yamazaki, G. F Gauze, V.L. Siqueira, R.F. Cardoso, Eugenol and derivatives activity against Mycobacterium tuberculosis, nontuberculous mycobacteria and other bacteria, Future Microbiol. 14 (2019) 331–344, https://doi.org/10.2217/fmb-2018-0333.

[99] A.B. Tiku, S.K. Abraham, R.K. Kale, Eugenol as an in vivo radioprotective agent, J. Radiat. Res. 45 (3) (2004 Sep) 435–440, https://doi.org/10.1269/jrr.45.435.

[100] S.A. Guenette, F. Beaudry, J.F. Marier, P. Vachon, Pharmacokinetics and anesthetic activity of eugenol in male Sprague-Dawley rats, J. Vet. Pharmacol. Therapeut. 29 (4) (2006) 265–270, https://doi.org/10.1111/j.1365-2885.2006.00740.x.

[101] H. Tsuchiya, Anesthetic agents of plant origin: a review of phytochemicals with anesthetic activity, Molecules 22 (8) (2017) 1369, https://doi.org/10.3390/molecules22081369.

[102] S.B. Mesole, O.O. Alfred, U.A. Yusuf, L. Lukubi, D. Ndhlovu, Apoptotic inducement of neuronal cells by aluminium chloride and the neuroprotective effect of eugenol in wistar rats, Oxid. Med. Cell. Longev. (2020), 8425643, https://doi.org/10.1155/2020/8425643, 2020.

[103] M.R. Wani, N. Maheshwari, G. Shadab, Eugenol attenuates TiO2 nanoparticles-induced oxidative damage, biochemical toxicity and DNA damage in Wistar rats: an in vivo study, Environ. Sci. Pollut. Res. Int. 28 (18) (2021) 22664–22678, https://doi.org/10.1007/s11356-020-12139-3.

[104] M.Z. Huang, Y.J. Yang, X.W. Liu, Z. Qin, J.Y. Li, Aspirin eugenol ester reduces H2O2-induced oxidative stress of HUVECs via mitochondria-lysosome Axis, Oxid. Med. Cell. Longev. (2019), 8098135, https://doi.org/10.1155/2019/8098135, 2019.

[105] N. Ma, Y. Yang, X. Liu, S. Li, Z. Qin, J. Li, Plasma metabonomics and proteomics studies on the anti-thrombosis mechanism of aspirin eugenol ester in rat tail thrombosis model, J. Proteonomics 215 (2020), 103631, https://doi.org/10.1016/j.jprot.2019.103631.
[106] E. Nagababu, J.M. Rifkind, S. Boindala, L. Nakka, Assessment of antioxidant activity of eugenol in vitro and in vivo, Methods Mol. Biol. 610 (2010) (2010) 165–180, https://doi.org/10.1007/978-1-60327-029-8_10.
[107] S.K. Jaganathan, E. Supriyanto, Antiproliferative and molecular mechanism of eugenol-induced apoptosis in cancer cells, Molecules 17 (6) (2012) 6290–6304, https://doi.org/10.3390/molecules17066290.
[108] M.L. Abdullah, M.M. Hafez, A. Al-Hoshani, O. Al-Shabanah, Anti-metastatic and anti-proliferative activity of eugenol against triple negative and HER2 positive breast cancer cells, BMC Compl. Alternative Med. 18 (1) (2018) 321, https://doi.org/10.1186/s12906-018-2392-5.
[109] J.N. Barboza, C. da Silva Maia Bezerra Filho, R.O. Silva, J.V.R. Medeiros, D.P. de Sousa, An overview on the anti-inflammatory potential and antioxidant profile of eugenol, Oxid. Med. Cell. Longev. (2018), 3957262, https://doi.org/10.1155/2018/3957262, 2018.
[110] S. Fujisawa, Y. Murakami, Eugenol and its role in chronic diseases, Adv. Exp. Med. Biol. 929 (2016) 45–66, https://doi.org/10.1007/978-3-319-41342-6_3.
[111] B.N. Harapan, H.J. Yoo, Neurological symptoms, manifestations, and complications associated with severe acute respiratory syndrome coronavirus 2 (SARS-CoV-2) and coronavirus disease 19 (COVID-19), J. Neurol. 268 (9) (2021) 3059–3071, https://doi.org/10.1007/s00415-021-10406-y.
[112] Y. Zhou, J. Xu, Y. Hou, J.B. Leverenz, A. Kallianpur, R. Mehra, Y. Liu, H. Yu, A.A. Pieper, L. Jehi, F. Cheng, Network medicine links SARS-CoV-2/COVID-19 infection to brain microvascular injury and neuroinflammation in dementia-like cognitive impairment, Alzheimer's Res. Ther. 13 (1) (2021) 110, https://doi.org/10.1186/s13195-021-00850-3.
[113] A.C. Yang, F. Kern, P.M. Losada, M.R. Agam, C.A. Maat, et al., Dysregulation of brain and choroid plexus cell types in severe COVID-19, Nature 595 (7868) (2021) 565–571, https://doi.org/10.1038/s41586-021-03710-0.
[114] G. Douaud, S. Lee, F. Alfaro-Almagro, C. Arthofer, C. Wang, P. McCarthy, F. Lange, J.L.R. Andersson, L. Griffanti, E. Duff, S. Jbabdi, B. Taschler, P. Keating, A. M. Winkler, R. Collins, P.M. Matthews, N. Allen, K.L. Miller, T.E. Nichols, S.M. Smith, SARS-CoV-2 is associated with changes in brain structure in UK Biobank, Nature 604 (7907) (2022) 697–707, https://doi.org/10.1038/s41586-022-04569-5.
[115] E.A. Albornoz, A.A. Amarilla, N. Modhiran, S. Parker, X.X. Li, et al., SARS-CoV-2 drives NLRP3 inflammasome activation in human microglia through spike protein [published online ahead of print, 2022 Nov 1], Mol. Psychiatr. (2022), https://doi.org/10.1038/s41380-022-01831-0, 10.1038/s41380-022-01831-0.
[116] B. Bowe, Y. Xie, Z. Al-Aly, Acute and postacute sequelae associated with SARS-CoV-2 reinfection, Nat. Med. 28 (11) (2022) 2398–2405, https://doi.org/10.1038/s41591-022-02051-3.
[117] B. Blomberg, K.G. Mohn, K.A. Brokstad, F. Zhou, D.W. Linchausen, B.A. Hansen, S. Lartey, T.B. Onyango, K. Kuwelker, M. Sævik, H. Bartsch, C. Tøndel, B. R. Kittang, , Bergen COVID-19 Research Group, R.J. Cox, N. Langeland, Long COVID in a prospective cohort of home-isolated patients, Nat. Med. 27 (9) (2021) 1607–1613, https://doi.org/10.1038/s41591-021-01433-3.
[118] E. Avolio, M. Carrabba, R. Milligan, M. Kavanagh Williamson, A.P. Beltrami, K. Gupta, K.T. Elvers, M. Gamez, R.R. Foster, K. Gillespie, F. Hamilton, D. Arnold, I. Berger, A.D. Davidson, D. Hill, M. Caputo, P. Madeddu, The SARS-CoV-2 Spike protein disrupts human cardiac pericytes function through CD147 receptor-mediated signalling: a potential non-infective mechanism of COVID-19 microvascular disease, Clin. Sci. 135 (24) (2021) 2667–2689, https://doi.org/10.1042/CS20210735.
[119] A. Kulasinghe, N. Liu, C.W. Tan, J. Monkman, J.E. Sinclair, D.D. Bhuva, D. Godbolt, L. Pan, A. Nam, H. Sadeghirad, K. Sato, G.L. Bassi, K. O'Byrne, C. Hartmann, A.F.R. Dos Santos Miggiolaro, G.L. Marques, L.Z. Moura, D. Richard, M. Adams, L. de Noronha, C.P. Baena, J.Y. Suen, R. Arora, G.T. Belz, K. R. Short, M.J. Davis, F.S. Guimaraes, J.F. Fraser, Transcriptomic profiling of cardiac tissues from SARS-CoV-2 patients identifies DNA damage, Immunology (2022) 15, https://doi.org/10.1111/imm.13577, 10.1111/imm.13577.
[120] Z. Ma, X. Li, R.L.Y. Fan, K.Y. Yang, C.S.H. Ng, R.W.H. Lau, R.H.L. Wong, K.K. Ng, C.C. Wang, P. Ye, Z. Fu, A.W.H. Chin, M.Y.A. Lai, Y. Huang, X.Y. Tian, L.L. M. Poon, K.O. Lui, A human pluripotent stem cell-based model of SARS-CoV-2 infection reveals an ACE2-independent inflammatory activation of vascular endothelial cells through TLR4, Stem Cell Rep. 17 (3) (2022) 538–555, https://doi.org/10.1016/j.stemcr.2022.01.015.
[121] Y. Xie, E. Xu, B. Bowe, Z. Al-Aly, Long-term cardiovascular outcomes of COVID-19, Nat. Med. 28 (3) (2022) 583–590, https://doi.org/10.1038/s41591-022-01689-3.
[122] T.M. Clausen, D.R. Sandoval, C.B. Spliid, J. Pihl, H.R. Perrett, C.D. Painter, A. Narayanan, S.A. Majowicz, E.M. Kwong, R.N. McVicar, B.E. Thacker, C.A. Glass, Z. Yang, J.L. Torres, G.J. Golden, P.L. Bartels, R.N. Porell, A.F. Garretson, L. Laubach, J. Feldman, X. Yin, Y. Pu, B.M. Hauser, T.M. Caradonna, B.P. Kellman, C. Martino, P.L.S.M. Gordts, S.K. Chanda, A.G. Schmidt, K. Godula, S.L. Leibel, J. Jose, K.D. Corbett, A.B. Ward, A.F. Carlin, J.D. Esko, SARS-CoV-2 infection depends on cellular heparan sulfate and ACE2, Cell 183 (4) (2020) 1043–1057.e15, https://doi.org/10.1016/j.cell.2020.09.033.
[123] Z. Raisi-Estabragh, J. Cooper, A. Salih, B. Raman, A.M. Lee, S. Neubauer, N.C. Harvey, S.E. Petersen, Cardiovascular disease and mortality sequelae of COVID-19 in the UK Biobank, Heart 109 (2) (2022) 119–126, https://doi.org/10.1136/heartjnl-2022-321492.
[124] J.J. Frere, R.A. Serafini, K.D. Pryce, M. Zazhytska, K. Oishi, I. Golynker, M. Panis, J. Zimering, S. Horiuchi, D.A. Hoagland, R. Møller, A. Ruiz, A. Kodra, J. B. Overdevest, P.D. Canoll, A.C. Borczuk, V. Chandar, Y. Bram, R. Schwartz, S. Lomvardas, V. Zachariou, B.R. tenOever, SARS-CoV-2 infection in hamsters and humans results in lasting and unique systemic perturbations after recovery, Sci. Transl. Med. 14 (664) (2022), eabq3059, https://doi.org/10.1126/scitranslmed.abq3059.
[125] J. Klein, J. Wood, J. Jaycox, P. Lu, R.M. Dhodapkar, J.R. Gehlhausen, A. Tabachnikova, L. Tabacof, A.A. Malik, K. Kamath, K. Greene, V.S. Monteiro, M. Peña-Hernandez, T. Mao, B. Bhattacharjee, T. Takahashi, C. Lucas, J. Silva, D. Mccarthy, E. Breyman, J. Tosto-Mancuso, Y. Dai, E. Perotti, K. Akduman, T.J. Tzeng, L. Xu, I. Yildirim, H.M. Krumholz, J. Shon, R. Medzhitov, S.B. Omer, D. van Dijk, A.M. Ring, D. Putrino, A. Iwasaki, Distinguishing features of Long COVID identified through immune profiling, medRxiv [Preprint] 10 (2022), https://doi.org/10.1101/2022.08.09.22278592, 2022.08.09.22278592.
[126] J.E. Gold, R.A. Okyay, W.E. Licht, D.J. Hurley, Investigation of long COVID prevalence and its relationship to epstein-barr virus reactivation, Pathogens 10 (6) (2021) 763, https://doi.org/10.3390/pathogens10060763.
[127] P. Brodin, M. Arditi, Severe acute hepatitis in children: investigate SARS-CoV-2 superantigens, Lancet Gastroenterol Hepatol 7 (7) (2022) 594–595, https://doi.org/10.1016/S2468-1253(22)00166-2.
[128] X. Wang, J. Luo, Z. Wen, L. Shuai, C. Wang, G. Zhong, X. He, H. Cao, R. Liu, J. Ge, R. Hua, Z. Sun, X. Wang, J. Wang, Z. Bu, Diltiazem inhibits SARS-CoV-2 cell attachment and internalization and decreases the viral infection in mouse lung, PLoS Pathog. 18 (2) (2022), e1010343, https://doi.org/10.1371/journal.ppat.1010343.
[129] E. Scarselli, H. Ansuini, R. Cerino, R.M. Roccasecca, S. Acali, G. Filocamo, C. Traboni, A. Nicosia, R. Cortese, A. Vitelli, The human scavenger receptor class B type I is a novel candidate receptor for the hepatitis C virus, EMBO J. 21 (19) (2002) 5017–5025, https://doi.org/10.1093/emboj/cdf529.
[130] M.B. Zeisel, G. Koutsoudakis, E.K. Schnober, A. Haberstroh, H.E. Blum, F.L. Cosset, T. Wakita, D. Jaeck, M. Doffoel, C. Royer, E. Soulier, E. Schvoerer, C. Schuster, F. Stoll-Keller, R. Bartenschlager, T. Pietschmann, H. Barth, T.F. Baumert, Scavenger receptor class B type I is a key host factor for hepatitis C virus infection required for an entry step closely linked to CD81, Hepatology 46 (6) (2007) 1722–1731, https://doi.org/10.1002/hep.21994.
[131] C. Wei, L. Wan, Q. Yan, X. Wang, J. Zhang, et al., HDL-scavenger receptor B type 1 facilitates SARS-CoV-2 entry, Nat Metab 2 (12) (2020) 1391–1400, https://doi.org/10.1038/s42255-020-00324-0.
[132] J.P. Dai, X.F. Zhao, J. Zeng, Q.Y. Wan, J.C. Yang, W.Z. Li, X.X. Chen, G.F. Wang, K.S. Li, Drug screening for autophagy inhibitors based on the dissociation of Beclin1-Bcl2 complex using BiFC technique and mechanism of eugenol on anti-influenza A virus activity, PLoS One 8 (4) (2013), e61026, https://doi.org/10.1371/journal.pone.0061026.
[133] G. Mustafa, M. Majid, A. Ghaffar, M. Yameen, H.A. Samad, H.S. Mahrosh, Screening and molecular docking of selected phytochemicals against NS5B polymerase of hepatitis c virus, Pak. J. Pharm. Sci. 33 (5) (2020) 2317–2322. Supplementary.
[134] S.M. Lam, X. Huang, G. Shui, Neurological aspects of SARS-CoV-2 infection: lipoproteins and exosomes as Trojan horses, Trends Endocrinol. Metabol. 33 (8) (2022) 554–568, https://doi.org/10.1016/j.tem.2022.04.011.
[135] Z. Saud, V.J. Tyrrell, A. Zaragkoulias, M.B. Protty, E. Statkute, et al., The SARS-CoV2 envelope differs from host cells, exposes procoagulant lipids, and is disrupted in vivo by oral rinses, J. Lipid Res. 63 (6) (2022), 100208, https://doi.org/10.1016/j.jlr.2022.100208.

[136] D. Wu, T. Shu, X. Yang, J.X. Song, M. Zhang, et al., Plasma metabolomic and lipidomic alterations associated with COVID-19, Natl. Sci. Rev. 7 (7) (2020) 1157–1168, https://doi.org/10.1093/nsr/nwaa086.
[137] L. Zhu, Z.G. She, X. Cheng, J.J. Qin, X.J. Zhang, et al., Association of blood glucose control and outcomes in patients with COVID-19 and pre-existing type 2 diabetes, Cell Metabol. 31 (6) (2020) 1068–1077.e3, https://doi.org/10.1016/j.cmet.2020.04.021.
[138] R. Adela, S.K. Banerjee, GDF-15 as a target and biomarker for diabetes and cardiovascular diseases: a translational prospective, J. Diabetes Res. 2015 (2015), 490842, https://doi.org/10.1155/2015/490842.
[139] X.J. Zhang, J.J. Qin, X. Cheng, L. Shen, Y.C. Zhao, et al., In-hospital use of statins is associated with a reduced risk of mortality among individuals with COVID-19, Cell Metabol. 32 (2) (2020) 176–187.e4, https://doi.org/10.1016/j.cmet.2020.06.015.
[140] H.H. Luan, A. Wang, B.K. Hilliard, F. Carvalho, C.E. Rosen, A.M. Ahasic, E.L. Herzog, I. Kang, M.A. Pisani, S. Yu, C. Zhang, A.M. Ring, L.H. Young, R. Medzhitov, GDF15 is an inflammation-induced central mediator of tissue tolerance, Cell 178 (5) (2019) 1231–1244.e11, https://doi.org/10.1016/j.cell.2019.07.033.
[141] E. Sefik, R. Qu, C. Junqueira, E. Kaffe, H. Mirza, et al., Inflammasome activation in infected macrophages drives COVID-19 pathology, Nature 606 (7914) (2022) 585–593, https://doi.org/10.1038/s41586-022-04802-1.
[142] C. Junqueira, Â. Crespo, S. Ranjbar, L.B. de Lacerda, M. Lewandrowski, J. Ingber, B. Parry, S. Ravid, S. Clark, M.R. Schrimpf, F. Ho, C. Beakes, J. Margolin, N. Russell, K. Kays, J. Boucau, U. Das Adhikari, S.M. Vora, V. Leger, L. Gehrke, L.A. Henderson, E. Janssen, D. Kwon, C. Sander, J. Abraham, M.B. Goldberg, H. Wu, G. Mehta, S. Bell, A.E. Goldfeld, M.R. Filbin, J. Lieberman, FcγR-mediated SARS-CoV-2 infection of monocytes activates inflammation, Nature 606 (7914) (2022) 576–584, https://doi.org/10.1038/s41586-022-04702-4.
[143] L. Liu, Q. Wei, Q. Lin, J. Fang, H. Wang, H. Kwok, H. Tang, K. Nishiura, J. Peng, Z. Tan, T. Wu, K.W. Cheung, K.H. Chan, X. Alvarez, C. Qin, A. Lackner, S. Perlman, K.Y. Yuen, Z. Chen, Anti-spike IgG causes severe acute lung injury by skewing macrophage responses during acute SARS-CoV infection, JCI Insight 4 (4) (2019), e123158, https://doi.org/10.1172/jci.insight.123158.
[144] C. Corpetti, A. Del Re, L. Seguella, I. Palenca, S. Rurgo, B. De Conno, M. Pesce, G. Sarnelli, G. Esposito, Cannabidiol inhibits SARS-Cov-2 spike (S) protein-induced cytotoxicity and inflammation through a PPARγ-dependent TLR4/NLRP3/Caspase-1 signaling suppression in Caco-2 cell line, Phytother Res. 35 (12) (2021) 6893–6903, https://doi.org/10.1002/ptr.7302.
[145] S.M. de Morais, N.S. Vila-Nova, C.M. Bevilaqua, F.C. Rondon, C.H. Lobo, A. de Alencar Araripe Noronha Moura, A.D. Sales, A.P. Rodrigues, J.R. de Figuereido, C.C. Campello, M.E. Wilson, H.F. de Andrade Jr., Thymol and eugenol derivatives as potential antileishmanial agents, Bioorg. Med. Chem. 22 (21) (2014) 6250–6255, https://doi.org/10.1016/j.bmc.2014.08.020.
[146] M.R. Charan Raja, A.B. Velappan, D. Chellappan, J. Debnath, S. Kar Mahapatra, Eugenol derived immunomodulatory molecules against visceral leishmaniasis, Eur. J. Med. Chem. 139 (2017) 503–518, https://doi.org/10.1016/j.ejmech.2017.08.030.
[147] T. Lane, M. Anantpadma, J.S. Freundlich, R.A. Davey, P.B. Madrid, S. Ekins, The natural product eugenol is an inhibitor of the ebola virus in vitro, Pharm. Res. (N. Y.) 36 (7) (2019) 104, https://doi.org/10.1007/s11095-019-2629-0.
[148] M.R. Charan Raja, A. Kar, S. Srinivasan, D. Chellappan, J. Debnath, S. Kar Mahapatra, Oral administration of eugenol oleate cures experimental visceral leishmaniasis through cytokines abundance, Cytokine 145 (2021), 155301, https://doi.org/10.1016/j.cyto.2020.155301.
[149] N. Turgeon, K. Michel, T.L. Ha, E. Robine, S. Moineau, C. Duchaine, Resistance of aerosolized bacterial viruses to four germicidal products, PLoS One 11 (12) (2016), e0168815, https://doi.org/10.1371/journal.pone.0168815.
[150] K.H. Dinnon 3rd, S.R. Leist, K. Okuda, H. Dang, E.J. Fritch, et al., SARS-CoV-2 infection produces chronic pulmonary epithelial and immune cell dysfunction with fibrosis in mice, Sci. Transl. Med. 14 (664) (2022), https://doi.org/10.1126/scitranslmed.abo5070 eabo5070.
[151] F. DI Pierro, A. Khan, A. Bertuccioli, P. Maffioli, G. Derosa, S. Khan, B.A. Khan, R. Nigar, I. Ujjan, B.R. Devrajani, Quercetin Phytosome® as a potential candidate for managing COVID-19, Minerva Gastroenterol. 67 (2) (2021) 190–195, https://doi.org/10.23736/S2724-5985.20.02771-3.
[152] A. Martínez-Herrera, A. Pozos-Guillén, S. Ruiz-Rodríguez, A. Garrocho-Rangel, A. Vértiz-Hernández, D.M. Escobar-García, Effect of 4-Allyl-1-hydroxy-2-methoxybenzene (eugenol) on inflammatory and apoptosis processes in dental pulp fibroblasts, Mediat. Inflamm. (2016), 9371403, https://doi.org/10.1155/2016/9371403, 2016.
[153] D.C. Thompson, D. Constantin-Teodosiu, P. Moldéus, Metabolism and cytotoxicity of eugenol in isolated rat hepatocytes, Chem. Biol. Interact. 77 (2) (1991) 137–147, https://doi.org/10.1016/0009-2797(91)90069-j.
[154] S. Fujisawa, T. Atsumi, Y. Kadoma, H. Sakagami, Antioxidant and prooxidant action of eugenol-related compounds and their cytotoxicity, Toxicology 177 (1) (2002) 39–54, https://doi.org/10.1016/s0300-483x(02)00194-4.
[155] W. Liang, W. Guan, R. Chen, W. Wang, J. Li, K. Xu, C. Li, Q. Ai, W. Lu, H. Liang, S. Li, J. He, Cancer patients in SARS-CoV-2 infection: a nationwide analysis in China, Lancet Oncol. 21 (3) (2020) 335–337, https://doi.org/10.1016/S1470-2045(20)30096-6.
[156] J. Yu, W. Ouyang, M.L.K. Chua, C. Xie, SARS-CoV-2 transmission in patients with cancer at a tertiary care hospital in wuhan, China, JAMA Oncol. 6 (7) (2020) 1108–1110, https://doi.org/10.1001/jamaoncol.2020.0980.
[157] Y. Wang, S. Liu, H. Liu, W. Li, F. Lin, L. Jiang, X. Li, P. Xu, L. Zhang, L. Zhao, Y. Cao, J. Kang, J. Yang, L. Li, X. Liu, Y. Li, R. Nie, J. Mu, F. Lu, S. Zhao, J. Lu, J. Zhao, SARS-CoV-2 infection of the liver directly contributes to hepatic impairment in patients with COVID-19, J. Hepatol. 73 (4) (2020) 807–816, https://doi.org/10.1016/j.jhep.2020.05.002.
[158] B.M. Popkin, S. Du, W.D. Green, M.A. Beck, T. Algaith, C.H. Herbst, R.F. Alsukait, M. Alluhidan, N. Alazemi, M. Shekar, Individuals with obesity and COVID-19: a global perspective on the epidemiology and biological relationships, Obes. Rev. 21 (11) (2020), e13128, https://doi.org/10.1111/obr.13128.